Doctoral Thesis

Development of Multifunctional Polymer-based Hydrogel with Controllable Physicochemical Properties for Biomedical Engineering

Mirae Kim

Department of Materials Science and Engineering

Ulsan National Institute of Science and Technology

2021

Development of Multifunctional Polymer-based Hydrogel with Controllable Physicochemical Properties for Biomedical Engineering

Mirae Kim

Department of Materials Science and Engineering

Ulsan National Institute of Science and Technology

Development of Multifunctional Polymer-based Hydrogel with Controllable Physicochemical Properties for Biomedical Engineering

A thesis/dissertation submitted to
Ulsan National Institute of Science and Technology
in partial fulfillment of the
requirements for the degree of
Doctor of Philosophy

Mirae Kim

12. 09. 2020

Approved by

Advisor
Chaenyung Cha

Development of Multifunctional Polymer-based Hydrogel with Controllable Physicochemical Properties for Biomedical Engineering

Mirae Kim

This certifies that the thesis/dissertation of Mirae Kim is approved.

12. 09. 2020

signature

Advisor: Chaenyung Cha

signature

Thesis Committee: Hyun-Wook Kang

signature

Thesis Committee: Dong-Woog Lee

signature

Thesis Committee: Jiyun Kim

signature

Thesis Committee: Jeyoung Park

ABSTRACT

Hydrogels consisting of aqueous 3D crosslinked polymer network are very similar to living tissue properties such as elasticity, biocompatibility, hydrophilicity and porosity, and are widely used in various biomedical applications. They are widely used as promising materials for therapeutic delivery, contact lenses, bone cements, wound dressings, and 3D tissue scaffolds for tissue engineering and so on. However, to control their properties independently to suit biomedical application purpose is often challenge.

One of challenge is interdependency of hydrogel properties, since controlling the crosslinking density can also affects their other properties such as the degradation rate, hydrophilicity and mechanical properties. Also, their fabrication mechanisms are often an issue. Free radical polymerization, most commonly used to form hydrogels, is usually initiated by free radical-generating compounds, radiation or heating, which activation and residual initiators often damage cells and tissues. In addition, it is difficult to control the crosslinking kinetics at low toxicity levels. Therefore, an "*in situ*" crosslinking reaction would be highly favored for hydrogel fabrication in biomedical application. because, they react under mild conditions without using initiator and their crosslinking kinetics can be widely controlled with low toxicity.

Due to many things in addition to the aforementioned challenges, it is important to control these properties at different levels to meet the specific requirements. Therefore, in this study, in order to overcome limitations while maintaining their intrinsic properties, a multifunctional polymer-based hydrogel was developed, and various properties were controlled. It is expected to exhibit superior properties to increase the potential use in the biomedical industry.

In chapter 2, the protein release rates from hydrogels were controlled by varying the physical properties of the hydrogels while maintaining their crosslinking density. In general, the degree of crosslinking is adjusted to control the protein release of the hydrogel as a carrier. However, it is not preferred because the crosslinking density affects the mechanical properties of the hydrogels, in which the mechanical and diffusional properties are inversely correlated. To overcome these issues, by presenting functional groups having positive charge, negative charge, and hydrophobicity, respectively, on the poly(ethylene glycol) (PEG) chains, the release of proteins having various isoelectric points was controlled through electrostatic interactions.

In the chapter 3, the mechanical properties and degradation behavior of PEG diacrylate (PEGDA)-polyethyleneimine (PEI) hydrogels prepared by *in situ* crosslinking between PEGDA and PEI via Michael addition were explored. Generally, cross-linked hydrogels involving the use of initiators to start the process often exhibit cytotoxicity depending on reagent concentrations. Therefore, their dosage must be applied carefully to prevent cytotoxicity while maintaining the ability to initiate a

crosslinking reaction. As the alternative to these issues, PEGDA and PEI were used to fabricate hydrogels through "*in situ*" crosslinking reactions that occur under mild conditions and do not involve the use of initiators. We also explored the drug release kinetics of PEGDA-PEI hydrogels depending on their physical properties and degradation behavior.

In the chapter 4, the mechanical properties of *in situ* forming chitosan hydrogels via Schiff base formation were controlled by introducing tunable polymer graft architecture. Due to the mechanical properties of *in situ* forming hydrogels depend on the crosslinking density which also controls the gelation rate, it is a significant challenge to independently control the mechanics and gelation kinetics. We synthesized PEG with varying lengths and densities conjugated to the chitosan backbone, which not only allowed dissolution in neutral aqueous solutions but also the control of mechanical properties of hydrogel while maintaining facile gelation kinetics. In addition, the tissue adhesive properties of resulting hydrogels were evaluated by *ex vivo* and *in vivo* models, demonstrating their clinical potential.

In the last chapter, polyaspartamide presenting amine groups with controllable grafting density and length was synthesized using diamines with varying length of poly(ethylene glycol) linker. Small molecules can only have a few functional groups and often-show limited solubility in various solvents, limiting their controllable range. On the other hand, polymers that have functional groups throughout their repeating units serving as sites for chemical reactions can present more reactive functional groups than small molecules, resulting considered highly effective crosslinkers to develop materials with variable mechanical properties. We demonstrated the potential application as an injectable drug delivery systems undergo facile degradation and complete dissolution in physiological conditions, regardless of mechanical properties, by adjusting the graft architecture of poly(2-hydroxyethyl aspartamide)-g-amino-poly(ethylene glycol) (PHEA-PEGAm) as polymer crosslinker..

CONTENTS

ABSTRACT ..... **I**
CONTENTS ..... **IV**
LIST OF FIGURES AND TABLES ..... **VII**

CHAPTER 1. Introduction **1**

1.1 Research Background **1**
1.2 Research Purpose and Motivation **2**

CHAPTER 2. Modulation of functional pendant chains within poly(ethylene glycol) hydrogels for refined control of protein release **3**

2.1 Introduction **3**
2.2 Materials and Methods **4**
2.2.1 Synthesis of Poly(ethylene glycol) dimethacrylate (PEGDA) 4
2.2.2 Synthesis of heterobifunctional poly(ethylene glycol) monomethacrylate (PEGMA) 4
2.2.3 Fabrication of hydrogels 8
2.2.4 Evaluation of mechanical properties of hydrogels 8
2.2.5 Evaluation of protein release from hydrogels 8
2.3 Results and Discussion **9**
2.3.1 Synthesis of heterobifunctional PEGMA 9
2.3.2 Mechanical properties of PEG hydrogel with functional pendant chains 11
2.3.3 Protein release from PEG hydrogel with functional pendant chains 14
2.4 Conclusion **23**

CHAPTER 3. Integrative control of mechanical and degradation properties of in situ crosslinkable polyamine-based hydrogels for dual-mode drug release kinetics **25**

3.1 Introduction **25**
3.2 Materials and Methods **26**
3.2.1 Synthesis of poly(ethylene glycol) diacrylate (PEGDA) 26
3.2.2 PEGDA-PEI hydrogel fabrication 27
3.2.3 Mechanical properties and degradation of PEGDA-PEI hydrogels 27
3.2.4 Drug release profiles from PEGDA-PEI hydrogels 28
3.3 Results and Discussion **29**
3.3.1 Mechanical properties of PEGDA-PEI hydrogels 29
3.3.2 Gelation kinetics 30
3.3.3 Rigidity 33

3.3.4 Degradation of PEGDA-PEI hydrogels 36
3.3.5 Degradation of PEGDA-PEI hydrogels 39
3.4 Conclusion **43**

CHAPTER 4. In situ facile-forming chitosan hydrogels with tunable physicomechanical and tissue adhesive properties by polymer graft architecture **44**

4.1 Introduction **44**
4.2 Materials and Methods **46**
4.2.1 Synthesis of PEG-grafted chitosan ('PEG-g-Cs') and PEG-dialdehyde 46
4.2.2 Fabrication of Cs-PEG hydrogels 48
4.2.3 Mechanical and rheological properties of Cs-PEG hydrogels 48
4.2.4 Diffusional properties of Cs-PEG hydrogels 49
4.2.5 Tissue adhesive properties of Cs-PEG hydrogels 49
4.2.6 Anti-microbial properties of PEG-g-Cs 51
4.2.7 Swept-Source Optical Coherence Tomography (SS-OCT) 51
4.3 Results and Discussion **52**
4.3.1 Synthesis and physical properties of PEG-g-Cs 52
4.3.2 Mechanical properties of Cs-PEG hydrogels 56
4.3.3 Diffusional properties of Cs-PEG hydrogels 60
4.3.4 Anti-microbial properties of Cs-PEG hydrogels 62
4.3.5 Gelation kinetics of Cs-PEG hydrogels 63
4.3.6 Tissue adhesive properties of Cs-PEG hydrogels 64
4.3.7 In vivo evaluation of Cs-PEG hydrogel as tissue sealant 66
4.4 Conclusion **70**

CHAPTER 5. In situ facile-forming chitosan hydrogels with tunable physicomechanical and tissue adhesive properties by polymer graft architecture **71**

5.1 Introduction **71**
5.2 Materials and Methods **72**
5.2.1 Synthesis of Polysuccinimide (PSI) 72
5.2.2 Synthesis of PEG-Diamine 72
5.2.3 Synthesis of Poly(2-hydroxyethyl aspartamide)-g-Amino-Poly(ethylene glycol) (PHEA–PEGAm) 74
5.2.4 Trinitrobenzene sulfonic acid (TNBS) assay 75
5.2.5 Synthesis of oxidized alginate 75
5.2.6 Fabrication of PHEA–PEGAm Hydrogels 75

5.2.7 Mechanical and Degradation Properties of Hydrogels 75
5.2.8 Drug Release Kinetics 76
5.2.9 Rheological Properties of Hydrogels 76
5.2.10 In Vitro Cytotoxicity 76
5.2.11 Ex Vivo Evaluation of Degradation Behavior of Hydrogel 77
5.3 Results and Discussion **77**
5.3.1 Synthesis and Characterization of Amine-Presenting Polyaspartamide with Tunable Graft Architecture 77
5.3.2 Fabrication and Mechanical Properties of PHEA-Linked Hydrogels 81
5.3.3 Degradation of PHEA-Linked Hydrogels 84
5.3.4 Drug Release Kinetics of PHEA-Linked Hydrogels 86
5.3.5 Ex Vivo Alg-PHEA Hydrogel Injection and Degradation 88
5.3.6 Dual Ionic Cross-Linked Alg-PHEA Hydrogels 89
5.4 Conclusion **91**

CHAPTER 6. Summary and Future Perspective **92**

REFERENCES **93**

LIST OF FIGURES AND TABLES

Figure 2-1. The molecular weight distributions of (a) Sulfo-PEG, (b) TMAC-PEG, and (c) Ph-PEG, determined from MALDI-TOF mass spectrometry. 5

Figure 2-2. ^{1}H-NMR spectra of (a) Sulfo-PEG, (b) TMAC-PEG, and (c) Ph-PEG. 6

Figure 2-3. ^{13}C-NMR spectra of (a) Sulfo-PEG, (b) TMAC-PEG, and (c) Ph-PEG. 7

Figure 2-4. Zeta potential values of (a) proteins (albumin, insulin, and trypsin) and (b) SulfoPEGMA and TMAC-PEGMA, measured at 0.1 % (w/v) in 10 mM NaCl. 8

Figure 2-5. (a) Fabrication of PEG hydrogels with functional pendant chains via radical copolymerization of PEGDA with heterobifunctional PEGMA. (b) Synthesis of heterobifunctional PEGMA via anionic polymerization of epoxide with an initiator containing the desired functional group, followed by the conjugation of methacrylate. The functional groups used in this study were sulfonate (negative charge), trimethylammonium chloride (positive charge) and phenyl (hydrophobicity) groups. 10

Figure 2-6. (a) The fraction of functional pendant chains (Φ) was varied while keeping the total number of pendant chains constant. Normalized elastic moduli (E/E_0) of PEG hydrogels with varying Φ, measured (b,c,d) right after fabrication and (e,f,g) after incubation in PBS for 24 hours. The moduli were normalized with that at $\Phi = 0$ (E_0). (b,e) 10% PEGDA and 2% PEGMA, (c,f) 8% PEGDA and 4% PEGMA, (d,g) 6% PEGDA and 6% PEGMA 11

Figure 2-7. Elastic moduli (E) of Sulfo-PEG, TMAC-PEG, and Ph-PEG hydrogels measured right after fabrication ('initial moduli'). The PEGDA and PEGMA concentrations of the hydrogels were (a) 10% and 2%, (b) 8% and 4%, and (c) 6% and 6%. 12

Figure 2-8. (a-c) Elastic moduli (E) and (d-e) swelling ratios (Q) of Sulfo-PEG, TMAC-PEG, and Ph-PEG hydrogels. The PEGDA and PEGMA concentrations of the hydrogels were (a,d) 10% and 2%, (b,e) 8% and 4%, and (c,f) 6% and 6%. E and Q were measured after 1 day of incubation in PBS. . 13

Figure 2-9. Scanning electron microscopic (SEM) images of non-functional mPEG hydrogel, Sulfo-PEG hydrogel, TMAC-PEG hydrogel, and Ph-PEG hydrogel at $\Phi = 1$ (scale bar: 5 μm). (a) 10% PEGDA and 2% PEGMA, (b) 8% PEGDA and 4% PEGMA. 13

Figure 2-10. Normalized swelling ratios (Q/Q_0) of PEG hydrogels with varying Φ. The swelling ratios were normalized with that at $\Phi = 0$ (Q_0). (a) 10% PEGDA and 2% PEGMA, (b) 8% PEGDA and 4% PEGMA, (c) 6% PEGDA and 6% PEGMA. 14

Figure 2-11. (a) Protein with pI lower than 7.4 becomes negatively charged, and thus expected to have a greater release rate in Sulfo-PEG hydrogels via repulsion than TMAC-PEG hydrogels. The release profiles of albumin from (b) Sulfo-PEG hydrogels, (c) TMAC-PEG hydrogels and (d) Ph-PEG hydrogels. (e) The kinetic rate constants (*k*) and (f) exponents (*n*) were obtained by fitting the curves with Eq. 2-1. (g) Diffusion coefficients (*D*) were obtained by fitting the curves with Eq. 2-2. The PEGDA and PEGMA concentrations of the hydrogels were 8% and 4%, respectively. (*$p < 0.05$).. 16

Figure 2-12. (a,b) Kinetic rate constants (*k*) and (c,d) diffusion coefficients (*D*) of albumin release from Sulfo-PEG, TMAC-PEG and Ph-PEG hydrogels, obtained by fitting the release profiles with Eq. (1) and Eq. 2-2, respectively. (*$p < 0.05$) (a,c) 10% PEGDA and 2% PEGMA, (b,d) 6% PEGDA and 6% PEGMA..... 18

Figure 2-13. The release profiles of insulin from (a) Sulfo-PEG hydrogels, (b) TMAC-PEG hydrogels and (c) Ph-PEG hydrogels. (d) The kinetic rate constants (*k*) and (e) exponents (*n*) obtained by fitting the curves with Eq. 2-1. (f) Diffusion coefficients (*D*) were obtained by fitting the curves with Eq. 2-2. (*$p < 0.05$) The PEGDA and PEGMA concentrations of the hydrogels were 8% and 4%, respectively. 19

Figure 2-14. (a,b) Kinetic rate constants (*k*) and (c,d) diffusion coefficients (*D*) of insulin release from Sulfo-PEG, TMAC-PEG and Ph-PEG hydrogels, obtained by fitting the release profiles with Eq. 2-1 and Eq. 2-2, respectively. (*$p < 0.05$) (a,c) 10% PEGDA and 2% PEGMA, (b,d) 6% PEGDA and 6% PEGMA. 20

Figure 2-15. (a) Protein with pI higher than 7.4 becomes positively charged, and thus expected to have a greater release rate in TMAC-PEG hydrogels via repulsion than Sulfo-PEG hydrogels. The release profiles of trypsin from (b) Sulfo-PEG hydrogels, (c) TMAC-PEG hydrogels and (d) Ph-PEG hydrogels. (e) The kinetic rate constants (*k*) and (f) exponents (*n*) were values obtained by fitting the curves with Eq. 2-1. (g) Diffusion coefficient (*D*) were obtained by fitting the curves with Eq. 2-2. The PEGDA and PEGMA concentrations of the hydrogels were 8% and 4%, respectively. 22

Figure 2-16. (a,b) Kinetic rate constants (*k*) and (c,d) diffusion coefficients (*D*) of trypsin release from Sulfo-PEG, TMAC-PEG and Ph-PEG hydrogels, obtained by fitting the release profiles with Eq. 2-1

and Eq. 2-2, respectively. (a) 10% PEGDA and 2% PEGMA, (b) 6% PEGDA and 6% PEGMA..... 23

Figure 3-1. A representative ^{1}H-NMR spectrum of PEGDA. The peak integration ratio between acrylic peaks (a, b, c) and hydroxyethyl peak (d) are listed. 27

Figure 3-2. Schematic representation of *in situ* crosslinkable PEGDA-PEI hydrogels prepared under physiological condition. The reaction parameters include the concentrations of PEGDA and PEI as well as M_W of PEGDA. 29

Figure 3-3. The viscosity of PEI at various concentrations, measured at room temperature (RT) or 37 °C. 29

Figure 3-4. (a) Photographic (top) and fluorescent microscopic (bottom) images of PEGDA-PEI hydrogels (scale bar: 100 μm). (A: 10 % PEGDA-5% PEI, B: 20 % PEGDA-5% PEI, C: 10 % PEGDA-3% PEI, D: 20 % PEGDA-3% PEI). (b) (Top) Photographs of PEGDA-PEI hydrogels conjugated with (E) or without (F) FITC after incubation in PBS. Greater swelling was observed for F due to accelerated degradation. (Bottom) After continuous swelling, F disintegrated while E remained intact. 30

Figure 3-5. Rheological properties of the reaction mixture of 10% PEGDA and 5% PEI, evaluated by the changes in storage (G') and loss (G'') moduli measured over time: (a) PEGDA400, (b) PEGDA700, (c) PEGDA1K, and (d) PEGDA2K. The arrows indicate the gel point. (e) The gelation times (t_{gel}) of 10% PEGDA or 20% PEGDA with 5% PEI. (f) t_{gel} values of 20% PEGDA700 with varying concentration of PEI. 31

Figure 3-6. Rheological properties of the reaction mixture of 10 % PEGDA and 5 % PEI, evaluated by the changes in storage (G') and loss (G'') moduli measured over time: (a) PEGDA3K and (b) PEGDA6K. 31

Figure 3-7. Rheological properties of the reaction mixture of 20 % PEGDA and 5 % PEI, evaluated by the changes in storage (G') and loss (G'') moduli measured over time: (a) PEGDA400, (b) PEGDA700, (c) PEGDA1K, (d) PEGDA2K, (e) PEGDA3K, and (f) PEGDA6K. The arrows indicate the gel point. 32

Figure 3-8. Rheological properties of the reaction mixture of 20 % PEGDA700 with (a) 3 % PEI, (b) 5 % PEI, and (c) 10 % PEI. The changes in storage (G') and loss (G'') moduli were measured over

time. The arrows indicate the gel point. 33

Figure 3-9. Elastic moduli (E) of PEGDA-PEI hydrogels: (a) 10% or 20% PEGDA with 5% PEI at varying M_W of PEGDA, (b,c) 10% PEGDA or 20% PEGDA with varying PEI concentration and M_W of PEGDA. (d) The ratio of the number densities of acrylate in PEGDA and amine in PEI ($\Phi_{Ac/Am}$) for varying M_W of PEGDA at different PEI concentrations. 34

Figure 3-10. Storage moduli (G') of PEGDA-PEI hydrogels, taken from the highest G' values after gelation from the rheological experiments. (a) 10% or 20% PEGDA with 5% PEI at varying M_W of PEGDA and (b) 20% PEGDA700 with varying PEI concentration. 36

Figure 3-11. (a) Degradation mechanism of PEGDA-PEI hydrogels; hydrolysis of ester bonds by increased local hydroxide ions and/or direct nucleophilic attack on ester bonds by unreacted amine groups. (b) The change in normalized elastic moduli (E/E_0) of 10% PEGDA-5% PEI hydrogels with varying M_W of PEGDA plotted over time. (c) The degradation rate constants (k_d) obtained by fitting (b) with Eq. 3-1. The k_d values for (d) 10% PEGDA and (e) 20% PEGDA linked with varying concentrations of PEI. 37

Figure 3-12. The change in normalized elastic moduli (E/E_0) of 20 % PEGDA-5 % PEI hydrogels with varying M_W of PEGDA plotted over time. The plots were fitted with Eq. 3-1 to obtain the degradation rate constants (k_d) which are shown in Figure 3-11. 38

Figure 3-13. (A) The drug release profiles of PEGDA-PEI hydrogels (10% PEGDA with 5% PEI). The profiles consisted of two separate modes of release occurring in sequence; initial swelling-controlled mechanism, followed by degradation-controlled mechanism. (b) The initial drug release profiles were fitted with Eq. 3-2 and (c) the kinetic rate constants (k_1) were obtained. (d) The latter drug release profiles were fitted with Eq. 3-3 and (e) the kinetic rate constants (k_2) were obtained.. 40

Figure 3-14. (a) The drug release profiles of PEGDA-PEI hydrogels (20 % PEGDA, 5 % PEI). The profiles consisted of two separate modes of release occurring in sequence; initial swelling-controlled mechanism, followed by degradation-controlled mechanism. (b) The initial drug release profiles were fitted with Eq. 3-2, and (c) the latter drug release profiles were fitted with Eq. 3-3. The k_1 and k_2 values obtained from (b) and (c) are shown in Figure 3-13 41

Figure 3-15. k_1 and k_2 values obtained from drug release profiles of PEGDA-PEI hydrogels. (a,b) 10% PEGDA and (c,d) 20% PEGDA linked with varying concentrations of PEI 42

Figure 3-16. The drug release profiles of PEGDA-PEI hydrogels. (a) 10 % PEGDA with 3 % PEI, (b) 10 % PEGDA with 10 % PEI, (c) 20 % PEGDA with 3% PEI, (d) 20 % PEGDA with 10% PEI..... 43

Figure 4-1. (a) PEG grafting of chitosan (PEG-*g*-Cs). mPEG was first oxidized to present aldehyde groups (mPEG-aldehyde), which was then reacted with chitosan via Schiff base formation. Sodium cyanoborohydride was used to irreversibly reduce the Schiff base into secondary amine. (b) Schematic representation of *in situ* forming PEG-*g*-Cs hydrogel, with PEG-dialdehyde (PEGDAld) as a crosslinker. (c) FT-IR spectra of PEG750-*g*-Cs (a: ν_s(C-H), b: ν_s(C-O-O)(anti) (carboxylic acid salt), c: ν_s(C-N), d: ν_s(C-O-C)(anti)). (d) DSC curves of PEG750(0.7)-*g*-Cs and PEG2K(0.7)-*g*-Cs. (e) The microbial inhibition rates of PEG750(1)-*g*-Cs and PEG750(1)-*g*-Cs. 46

Figure 4-2. Representative ^{1}H-NMR spectra of (a) N-carboxyethyl chitosan (NCE-Cs) and (b) PEG-*g*-Cs. Characteristic peaks corresponding to N-carboxyethyl and PEG are assigned. 54

Figure 4-3. FT-IR spectra of PEG2K-*g*-Cs. a: ν_s(C-H), b: ν_s(C-O-O)(anti) (carboxylic acid salt), c: ν_s(C-N), d: ν_s(C-O-C)(anti)..... 55

Figure 4-4. Representative DSC curves of (a) N-carboxyethyl chitosan (NCE-Cs) and (b) PEG-*g*-Cs. (c) T_m and ΔH of PEG chains obtained from the peaks corresponding to the melting of PEG chains on Cs..... 55

Figure 4-5. Anti-bacterial properties of (a) PEG750(1)-*g*-Cs and (b) PEG2K(1)-*g*-Cs at various concentrations by measuring the viability of *E. coli* over time. 56

Figure 4-6. Elastic moduli (E) and swelling ratios (Q) of Cs-PEG hydrogels. (a, c) PEG750-*g*-Cs, (b, d) PEG2K-*g*-Cs. PEG-*g*-Cs was crosslinked by 20 % PEGDAld with varying M_W. The PEG graft density and length, and the concentration of PEG-*g*-Cs were controlled. Possible physical interaction mechanisms between varying M_W of PEGDAld with (e) PEG750-*g*-Cs and (f) PEG2K-*g*-Cs. 58

Figure 4-7. Elastic moduli (E) of Cs-PEG hydrogels. (a) 5 % PEG750(0.7)-*g*-Cs and (b) PEG2K(0.7)-*g*-Cs crosslinked by PEGDAld with varying M_W and concentration. 60

Figure 4-8. (a) Elastic moduli (E) of Cs-PEG hydrogels made by crosslinking NCE-Cs with varying M_W of PEGDAld. (b) Possible mechanisms of PEGDAld interaction with PEG-*g*-Cs and NCE-Cs. 60

Figure 4-9. (a) Scanning electron microscopic visualization of pore networks of Cs-PEG hydrogels

(scale bar: 50 μm). (b-e) Cumulative amount of BSA release profiles from Cs-PEG hydrogels, and kinetic constants (*k*) and exponents (*n*) obtained by fitting the profiles with a mathematical model (Eq. 4-2); (b, c) PEG750(0.7)-*g*-Cs crosslinked with varying M_W of PEGDAld, (d, e) different types of PEG-*g*-Cs crosslinked with PEGDAld6K. 61

Figure 4-10. *E. coli* growth on various Cs-PEG hydrogel surfaces, visualized by staining with MTT, which turns live bacterial cells brown-purple. LB agarose hydrogel was used as a control. 63

Figure 4-11. Rheological characterization of PEG-*g*-Cs and PEGDAld during gelation by measuring storage (*G'*) and loss (*G"*): (a) PEG750(0.7)-*g*-Cs, (b) PEG2K(0.7)-*g*-Cs, (c) PEG750(1)-*g*-Cs, and (d) PEG2K(1)-*g*-Cs. In (c) and (d), PEGDAld6K was used. Gelation time for (e) PEG750-*g*-Cs and (f) PEG2K-*g*-Cs, determined by the time for *G'* and *G"* curves to cross (identified with arrows).... 64

Figure 4-12. (a) Schematic illustrations of (a) a lap shear test and (b) a burst pressure test. Adhesive strength (σ_{max}), adhesive energy (J_A), and burst pressure (*BP*) of CsPEG hydrogels: (c, d, e) PEG750(0.7)-*g*-Cs and PEG2K(0.7)-*g*-Cs crosslinked with varying M_W of PEGDAld, (f, g, h) PEG750(1)-*g*-Cs and PEG2K(1)-*g*-Cs crosslinked with PEGDAld6K. (*$p < 0.05$, $n = 12$)..... 65

Figure 4-13. (a) Cs-PEG hydrogel was applied to a rat skin wound model via syringe to close the wound gap. (b) OCT imaging was used to visualize the detailed skin tissue around the wound area. (c) After applying tissue sealants, the wound closure and subsequent healing process was monitored over time up to 5 days: (c-1) untreated, (c-2) suture, (c-3) Beriplast-P, (c-4) PEG750-*g*-Cs hydrogel, (c-5) PEG2K-*g*-Cs hydrogel, (c-6) PEG2K-*g*-Cs hydrogel encapsulated with EGF. The markers on OCT images identify the wound area. 67

Figure 4-14. The wound dimensions, width and depth, measured from the OCT images (marked with arrows in Figure 4-13) 68

Figure 4-15. Detailed schematics of Swept-Source Optical Coherence Tomography (SS-OCT) imaging apparatus to visualized skin tissue; C: Collimator, L: Lens, RM: Reference mirror, FC: Fiber coupler, CIR: Circulator, BPD: Balanced photo-detector, GS: Galvanometer scanner. 68

Figure 4-16. Histological evaluation of the skin wound tissues after tissue sealant treatment. The tissues harvested at day 3 and 5 were stained with hematoxylin & eosin (scale bar: 500 μm). E: epidermis, D: dermis, Sc: scab, arrows and highlighted area: fibrotic tissue. 69

Figure 5-1. ^{1}H-NMR spectra of PEG-diamine with varying molecular weights; 200, 600, 1000 (1K) g mol-1. Characteristic peaks of ethylene oxide repeating are noted (a-c). 73

Figure 5-2. The amount of amine in (a) PEG-diamine and (b) PHEA-PEGAm600 with varying DS_{Am} determined by TNBS assay (absorbance at 335 nm). 74

Figure 5-3. (a) Synthesis of poly(2-hydroxylethyl aspartamide)-*g*-amino-poly(ethylene glycol), termed PHEA–PEGAm, via ring-opening addition of polysuccinimide (PSI) with ethanolamine and PEG-diamine. (b) Synthesis of poly(ethylene glycol)(PEG) diamine via Mitsunobu reaction of PEG. (c) Schematic illustration of controlling the length and density of amine grafts of PHEA–PEGAm. 78

Figure 5-4. ^{1}H-NMR spectra of PHEA-PEGAm with varying DS_{Am}; (a) PHEA-PEGAm200, (b) PHEAPEGAm600 and (c) PHEA-PEGAm1K. Characteristic peaks corresponding to hydroxyl grafts (a, c), amine grafts (b, d) and PEG linkers (e) are noted. 79

Figure 5-5. Representative FT-IR spectra of PHEA-PEGAm with varying DS_{Am}. Characteristic peaks corresponding to amide vs(C=O) of hydroxyl grafts (a) and amine grafts (b) are noted. 80

Figure 5-6. Cytotoxicity of PHEA-PEGAm assessed by measuring the viability of cells exposed to various concentrations of PHEA-PEGAm. 80

Figure 5-7. Elastic moduli (E) of Alg-PHEA hydrogels controlled with DS_{Am} of PHEA, (a) PHEA-EtAm, (b) PHEA–PEGAm200, (c) PHEA–PEGAm600, and (d) PHEA–PEGAm1K. 81

Figure 5-8. Schematic illustration of possible mechanisms of cross-linking reactions: (a) PHEA-EtAm or PHEA–PEGAm200 with varying DS_{Am}; (b) PHEA–PEGAm with varying graft lengths..... 82

Figure 5-9. Gelation time (t_{gel}) of Alg-PHEA hydrogels controlled with concentration and DS_{Am} of PHEA, (a) PHEA-EtAm, (b) PHEA–PEGAm200, (c) PHEA–PEGAm600, and (d) PHEA–PEGAm1K. 84

Figure 5-10. Time-resolved fractional change in elastic moduli (E_t/E_0) and degradation rates (k_D) of Alg-PHEA hydrogels: (a, d) PHEA–PEGAm200, (b, e) PHEA–PEGAm600, and (c, f) PHEA–PEGAm1K. 85

Figure 5-11. Time-resolved fractional drug release profiles (M_t/M_∞) and release rate constants (k_R) of

Alg-PHEA hydrogels: (a, e) PHEA–PEGAm600 (DS4), (b, f) PHEA–PEGAm1K (DS4) with varying concentrations, (c, g) 15% PHEA–PEGAm600 with varying DS_{Am}, and (d, h) 15% PHEA–PEGAm (DS4) with varying graft lengths. Elastic modulus (E) and degradation rate constant (k_D) for each condition are noted. 86

Figure 5-12. Exponent (n) values obtained by fitting the time-resolved drug releases of Alg-PHEA hydrogels with Eq. 5-2 (Ritger-Peppas model): (a) PHEA-PEGAm600 (DS4), (b) PHEA-PEG1K (DS4) with varying concentrations, (c) 15 % PHEA-PEGAm600 with varying DS_{Am}, and (d) 15 % PHEAPEGAm (DS4) with varying graft lengths. 87

Figure 5-13. (a) Schematic representation of Alg-PHEA hydrogel injection into a tissue explant and subsequent degradation in neutral buffered solution. (b) Representative H&E histological images of Alg-PHEA hydrogel formed within tissue (left) and the same tissue area after hydrogel dissolution in 24 h (right; scale bar: 100 μm). (c) H&E histological images (top) and photographs (bottom) of various Alg-PHEA hydrogels within tissues after 4 h (scale bar: 100 μm). Boxed sections in photographs show embedded hydrogels. 88

Figure 5-14. (a) Elastic moduli and (b) SEM cross-sectional images of Alg-PHEA hydrogels further cross-linked with various concentrations of Ca^{2+} up to 5 M (scale bar: 30 μm). 89

Figure 5-15. (a) Photographs of Alg-PHEA (control) and Ca-Alg-PHEA hydrogel disks, with the initial diameter of 8 mm, taken at various times during incubation in aqueous buffered solution. The concentration of Ca^{2+} cross-linker was controlled up to 5 M. The diameter before complete dissolution are noted. (b, c) Time-resolved fractional change in elastic moduli (E_t/E_0) and degradation rates (k_D), and (d, e) time-resolved fractional drug release profiles (M_t/M_∞) and release kinetics (k_R) of Alg-PHEA and Ca-Alg-PHEA hydrogels (*$p < 0.05$). 90

Table 3-1. The number densities (mol mL^{-1}) of (a) acrylate in PEGDA and (b) amine in PEI at different concentrations. 35

Table 4-1. DS_{PEG} of various PEG-*g*-Cs 48

CHAPTER 1. Introduction

1.1 Research Background

Hydrogel for biomedical engineering

Hydrogel is a three-dimensional (3D) network consisting of a group of hydrophilic polymers which that hold large amounts of water and can be extensively swelled with water. Due to their unique properties such as porosity, elasticity, biocompatibility and hydrophilicity are very similar to living tissue, they widely investigated as promising material for biomedical engineering application. [1-3] Currently, they are used for carrier for various biological molecules, tissue engineering scaffold, contact lens and wound dressings.

Hydrogel networks are commonly formed through physical or chemical crosslinking of functional monomer. Physically cross-linked hydrogels possess temporary connections such as polymeric chain entanglement or physically induced gelation through hydrogen bonding, ionic interaction and hydrophobic interactions. These hydrogels are often called reversible gels, as they can be dissolved by changing environmental conditions (by pH, ionic strength, or temperature). Biomedical safety is a significant advantage of physical crosslinking, because the absence of chemical crosslinking agents can avoid the potential cytotoxicity of unreacted chemical crosslinkers. [4] These hydrogels can be obtained from poly(vinyl alcohol), poly(ethylene glycol), poly(Nisopropylacrylamide), poly(acrylic acid), poly(vinyl imidazole).

Chemically cross-linked hydrogels are obtained through covalent bonds between polymer chains, and most of linkages are stable in physiological conditions and irreversible compared to physical crosslinked hydrogel. [4] Moreover, they exhibit good mechanical properties and adjustable decomposition behavior. Up to now, several crosslinking methods have been reported, generally include free radical polymerization and *in situ* crosslinking reaction such as Schiff base formation and Michael addition.

Free radical polymerization is commonly used to form hydrogel. Because, it is highly reactive and tolerates variety of functional groups. Also, it occurs in mild conditions, even in aqueous solution and room temperature. Polymerization is usually initiated by free radical generating compound, radiation or heating. However, these activations and residual initiator often damage the cells and tissue.

In situ crosslinked hydrogel can be prepared spontaneously without the use of initiator or harmful activation through chemical reactions between complementary functional groups. These reactions have advantages such as high yields under mild condition, low by-products, high specificity and selectivity.

The Michael reaction typically refers to the addition of a nucleophile (Michael donors) to an activated α,β-unsaturated carbonyl-containing compound (Michael acceptors). [5, 6] This reaction benefits from

mild reaction conditions, various compatible reagents, high conversions, and the absence of side-products or toxic metal catalysts. Accordingly, this reaction is well-suited for gene transfection, cellular scaffold and tissue replacement and widely exploited for the preparation of injectable hydrogels for biomedical applications.

A Schiff base is usually formed by condensation of an aldehyde or ketone with a primary amine such as HA, chitosan, and dextran under physiological conditions. In general, depending on the ratio of amine to aldehyde groups, their gelation time and physical properties can be varied. It can be easily applied to construction of an injectable hydrogel due to aldehyde groups can react with other amine groups in tissue or organs. The dynamic equilibrium between Schiff base bonds and aldehyde and amine reactants provides advantages for Schiff base formation and provides self-healing capabilities of the hydrogel network through reversible reactions such as uncoupling and recoupling of imine bonds.

1.2 Research Purpose and Motivation

Currently, hydrogels are applied in many important biomedical applications such as therapeutic delivery, contact lenses, corneal prosthetics, bone cement, wound dressing, 3D tissue scaffolds for tissue engineering, and more. However, their properties, such as low mechanical strength, antimicrobial, biological interactions, water sorption and diffusion, degradation and others, are often hindered to use in biomedical application. Moreover, it is difficult to control properties effectively because of their interdependent properties as well as their fabrication mechanisms which cause toxicity. Therefore, it is important to control these properties at various levels while maintaining their unique properties to meet the specific requirements.

Herein, we have developed advanced hydrogels with controllable physicochemical properties, as multifunctional systems, which are expected to exhibit superior properties to increase the potential uses of these materials in the biomedical industry.

CHAPTER 2. Modulation of functional pendant chains within poly(ethylene glycol) hydrogels for refined control of protein release

2.1 Introduction

Hydrogels are a popular class of carriers for various biological molecules, such as proteins and DNA, as well as cells and tissues for biomedical applications. [7-10] Highly favorable physical properties of hydrogels prepared using biocompatible polymers, such as elasticity and hydrophilicity, help provide the encapsulated entities with optimal mechanical and aqueous environment and protection for prolonged life-time. In addition, the fabrication methods are generally mild enough to allow for safe encapsulation with high efficiency. The cellular activities within the hydrogels could be further promoted by modifying the polymer network with cell-responsive moieties. [11, 12]

For controlled release applications, the release rates of encapsulated biomolecules from hydrogels are often controlled in an efficient manner by simply varying the crosslinking density of the polymeric network, which in effect controls the porosity of the hydrogel. [13-15] However, this approach is also often encountered with a few critical drawbacks. First, the crosslinking density, according to the rubber elasticity theory, also affects the mechanical properties of the hydrogels, in which the mechanical and diffusional properties are inversely correlated. [16, 17] Thus, this interdependency could lead to an inadvertent change in mechanical properties while attempting to control the release rates via crosslinking density; hydrogels may become structurally too weak at lower crosslinking density to increase the release rate, or they may become too brittle at higher crosslinking density. Furthermore, the release may be severely hindered for the hydrogel having significantly reduced pores, which is especially critical for the release of larger macromolecules such as large proteins and DNA. [14, 18] To overcome these issues, it would be ideal to control the release rates of encapsulated species in a wide range while minimally affecting the crosslinking density of the hydrogels.

In this study, protein release rates from hydrogels were controlled by varying the physical properties of the hydrogels while maintaining their crosslinking density. Poly(ethylene glycol) dimethacrylate (PEGDA) hydrogels presenting pendant chains with end functional groups with varying physical properties (i.e. charge density and hydrophobicity) were fabricated by radical copolymerization with heterobifunctional PEG monomethacrylate (PEGMA) (Figure 2-5a). There have been previously published reports of engineering charged or hydrophobic hydrogels, but their approaches generally involved utilizing the monomers or macromers with charged or hydrophobic functional domains (e.g. acrylate, vinyl sulfonate, [2-(methacryloxy)ethyl] trimethylammonium chloride), poloxamers, and

heparin), and thus maintaining their crosslinking densities were not factored. [19-25] However, in this study, by changing the number of "functional" pendant chains while keeping the total number of pendant chains constant, the crosslinking density of the PEG hydrogels could be controlled, thereby minimally affecting the mechanical properties, while varying the physical properties of the hydrogels. With PEG pendant chains with charged functional groups, (e.g. negatively charged sulfonate and positively charged trimethylammonium chloride), the release of proteins having different charge densities at physiological pH due to different isoelectric points (pI) could be controlled via electrostatic interaction. Three model proteins, namely albumin, insulin and trypsin, having different pI values, were used. Their release rates from the PEG hydrogels with varying number of charged pendant chains were measured. Furthermore, since proteins have varying degrees of hydrophobicity based on amino acid compositions, the release from PEG hydrogels with hydrophobic phenyl pendant chains was also explored.

2.2 Materials and Methods

2.2.1 Synthesis of Poly(ethylene glycol) dimethacrylate (PEGDA)

PEGDA was synthesized following a previously published method. [26] Briefly, poly(ethylene glycol) (PEG, average M_W of 2,000 g mol^{-1}, Sigma Aldrich) and triethylamine (Sigma Aldrich) were first dissolved in dichloromethane. Methacryloyl chloride (Sigma Aldrich) was added dropwise to the mixture, and continuously stirred for 24 hours under dry N_2 gas. The molar ratio of PEG, methacryloyl chloride and triethylamine was 1:4:5. The insoluble salt formed during the reaction was filtered out, and excess diethyl ether was added to the mixture to precipitate the product. The product was obtained by filtration, washed twice with diethyl ether, and dried under vacuum.

2.2.2 Synthesis of heterobifunctional poly(ethylene glycol) monomethacrylate (PEGMA)

Heterobifunctional PEGMA having a functional end group was developed by two-step synthesis: (1) the ring-opening anionic polymerization of ethylene oxide to synthesize heterobifunctional PEG, followed by (2) the conjugation of methacrylate onto the hydroxyl group on the PEG (Figure 2-5b). [26-28]

Potassium naphthalenide, a strong base that activates the hydroxyl-based initiator to alkoxide, was prepared by dissolving molar equivalents of potassium and naphthalene (9 mmol each) in 20 mL of dry tetrahydrofuran (THF, Samchun Chemical, Korea) for 5 hours. The mixture became dark green with the formation of potassium naphthalenide. Hydroxyl-based initiator (11 mmol) was dissolved separately in 30 mL of dry THF, and the potassium naphthalenide mixture was slowly added and stirred for one hour, resulting in the alkoxide formation. 30 mL of ethylene oxide (EO, Asia Chemical, Korea)

was then added to the mixture and continuously stirred for 48 hours at room temperature (note: the mixture and EO was chilled on ice to prevent evaporation during the mixing process). The entire process was done under dry N_2 gas.

HCl (10 mmol) was added to stop and neutralize the reaction, from which the insoluble salt (KCl) being formed was filtered out. After condensing the mixture via rotary evaporation, the crude product was obtained by precipitation in excess diethyl ether. After washing with diethyl ether twice, the final product was obtained by filtration and drying under vacuum. The initiators used for synthesizing sodium sulfoethyl, trimethylammonium chloride, and phenyl-capped PEG, namely Sulfo-PEG, TMAC-PEG, and Ph-PEG, were sodium isethionate, choline chloride, and 2-phenylethanol (all purchased from Sigma Aldrich), respectively. The molecular weights (M_W) of Sulfo-PEG, TMAC-PEG, and Ph-PEG, as determined from MALDI-TOF mass spectrometry (Ultraflex III, Bruker), were 2341, 2200, and 1770 g mol^{-1}, respectively (Figure 2-1). For Sulfo-PEG and TMAC-PEG, tetrahydrofuran and 2,5-dihydroxybenzoid acid (Sigma Aldrich) were used as solvent and matrix, respectively, while chloroform and dithranol (Sigma Aldrich) were used for Ph-PEG.

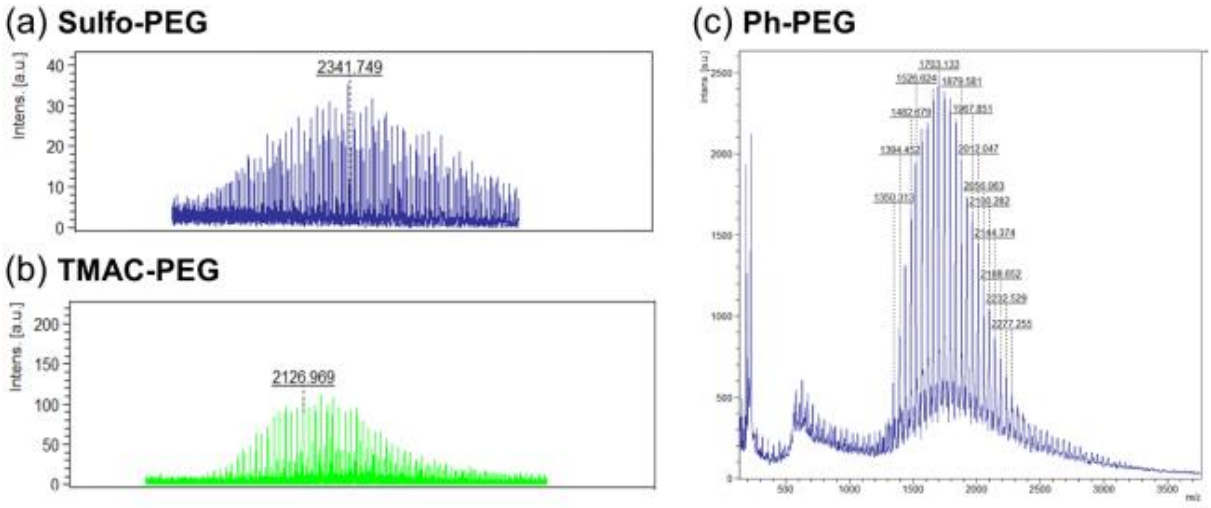

Figure 2-1. The molecular weight distributions of (a) Sulfo-PEG, (b) TMAC-PEG, and (c) Ph-PEG, determined from MALDI-TOF mass spectrometry.

The conjugation of methacrylate was done using the same procedure for the synthesis of PEGDA. The molar ratio of heterobifunctional PEG, methacryloyl chloride and TEA here was 1:2:3, as there is only one hydroxyl group in a polymer chain.

The chemical structures of the heterobifunctional PEGMAs were analyzed with ^{1}H-NMR and ^{13}C-NMR spectra (400-MR DD2, Agilent) (Figure 2-2 and Figure 2-3). The M_W of Sulfo-PEGMA, TMAC-PEGMA and Ph-PEGMA, determined by the ratio of integration peaks corresponding to methacrylate and ethylene oxide unit, were 3370, 3211, and 4120 g mol^{-1}, respectively. The zeta potentials of sulfonate and trimethylammonium chloride linked PEG were determined at 0.1 wt% in 10 mM NaCl, pH 7 (Nano ZS, Malvern) (Figure 2-4).

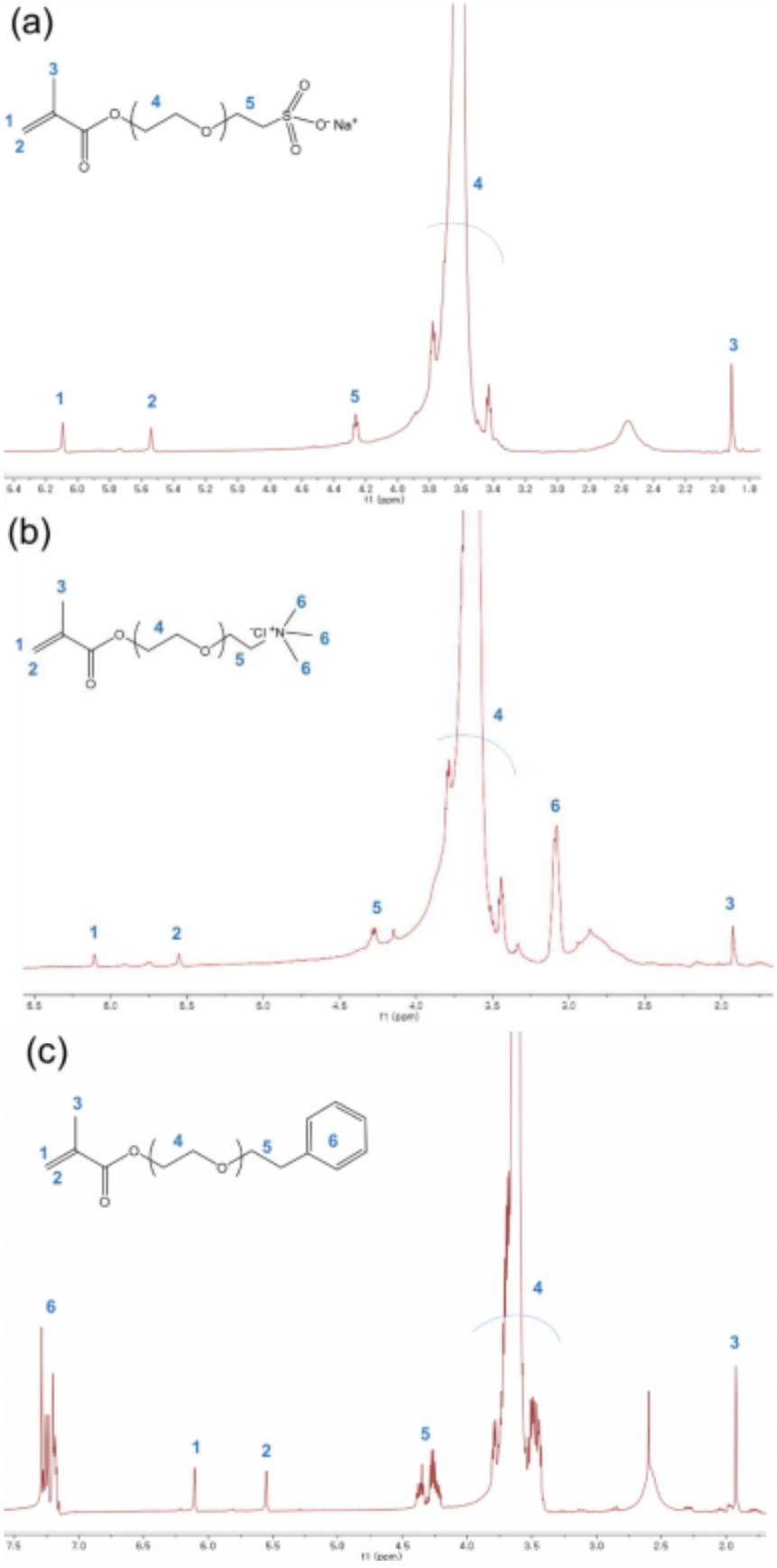

Figure 2-2. ^{1}H-NMR spectra of (a) Sulfo-PEG, (b) TMAC-PEG, and (c) Ph-PEG.

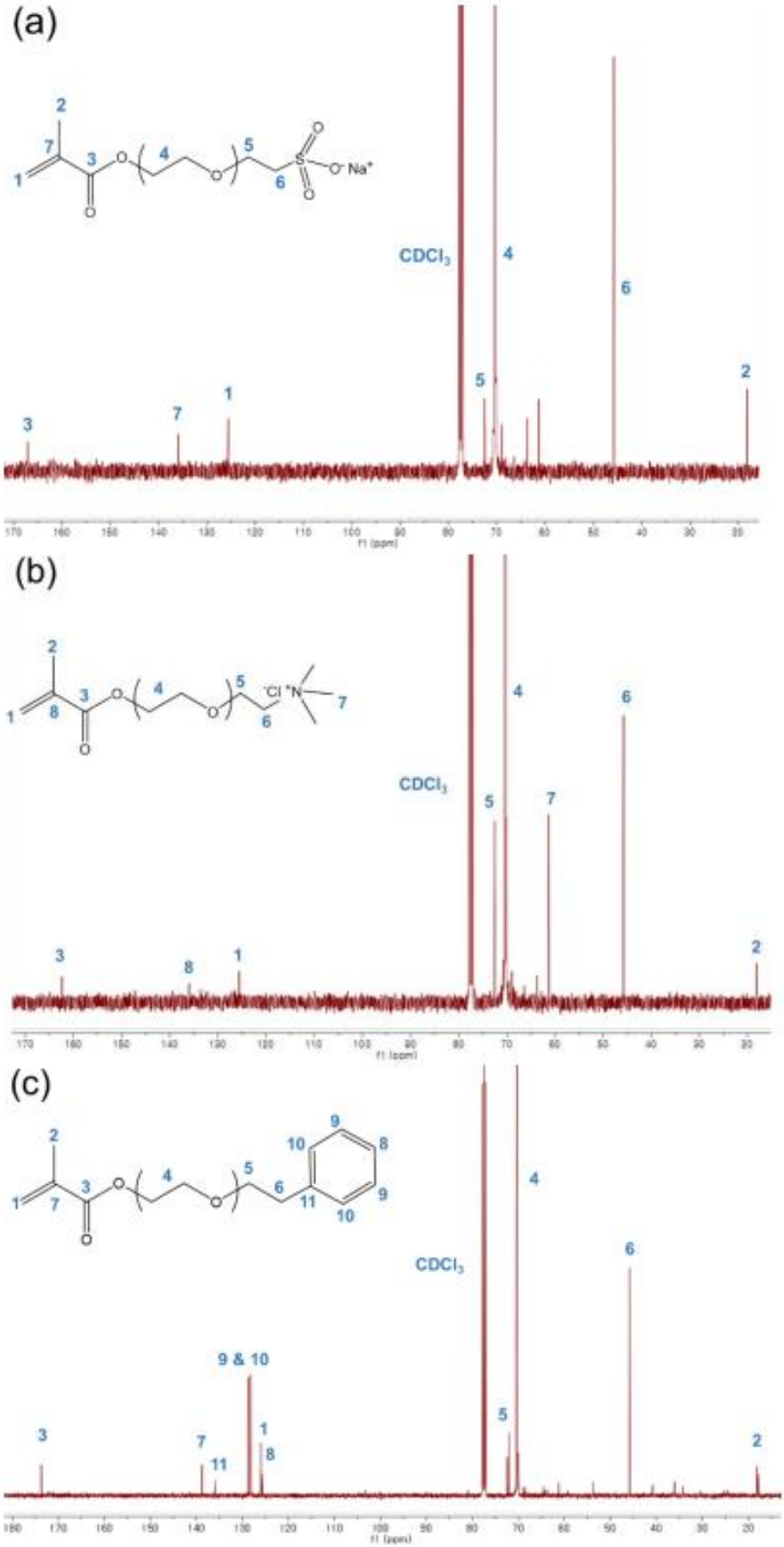

Figure 2-3. ^{13}C-NMR spectra of (a) Sulfo-PEG, (b) TMAC-PEG, and (c) Ph-PEG.

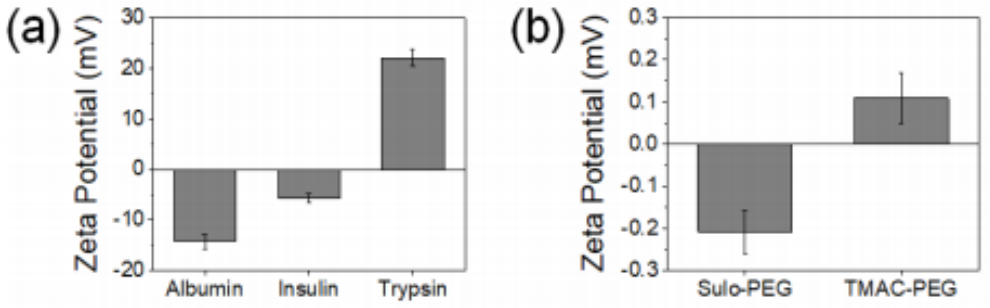

Figure 2-4. Zeta potential values of (a) proteins (albumin, insulin, and trypsin) and (b) SulfoPEGMA and TMAC-PEGMA, measured at 0.1 % (w/v) in 10 mM NaCl.

2.2.3 Fabrication of hydrogels

A precursor solution was prepared by mixing PEGDA and PEGMA in various ratios, while keeping the overall concentration at 12% (w/v). The total PEGMA content consisted of 'non-functional' methoxy PEGMA (M_n 2000 g mol^{-1}, Sigma Aldrich) and the heterobifunctional PEGMA. At a given PEGMA concentration, the fraction of heterobifunctional PEGMA was varied to control the physical properties of the pendant PEG chains. 10 μL of ammonium persulfate (1 M) and 1 μL of tetramethylethylenediamine as co-initiators were added to 1 mL of a precursor solution, and placed in a custom-made mold with 1 mm spacer to prepare disk-shaped hydrogels with a diameter of 8 mm. The hydrogel disks were incubated in phosphate buffered saline (PBS) at room temperature for 24 hours before mechanical characterization.

2.2.4 Evaluation of mechanical properties of hydrogels

The mechanical properties of hydrogels were evaluated by calculating elastic moduli from stress-strain curves obtained from uniaxial compression experiments (Model 3343, Instron). [29-31] Each hydrogel disk was compressed at a rate of 1 mm min^{-1}. The elastic modulus was calculated from the slope of a stress-strain curve at the initial 10% strain region where the curve was linear.

2.2.5 Evaluation of protein release from hydrogels

The effect of physical properties of hydrogels on drug release kinetics was evaluated by measuring time-dependent release profiles of proteins with varying pI values. Albumin (from human serum, Sigma Aldrich), trypsin (from bovine pancreas, Sigma Aldrich) and insulin (human recombinant, Sigma Aldrich) having pI values of 4.7, 5.3, and 10.5, respectively, were used as model proteins. Their zeta potentials were measured at −14.2 mV, −5.7 mV, and 22.1 mV, respectively (0.1 wt% in 10 mM NaCl, pH 7) (Figure 2-4). The protein was first encapsulated into the hydrogel by dissolving the protein (2 mg mL^{-1}) in a precursor solution prior to fabrication. The hydrogel disks were prepared as mentioned

above. The hydrogel disks were incubated in PBS at 37 °C, and at each designated time point, the incubating media were collected and the protein concentrations were obtained using BCA™ Protein Assay kit (Thermo Fisher), following the manufacturer's instructions. The cumulative protein release profiles were fitted to the Ritger-Peppas equation,

$$\frac{M_t}{M_\infty} = k \cdot t^n \qquad \text{Eq. 2-1}$$

where M_t was the cumulative amount of protein released at a time, t, M_∞ was the total amount of protein in the hydrogel, k was the kinetic rate constant, and n is the exponent related to the release mechanism. [26, 30, 32]

Alternatively, the cumulative protein release profiles were fitted to the following power-law equation following Fickian diffusion mechanism,

$$\frac{M_t}{M_\infty} = 4\left(\frac{Dt}{\pi h^2}\right)^{1/2} \qquad \text{Eq. 2-2}$$

where D was the diffusion coefficient and h was the thickness of the hydrogel disk samples. [33-35] This relationship generally fits well for the first 60% of the release due to the fixed time dependency ($t^{1/2}$).

2.3 Results and Discussion

2.3.1 Synthesis of heterobifunctional PEGMA

PEG hydrogels have long been used as drug delivery systems due to biocompatibility, abundant source, bioinertness, and efficient processing. [12, 36] In particular, PEG with vinyl end groups, such as PEGDA, are widely used to develop hydrogels via radical polymerization either by itself or hybridizing with other vinyl-based polymers. The drug release rates from PEG hydrogels can be accomplished by controlling the crosslinking density which in turn controls the porosity of the polymeric network. [13, 14, 37] The physical properties of the PEG hydrogels can be further varied by introducing different moieties into the PEG network; copolymerization with other polymers or hybridizing with nanostructures (i.e. nanocomposite hydrogels). [38, 39] However, these strategies are often accompanied by unwanted changes in mechanical and swelling properties of the hydrogels, which may complicate the control of drug release.

Here, PEG hydrogels presented with varying number of pendant PEG chains with functional end groups were developed by copolymerizing PEGDA with heterobifunctional PEG monomethacrylate (PEGMA) to control the physical properties (e.g. charge density and hydrophobicity) while maintaining the crosslinking density (Figure 2-5a). By keeping the number of pendant chains, it would prevent unwanted change in mechanical and swelling properties that could also influence the release of

encapsulated drugs.

Three different types of heterobifunctional PEGMA was synthesized; sodium sulfoethyl PEGMA (Sulfo-PEGMA), trimethylammonium chloride PEGMA (TMAC-PEGMA), and phenyl PEGMA (Ph-PEGMA) in order to impart negative charge, positive charge and hydrophobicity, respectively (Figure 2-5b). The ring-opening polymerization of epoxide with the anionic initiator having the desired functional group was employed to synthesize the heterobifunctional PEG, which was followed by the conjugation of methacrylate via nucleophilic substitution of the hydroxyl group of PEG using methacryloyl chloride. The chemical compositions of various heterobifunctional PEGMA were confirmed with ^{1}H-NMR and ^{13}C-NMR (Figure 2-2 and Figure 2-3). The zeta potentials of Sulfo-PEGMA and TMAC-PEGMA were also determined to be −0.208 mV and 0.11 mV (0.1 wt% in 10 mM NaCl), respectively, which further confirmed the difference in the type and density of charges (Figure 2-1).

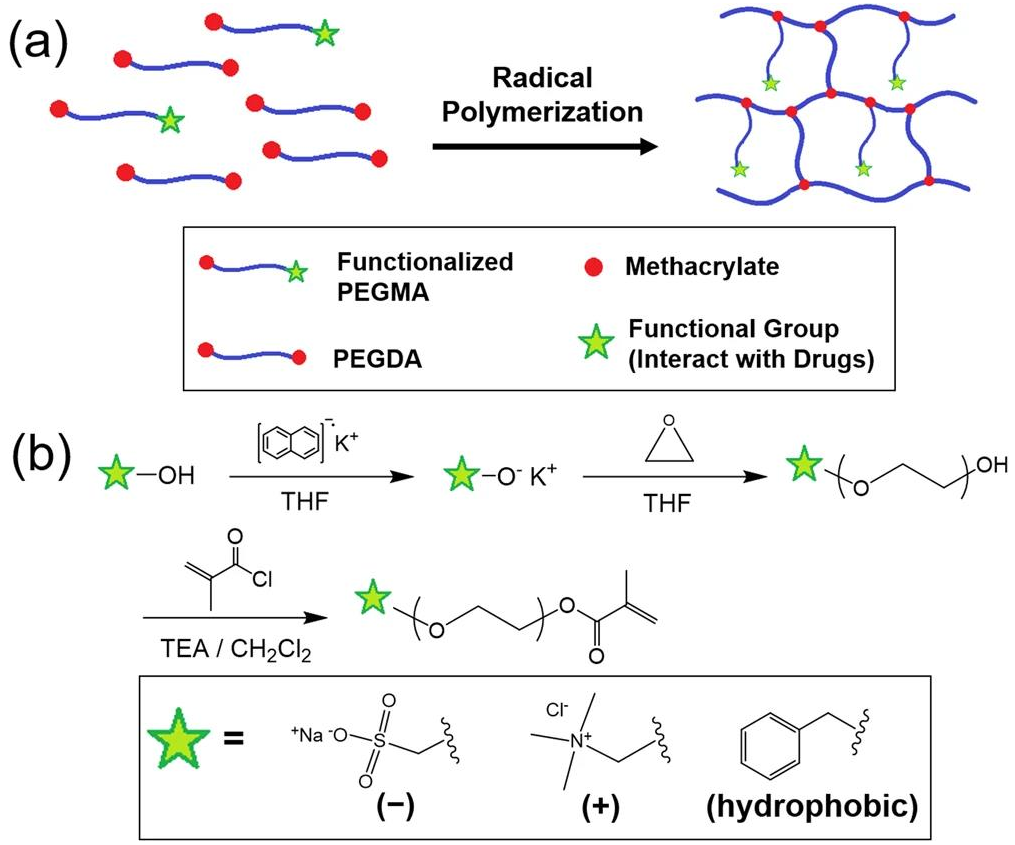

Figure 2-5. (a) Fabrication of PEG hydrogels with functional pendant chains via radical copolymerization of PEGDA with heterobifunctional PEGMA. (b) Synthesis of heterobifunctional PEGMA via anionic polymerization of epoxide with an initiator containing the desired functional group, followed by the conjugation of methacrylate. The functional groups used in this study were sulfonate (negative charge), trimethylammonium chloride (positive charge) and phenyl (hydrophobicity) groups.

2.3.2 Mechanical properties of PEG hydrogel with functional pendant chains

In order to control the physical properties of PEG hydrogels while minimizing the difference in crosslinking density among different pendant chains, the total number of pendant chains were kept constant while varying the fraction of functional pendant chains (Φ) (Figure 2-6a). This was accomplished by varying the ratio of heterobifunctional PEGMA with methoxy PEGMA as a non-functional control, while keeping the total concentration of PEGMA in a precursor solution (e.g. Φ = 0 when all the pendant chains are non-functional, Φ = 1 when all the pendant chains are functional).

The rigidity of the PEG hydrogels with varying Φ was measured to assess the effect of functional pendant chains. The concentrations of PEGDA and PEGMA were first kept at 10% and 2% (w/v) respectively. Increasing Φ did not result in a significant change in elastic moduli of the hydrogels, and the moduli at a given Φ were similar for all types of pendant chains (Figure 2-6b, Figure 2-7). This result demonstrated that the crosslinking density of hydrogels at varying Φ was not significantly affected for all types of pendant chains at the given PEGDA and PEGMA concentrations.

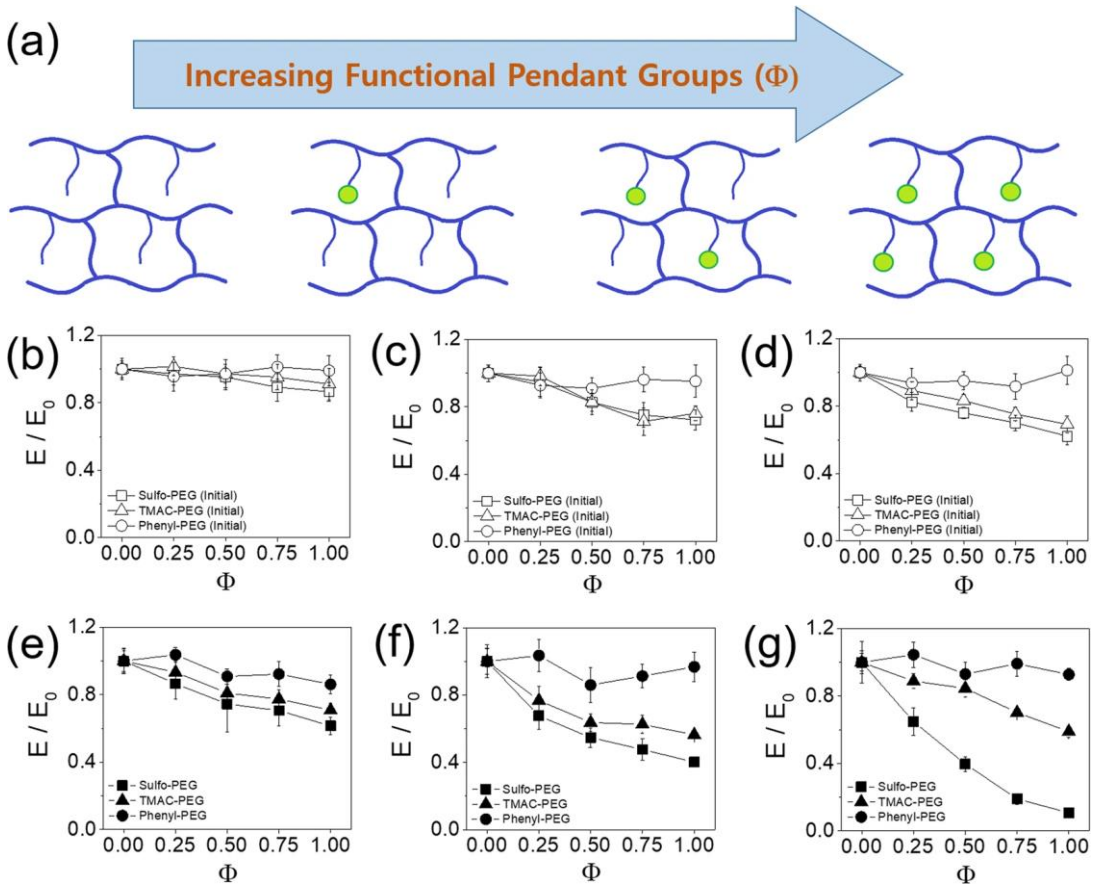

Figure 2-6. (a) The fraction of functional pendant chains (Φ) was varied while keeping the total number of pendant chains constant. Normalized elastic moduli (E/E_0) of PEG hydrogels with varying Φ, measured (b,c,d) right after fabrication and (e,f,g) after incubation in PBS for 24 hours. The moduli were normalized with that at Φ = 0 (E_0). (b,e) 10% PEGDA and 2% PEGMA, (c,f) 8% PEGDA and 4% PEGMA, (d,g) 6% PEGDA and 6% PEGMA.

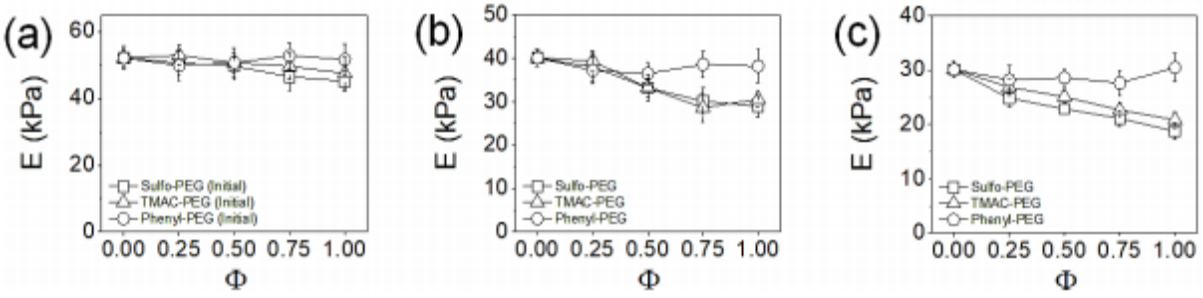

Figure 2-7. Elastic moduli (E) of Sulfo-PEG, TMAC-PEG, and Ph-PEG hydrogels measured right after fabrication ('initial moduli'). The PEGDA and PEGMA concentrations of the hydrogels were (a) 10% and 2%, (b) 8% and 4%, and (c) 6% and 6%.

The relative concentrations of PEGDA and PEGMA were varied to further evaluate the possible change in crosslinking density by varying Φ; the PEGMA concentration was increased to 4% and 6% (w/v) while decreasing PEGDA concentration to 8% and 6% (w/v), thus keeping the total polymer concentration at 12% (w/v). Since the PEGDA molecules are mainly responsible for the crosslinking of the polymeric network, the overall elastic moduli became smaller at higher PEGMA concentrations (Figure 2-7). There was a small decrease in moduli above $\Phi = 0.5$ for Sulfo-PEG and TMAC-PEG hydrogels, and the decrease became larger at higher PEGMA concentration (e.g. 15% and 25% decreases at $\Phi = 1$ for 4% and 6% PEGMA, respectively) (Figure 2-6c and d, Figure 2-8). This result may have been due to the increased charge density pushing the polymer chains further apart via repulsion, leading to a diminished degree of crosslinking. It is further corroborated by the lack of change in moduli of uncharged Ph-PEG hydrogels regardless of Φ and PEGMA concentration. Scanning electron microscopic (SEM) images of the hydrogels with 2% and 4% PEGMA also showed that the porosity, which generally correlates with the crosslinking density, was not significantly affected by the type of pendant chains at a given Φ (Figure 2-9). [29, 40] Taken together, except at the higher Φ of Sulfo-PEG and TMAC-PEG hydrogels with lower crosslinking density (i.e. higher PEGMA concentration), the mechanical properties of the hydrogels were generally well maintained at varying Φ. Even in those conditions, the crosslinking densities of Sulfo-PEG and TMAC-PEG hydrogels at a given Φ were similar, and thus the protein release from the two hydrogel systems could be analyzed based only on the difference in charge density.

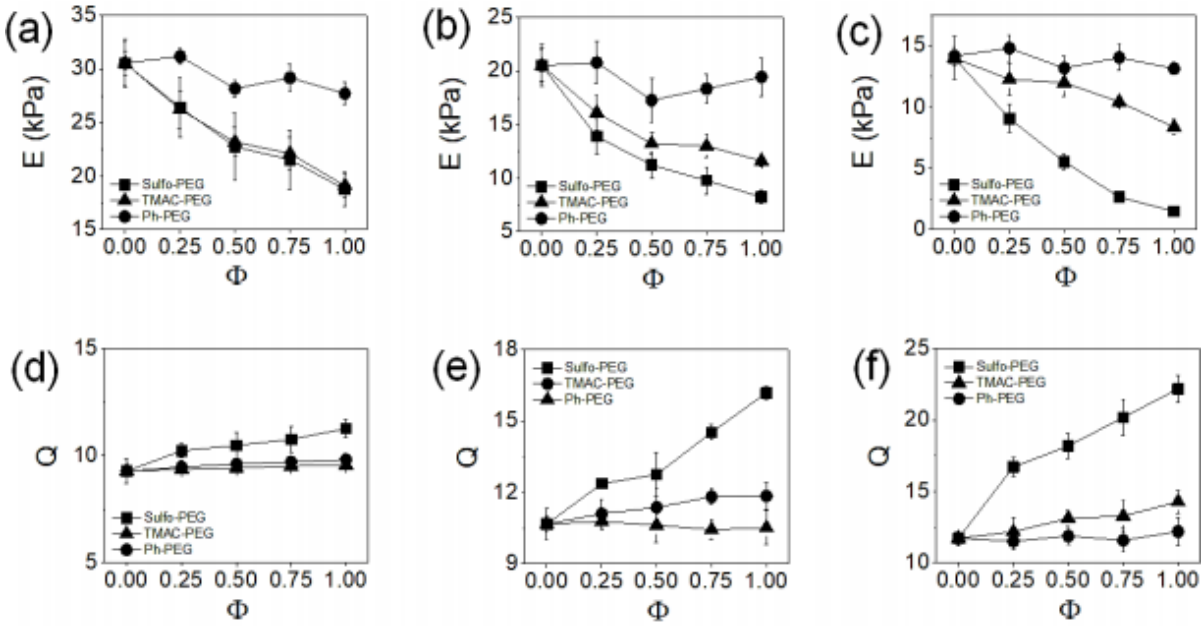

Figure 2-8. (a-c) Elastic moduli (E) and (d-e) swelling ratios (Q) of Sulfo-PEG, TMAC-PEG, and Ph-PEG hydrogels. The PEGDA and PEGMA concentrations of the hydrogels were (a,d) 10% and 2%, (b,e) 8% and 4%, and (c,f) 6% and 6%. E and Q were measured after 1 day of incubation in PBS.

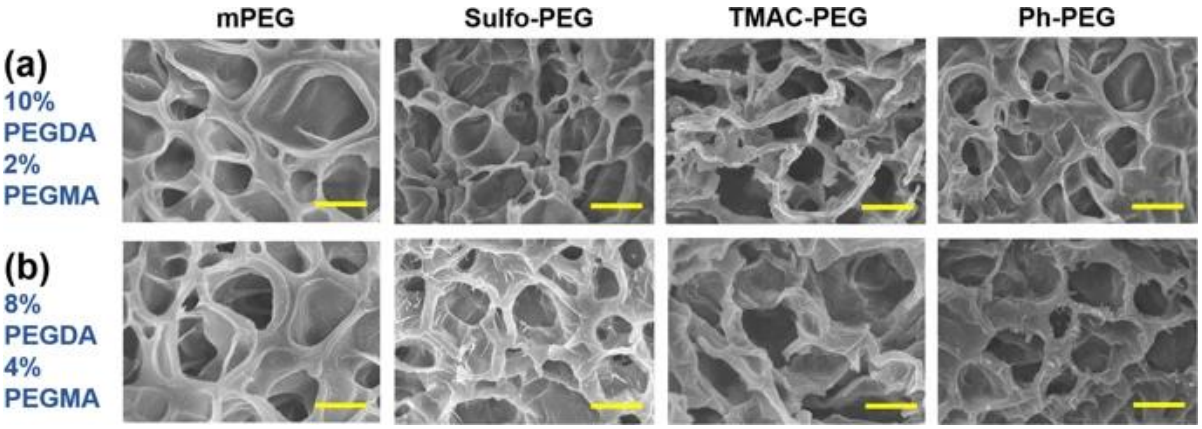

Figure 2-9. Scanning electron microscopic (SEM) images of non-functional mPEG hydrogel, Sulfo-PEG hydrogel, TMAC-PEG hydrogel, and Ph-PEG hydrogel at $\Phi = 1$ (scale bar: 5 μm). (a) 10% PEGDA and 2% PEGMA, (b) 8% PEGDA and 4% PEGMA.

Next, the moduli of the hydrogels were measured after incubation in PBS in order to evaluate the effect of swelling into hydrogels controlled by different charge densities (Figure 2-6e-g). It was hypothesized that the decrease in moduli by the swelling would be varied by the type and density of charge within the hydrogels. The moduli of Ph-PEG hydrogels were not affected by Φ, as expected, regardless of the concentrations of PEGDA and PEGMA, due to the lack of charge. However, the decrease in moduli of Sulfo-PEG hydrogels by Φ became more prominent with decreasing PEGDA (increasing PEGMA), especially more so than TMAC-PEG hydrogels. For example, the moduli of

Sulfo-PEG hydrogels decreased with Φ by 60% and 85% for hydrogels with 8% PEGDA and 4% PEGMA and 6% PEGDA and 6% PEGMA, respectively. On the other hand, the moduli of TMAC-PEG hydrogels decreased with Φ only by 40% and 50% for hydrogels with 8% PEGDA and 4% PEGMA and 6% PEGDA and 6% PEGMA, respectively. These results indicated that (1) the increased charge density within the Sulfo-PEG hydrogels and TMAC-PEG hydrogels with increasing Φ likely pushed the polymer chains further apart via repulsion during swelling and resulted in greater chain relaxation, and (2) the larger decrease in moduli for Sulfo-PEG hydrogels compared to TMAC-hydrogels is likely due to the greater charge density of the Sulfo group compared to TMAC groups, as evidenced by their zeta potentials. [41, 42]

The trends of swelling ratios of PEG hydrogels with functional pendant chains were in conjunction with those of elastic moduli shown in Figure 2-6, as expected, since the degree of swelling and rigidity are inversely related according to the rubber elasticity theory (Figure 2-10). Interestingly, the swelling ratios of TMAC-PEG hydrogels were not significantly affected by Φ especially compared to the decrease in moduli. It is likely a result of smaller ionic strength and increased local hydrophobicity by the methyl groups in TMAC, preventing further swelling behavior. This is further highlighted in comparison with the Sulfo-PEG hydrogels, which do not have hydrophobic groups and have greater ionic strength than TMAC, showing much greater increase in swelling ratios with Φ.

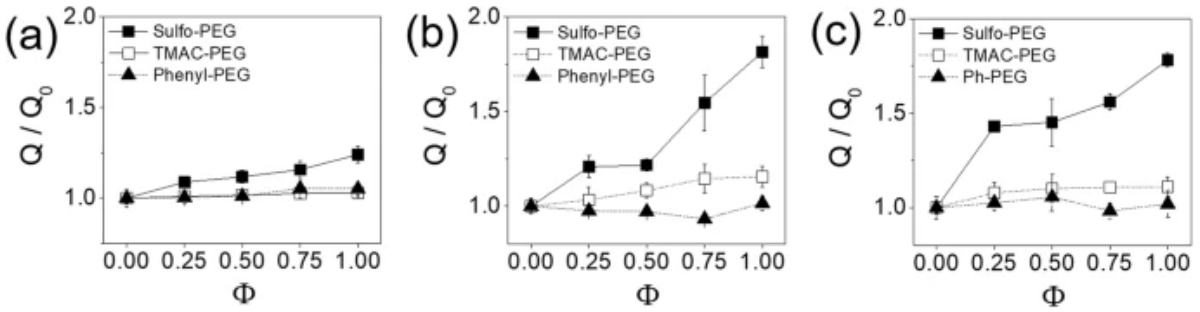

Figure 2-10. Normalized swelling ratios (Q/Q_0) of PEG hydrogels with varying Φ. The swelling ratios were normalized with that at $\Phi = 0$ (Q_0). (a) 10% PEGDA and 2% PEGMA, (b) 8% PEGDA and 4% PEGMA, (c) 6% PEGDA and 6% PEGMA.

2.3.3 Protein release from PEG hydrogel with functional pendant chains

Three proteins having different isoelectric points (pI), albumin, insulin, and trypsin, were used as model protein drugs, and their release profiles from the PEG hydrogels with varying Φ were measured. Albumin and insulin have the pI values of 4.9 and 5.3, so they are expected to be negatively charged at the physiological pH of 7.4. The pI of trypsin, on the other hand, is 10.5, thus it would be positively charged at the physiological pH. By comparing their release profiles, the effect of charge type and density in the hydrogels could be evaluated. Furthermore, between albumin and insulin, their molecular weights are 66 kDa and 5.8 kDa, respectively, so the effect of the size of the protein on the release could

also be determined. The protein release profiles with respect to time was then fitted with either (1) the Ritger-Peppas model in order to obtain the kinetic rate constants (k) and exponents (n) (Eq. 2-1), or the Fickian diffusion model to obtain diffusion coefficients (D) (Eq. 2-2), in order to analyze the drug release kinetics. Compared to the traditional Fickian diffusion model which is based on a fixed square root dependence on time, the Ritger-Peppas model allows the determination of both kinetic rate constant and power-law dependence on time. [43] The exponents indicate the release mechanism which depends heavily on the permeability and physical characteristics (e.g. chain relaxation) of the drug carriers. For hydrogels which undergo significant swelling due to the osmotic pressure from the surrounding medium as well as the chain relaxation of the polymeric network, the Fickian diffusion model is often limited when describing the overall release profiles (i.e. this model is more accurate at the initial protein release in which the release is mostly governed by the diffusion, whereas the release by chain relaxation deviates from the square root time dependence).

Albumin. Albumin is the most abundant type of protein commonly found in the plasma of most mammalian species, responsible for the transport of various molecules and maintaining the oncotic pressure. [44] It is negatively charged at physiological pH due to its lower pI value of 4.9. Therefore, the albumin encapsulated in Sulfo-PEG hydrogel was expected to have higher release rates than that of TMAC-PEG hydrogels due to electrostatic repulsion (Figure 2-11a). The albumin release profiles from Sulfo-PEG hydrogels and TMAC-PEG hydrogels were measured (Figure 2-11b and c), and the kinetic rate constants (k) were obtained via Ritger-Peppas model (Figure 2-11e). The concentrations of PEGDA and PEGMA were first kept at 8% and 4%, respectively. As expected, the k values of Sulfo-PEG hydrogels increased with Φ, and were significantly larger than those of TMAC-PEG hydrogels at all Φ, demonstrating that the increased negative charge by Sulfo-PEG facilitated the release of albumin (Figure 2-11e). Although the k values in TMAC-PEG hydrogels were lower than those of Sulfo-PEG hydrogels, increasing Φ did not result in the decrease of k values via electrostatic attraction as expected, likely due to the lower charge density of TMAC-PEG compared to Sulfo-PEG (i.e. TMAC-PEG has the lower absolute value of zeta potential than Sulfo-PEG).

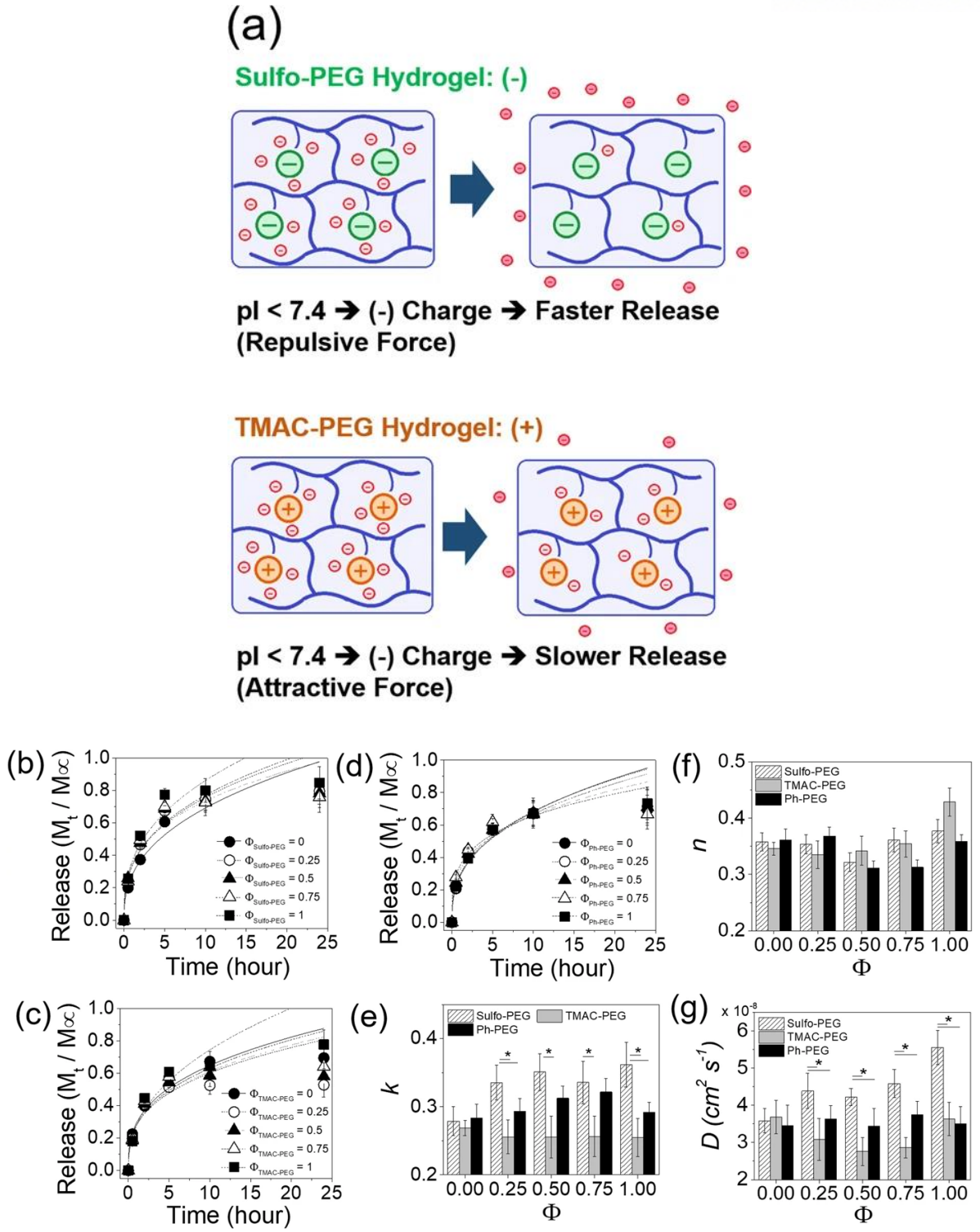

Figure 2-11. (a) Protein with pI lower than 7.4 becomes negatively charged, and thus expected to have a greater release rate in Sulfo-PEG hydrogels via repulsion than TMAC-PEG hydrogels. The release profiles of albumin from (b) Sulfo-PEG hydrogels, (c) TMAC-PEG hydrogels and (d) Ph-PEG hydrogels. (e) The kinetic rate constants (k) and (f) exponents (n) were obtained by fitting the curves with Eq. 2-1. (g) Diffusion coefficients (D) were obtained by fitting the curves with Eq. 2-2. The PEGDA and PEGMA concentrations of the hydrogels were 8% and 4%, respectively. (*$p < 0.05$).

The release profiles and their *k* values of albumin from PEG hydrogels with phenyl groups (Ph-PEG) were also obtained not only as a control to the Sulfo-PEG and TMAC-PEG hydrogels but also as a hydrogel with hydrophobicity (Figure 2-11d and e). The *k* values of Ph-PEG hydrogels at each Φ was in between those of Sulfo-PEG and TMAC-PEG hydrogel, demonstrating their charge neutrality. The values were not as significantly influenced by the increase in Φ, which showed the increase in hydrophobicity had little effect on the interaction between albumin and the polymeric network.

The exponents (*n*) from the Ritger-Peppas models were between 0.3 and 0.4 for all conditions, indicating the drug release was governed mostly by the Fickian diffusion and the release mechanism was not affected by the type of pendant functional groups (Figure 2-11f). [26, 33, 45] However, the release mechanism here showed smaller time-dependency (e.g. greater initial release) than a pure Fickian diffusion (i.e. the *n* value for a pure Fickian diffusion is 0.5). This 'quasi' Fickian diffusion mechanism suggested that the presence of more freely moving pendant chains, as compared to fully linked chains with limited mobility, likely promoted the faster drug release than what would be expected for the pure Fickian diffusion.

The drug release profiles were alternatively fitted with a Fickian diffusion model (Eq. 2-2) which assumes the square root of time dependence ($\sim t^{1/2}$), and obtained the diffusion coefficients (D) (Figure 2-11g). Because of the greater time dependence, the Fickian diffusion model did not ft well after first 10 hours of release (i.e. approximately 60% of total release) and overestimated the D values compared to k values from the Ritger-Peppas model. [34] Nonetheless, the trend in *D* values were similar to that of *k* values shown in Figure 2-11e, as they were expected to correlate with each other if *n* values from the Ritger-Peppas model were close to 0.5 and similar among different conditions.

The albumin release from PEG hydrogels at different PEGMA concentrations were further evaluated to assess the effect of crosslinking density on the protein release (Figure 2-12). When the PEGMA concentration was lowered to 2% (w/v) (PEGDA concentration increased to 10% (w/v)), the *k* and *D* values were generally low for all hydrogel types (Figure 2-12a and c). In addition, there was also negligible effect of Φ on the *k* values. This result suggests that albumin release was significantly hindered by the diminished porosity of the hydrogels at higher crosslinking density, and as a result the effect of charged groups on albumin release became minimal. When the PEGMA concentration was increased to 6% (w/v) (PEGDA concentration decreased to 6% (w/v)), there was a substantial increase in *k* and *D* values with Φ for all types of hydrogels (Figure 2-12b and d). The albumin release from Sulfo-PEG hydrogels was larger than other hydrogels, as expected. But there were smaller increases in albumin release from TMAC-PEG hydrogels and Ph-PEG hydrogels with Φ, despite the increasing positive charge and hydrophobicity. This is due to the increased porosity of the hydrogels, as evidenced by the swelling ratio shown in Figure 2-10, facilitating the protein release from the hydrogels and thereby diminishing the effect of functional pendant groups.

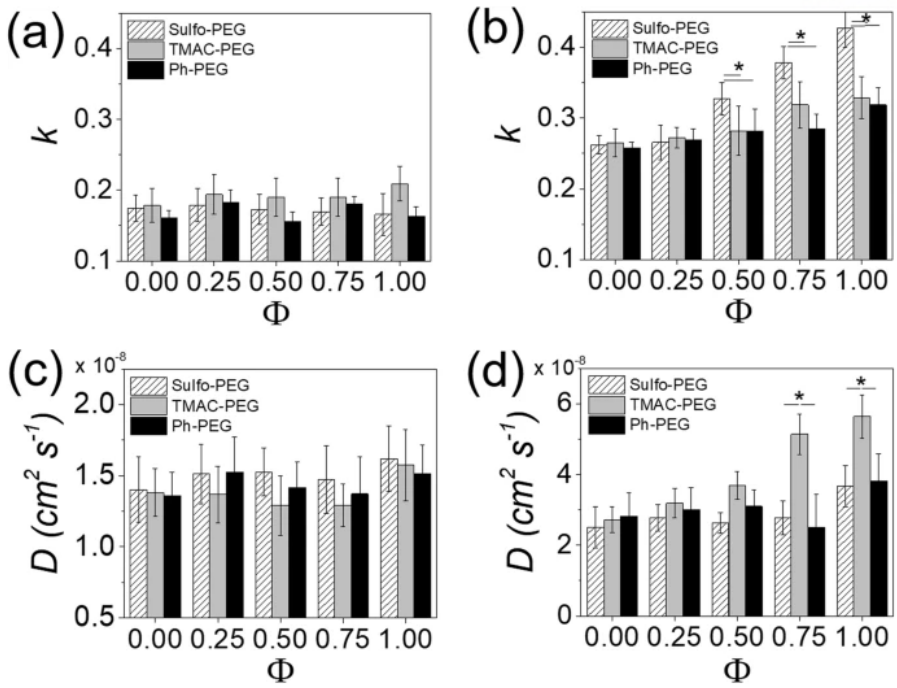

Figure 2-12. (a,b) Kinetic rate constants (*k*) and (c,d) diffusion coefficients (*D*) of albumin release from Sulfo-PEG, TMAC-PEG and Ph-PEG hydrogels, obtained by fitting the release profiles with Eq. (1) and Eq. 2-2, respectively. (*$p < 0.05$) (a,c) 10% PEGDA and 2% PEGMA, (b,d) 6% PEGDA and 6% PEGMA.

Insulin. Insulin, a hormone produced by beta cells in pancreatic islets, regulates the glucose level in our body. It is the de facto glucose-lowering drug for diabetes, and biomaterial-based delivery systems have been widely investigated for its controlled release. [46] It has a pI value of 5.3, thus possessing negative charge at physiological pH, much like albumin. But since insulin (5.8 kDa) is much smaller than albumin (66 kDa), it was hypothesized that the level of control of insulin release from the charged PEG hydrogels would be different from that of albumin.

The concentration of PEGMA was first kept at 4% (w/v) (PEGDA concentration of 8% (w/v)). The *k* values of insulin in Sulfo-PEG hydrogels began to increase significantly when Φ was increased above 0.5, unlike the albumin whose release was promoted below 0.5 (Figure 2-13a and d). Since there is less positive charge on insulin than albumin due to higher pI, more negative charges may have been needed to facilitate the release. It is also possible that the smaller size of insulin likely conferred more interaction with the polymeric network, requiring more negative charges to facilitate the release.

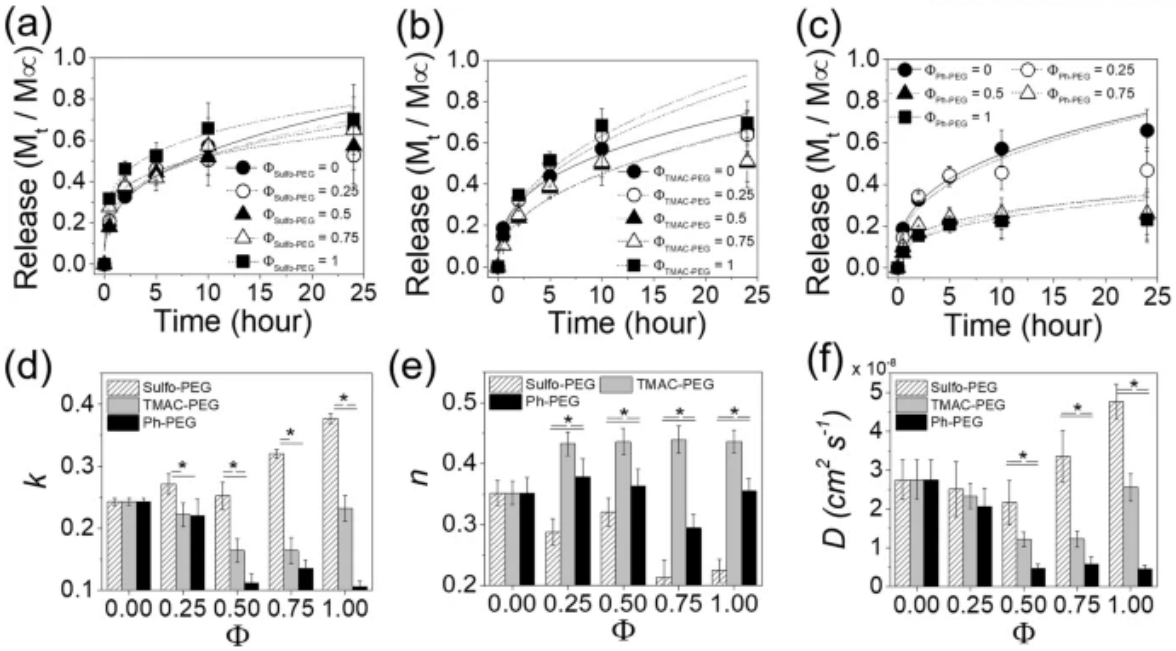

Figure 2-13. The release profiles of insulin from (a) Sulfo-PEG hydrogels, (b) TMAC-PEG hydrogels and (c) Ph-PEG hydrogels. (d) The kinetic rate constants (k) and (e) exponents (n) obtained by fitting the curves with Eq. 2-1. (f) Diffusion coefficients (D) were obtained by fitting the curves with Eq. 2-2. (*$p < 0.05$) The PEGDA and PEGMA concentrations of the hydrogels were 8% and 4%, respectively.

More significantly, the k values of insulin in TMAC-PEG hydrogels decreased above $\Phi = 0.5$, demonstrating the increased positive charge helped delay the release of insulin, more so than albumin despite less negative charge (Figure 2-13b and d). The smaller insulin likely was better able to interact with TMAC groups than bulkier albumin. The release from hydrophobic Ph-PEG hydrogels also showed significant decrease with Φ, demonstrating the increased number of phenyl groups was able to undergo extensive hydrophobic interaction with insulin, thereby delaying the release. Compared to albumin, less negative charge and smaller size of insulin likely contributed to this phenomenon.

Like albumin, the exponents (n) of insulin release from the hydrogels were all below 0.5, indicating the quasi-Fickian release with greater initial release (Figure 2-13e). However, the n values from Sulfo-PEG hydrogels were significantly lower than those of TMAC-PEG and Ph-PEG hydrogels, which further highlight the much accelerated release of insulin from the Sulfo-PEG hydrogels as compare with other hydrogels, likely attributed to the smaller size compared to albumin. In addition, similar to the albumin release, the changes in diffusion coefficients (D) calculated from fitting with Eq. 2-2 with Φ and type of pendant chains were generally in line with the k values shown in Figure 2-13d obtained from Eq. 2-1 (Figure 2-13f).

As similarly done with albumin, the insulin release from hydrogels were evaluated at different PEGMA concentrations to assess the effect of crosslinking density (Figure 2-14). Interestingly, when the PEGMA concentration was reduced to 2% (w/v) (increasing PEGDA concentration to 10% (w/v)),

the *k* and *D* values of insulin from Sulfo-PEG hydrogels showed significant increase with Φ up to 0.5, but decreased with Φ afterwards (Figure 2-14a and c). Similarly, to lesser extent, the release profiles of TMAC-PEG hydrogels and Ph-PEG hydrogels followed the similar patterns. This biphasic behavior was not shown for albumin at the same PEGMA concentration in Figure 2-12, in which the overall release was diminished, and suggested that there is an optimal level of diffusion of smaller protein in a more crosslinked network. The initial increase in *k* values with Φ up to 0.5 could possibly be a result of insulin, which is much smaller than albumin, being able to diffuse from the hydrogels even through diminished porosity at higher crosslinking density via pressure-driven flow enhancement in confined spaces. [47, 48] However, further increase in Φ likely reduced the flow enhancement, as the increased functional groups facilitated the increased porosity via the polymeric chain relaxation, eliminating the pressure gradient within the hydrogel. This interesting aspect of protein release in confined polymeric networks warrants further investigation in future studies.

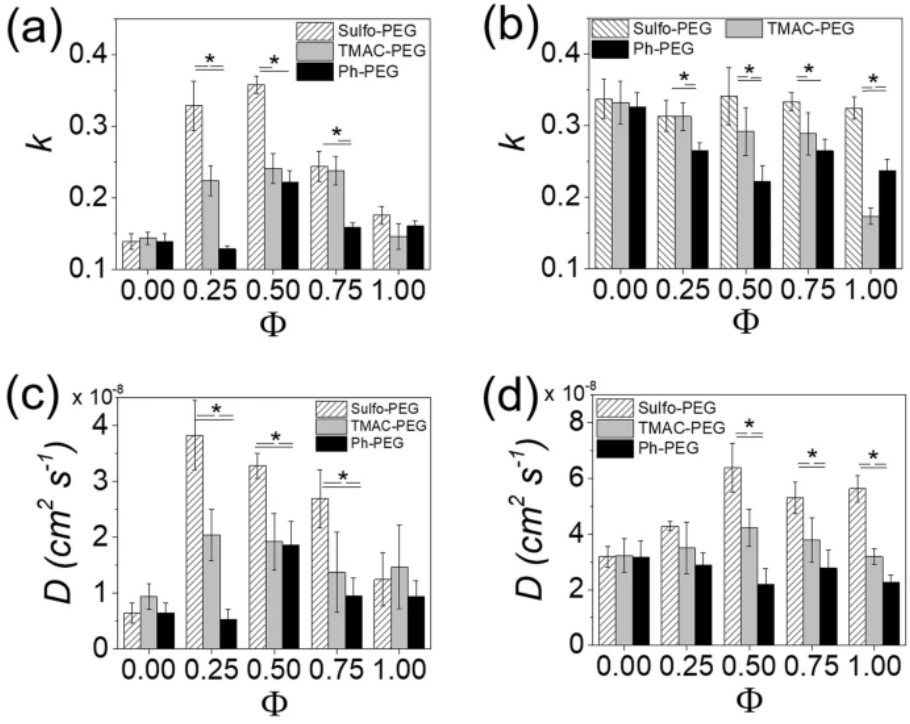

Figure 2-14. (a,b) Kinetic rate constants (*k*) and (c,d) diffusion coefficients (*D*) of insulin release from Sulfo-PEG, TMAC-PEG and Ph-PEG hydrogels, obtained by fitting the release profiles with Eq. 2-1 and Eq. 2-2, respectively. (*$p < 0.05$) (a,c) 10% PEGDA and 2% PEGMA, (b,d) 6% PEGDA and 6% PEGMA.

For the hydrogels with higher PEGMA concentration of 6% (w/v) (the PEGDA concentration of 6% (w/v)), the overall *k* and *D* values were much larger than those at lower PEGMA concentrations, as expected, due to lower crosslinking density (Figure 2-14b and d). The *k* values of Sulfo-PEG hydrogels remained high at all Φ, suggesting the increased negative charge density did not contribute to the release

rates as they were already high. On the other hand, the *k* values of TMAC-PEG hydrogels decreased with Φ, demonstrating the enhanced electrostatic interaction with insulin by the increased positive charge density helped delay the release. The increased hydrophobic interaction by increasing Φ of Ph-PEG hydrogels also resulted in decreasing *k* values. Interestingly, the increase in *D* for Sulfo-PEG hydrogels with Φ was larger, and the difference between Sulfo-PEG, TMAC-PEG, and Ph-PEG at a given Φ was also much larger than *k* values shown in Figure 2-14b (Figure 2-14d). This was due to the overestimation by the Fickian diffusion model, which was accentuated by the larger initial drug release for hydrogels with lower crosslinking density. Regardless, the *D* values further demonstrated the greater release rates from Sulfo-PEG hydrogels. Taken together, the insulin release was more heavily influenced by the changes in charge density of PEG hydrogels with functional pendant chains, which suggested that insulin was better able to interact with the functional groups owing to the smaller size, as compared to albumin.

Trypsin. Trypsin is a well-known serine protease responsible for protein digestion in many mammalian species, and also widely used for breaking cell aggregates and detaching cells from culture substrates in routine biological experiments. Unlike albumin and insulin, trypsin has the pI value of 10.5, thus possessing positive charge at physiological pH. Therefore, trypsin encapsulated in Sulfo-PEG hydrogels was expected to show lower release rates than TMAC-PEG hydrogels (Figure 2-15a).

The concentration of PEGMA was first kept at 4% (w/v) (PEGDA concentration of 8% (w/v)). The *k* and *D* values indicate that the trypsin release from Sulfo-PEG hydrogels was significantly reduced at all Φ, compared to albumin and insulin, demonstrating the increased negative charge density of Sulfo-PEG hydrogels was able to decrease the release rate of positively-charged trypsin (Figure 2-15b,e and f). However, the release rates of trypsin from TMAC-PEG hydrogels was not significantly enhanced by the increased positive charge via electrostatic repulsion as predicted (Figure 2-15c and e). This result suggests the positive charge density conferred by TMAC groups was not strong enough to exert enough repulsive force to facilitate the release of trypsin, which was in part evidenced by the lower absolute zeta potential value of TMAC (0.11 mV) compared to Sulfo group (0.21 mV). The exponents, like albumin, were not significantly affected by the type of pendant chains in the hydrogels (Figure 2-15f).

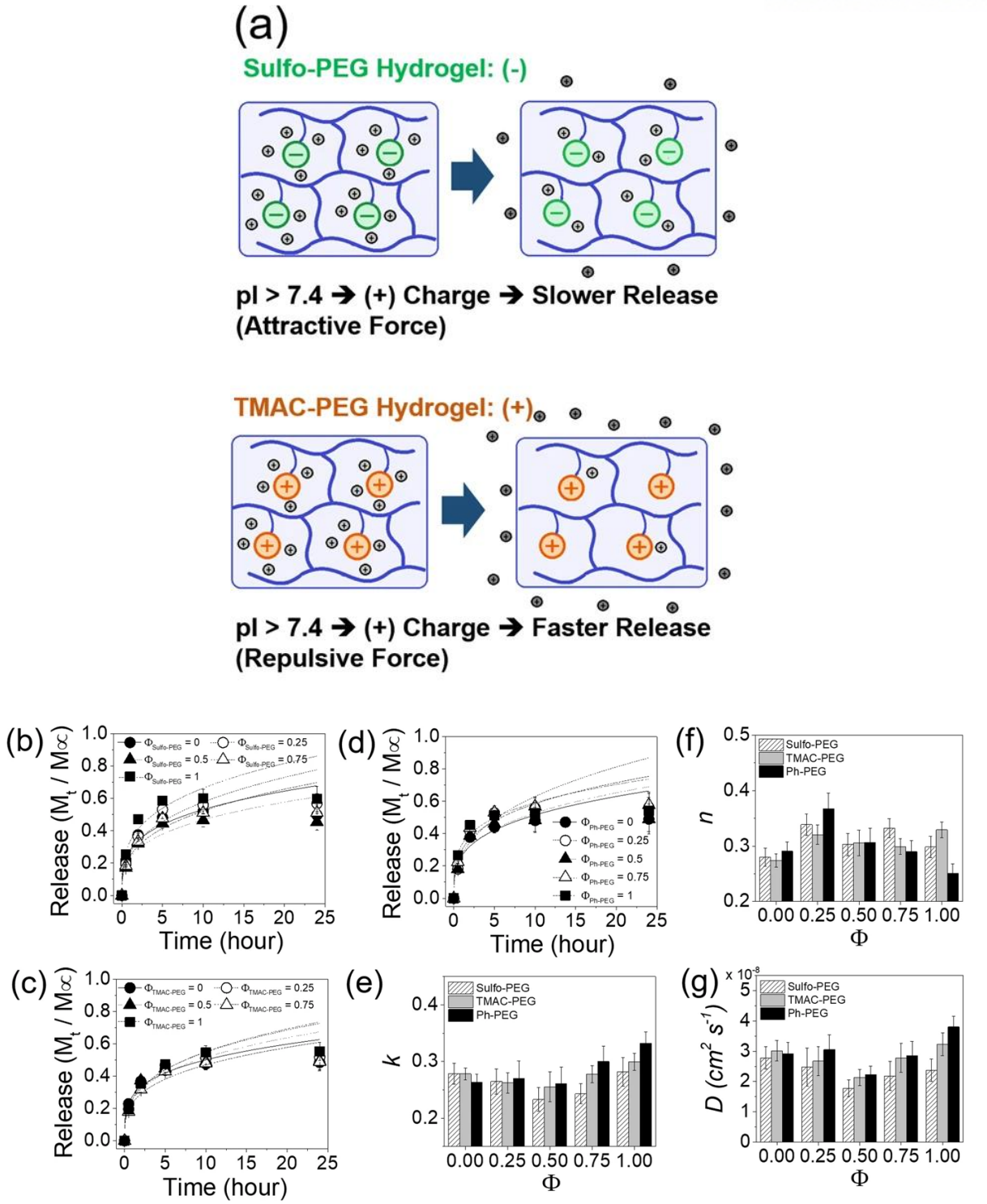

Figure 2-15. (a) Protein with pI higher than 7.4 becomes positively charged, and thus expected to have a greater release rate in TMAC-PEG hydrogels via repulsion than Sulfo-PEG hydrogels. The release profiles of trypsin from (b) Sulfo-PEG hydrogels, (c) TMAC-PEG hydrogels and (d) Ph-PEG hydrogels. (e) The kinetic rate constants (k) and (f) exponents (n) were values obtained by fitting the curves with Eq. 2-1. (g) Diffusion coefficient (D) were obtained by fitting the curves with Eq. 2-2. The PEGDA and PEGMA concentrations of the hydrogels were 8% and 4%, respectively.

Similarly, for the hydrogels at other PEGMA concentrations, the *k* and *D* values of trypsin in Sulfo-PEG hydrogels were significantly reduced as compared to albumin and insulin, whereas those in TMAC-PEG hydrogels did not significantly change with Φ (Figure 2-16). The *k* values in Ph-PEG hydrogels, regardless of the crosslinking density of the hydrogels, were also not substantially affected by Φ. It is possible that the range of physical properties tuned by the TMAC-PEG hydrogels and Ph-PEG hydrogels used in this study were not enough to significantly influence the release rate of trypsin.

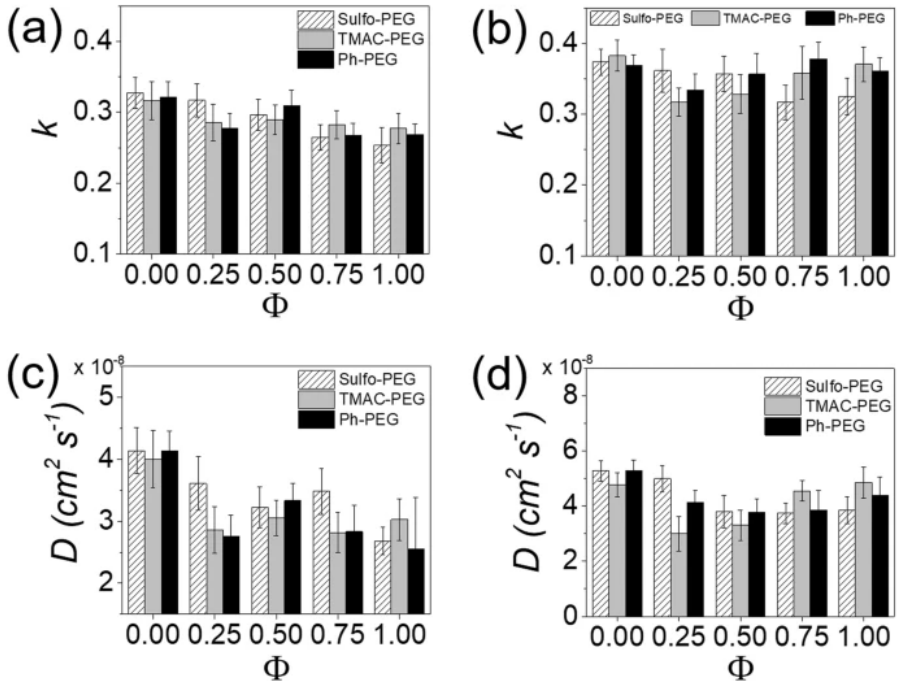

Figure 2-16. (a,b) Kinetic rate constants (*k*) and (c,d) diffusion coefficients (*D*) of trypsin release from Sulfo-PEG, TMAC-PEG and Ph-PEG hydrogels, obtained by fitting the release profiles with Eq. 2-1 and Eq. 2-2, respectively. (a) 10% PEGDA and 2% PEGMA, (b) 6% PEGDA and 6% PEGMA.

2.4 Conclusion

In this study, various physical properties (i.e. charge density and hydrophobicity) of PEG hydrogels were controlled independent of the crosslinking density by presenting pendant PEG chains with characteristic end functional groups in order to control the release of proteins having different isoelectric points (pI). The PEG hydrogels were fabricated by crosslinking PEGDA with PEGMA which becomes pendant PEG chains. While keeping the PEGDA and PEGMA concentrations, the ratio of non-functional PEGMA and heterobifunctional PEGMA was varied to control the physical properties of the hydrogels without changing the crosslinking density nor the number of total pendant chains. Therefore, only the change in physical properties were expected to significantly influence the changes in protein release rates. Here, the heterobifunctional PEGMA with sulfonate (‘Sulfo-PEG’),

trimethylammonium chloride ('TMAC-PEG'), and phenyl group ('Ph-PEG') were synthesized to confer negative charge, positive charge, and hydrophobicity, respectively. The releases of albumin and insulin, whose pI values are lower than physiological pH, negatively charged, are more facilitated in Sulfo-PEG hydrogels due to electrostatic repulsion as compared to TMAC-PEG hydrogels capable of providing attractive force. In addition, the effect of charge type and density was more noticeable for insulin, likely due to its smaller size than albumin allowing more interactions with the functional groups. On the other hand, the release of trypsin, having positive charge due to higher pI value than physiological pH, was significantly diminished in Sulfo-PEG hydrogels via repulsive force. These results demonstrate that the PEG hydrogels with pendant functional groups could be successfully utilized as vehicles for refined control of protein release for biomedical applications.

CHAPTER 3. Integrative control of mechanical and degradation properties of in situ crosslinkable polyamine-based hydrogels for dual-mode drug release kinetics

3.1 Introduction

Hydrogels are extensively investigated in biomedical applications, most notably as drug delivery systems and tissue engineering scaffold materials. [15, 49] Their unique blend of physical properties, such as hydrophilicity, elasticity and permeability, is ideally suited for those purposes. In addition, these properties could be controlled in an efficient manner by varying the crosslinking density of the polymeric network or hybridizing with another reinforcing materials (e.g. nanoparticles, interpenetrating network). [9, 50, 51] Furthermore, biological activities of cells and tissues incorporated within the hydrogel could be modulated by conjugation of cell-responsive moieties (e.g. collagen, fibronectin, and laminin). [52, 53]

The crosslinking reactions to form hydrogels generally involve the use of initiators to start the process. For example, radical polymerization with vinyl-based functional groups need radical initiators, such as persulfates and phenones. [54-57] However, these reagents often display cytotoxicity, depending on their concentrations, so their dosages must be chosen carefully to prevent the cytotoxicity while maintaining the ability to start the crosslinking reaction. [58, 59] Therefore, an "*in situ*" crosslinking reaction which occurs under mild conditions and does not involve the use of initiator would be highly favored for hydrogel fabrication. [5, 60-64]

Recently, Michael addition involving amine or thiol as a nucleophilic Michael donor has been increasingly adopted to develop *in situ* crosslinkable hydrogels, because the reaction generally occurs at physiologically buffered conditions (i.e. neutral pH, body temperature, ionic strength). [62, 65, 66] In addition, amine and thiol are strong enough nucleophiles that often do not require base catalyst for initiation. For example, Hubbell and co-workers are one of the first to report the biocompatible reaction between 4-arm poly (ethylene glycol) with vinyl sulfone groups as the Michael acceptor and cysteine (thiol)-linked oligopeptide as the Michael donor under mild aqueous conditions to fabricate hydrogels. [67]

In this study, *in situ* crosslinkable hydrogel system between poly (ethylene glycol) diacrylate (PEGDA) and polyethyleneimine (PEI) having variable mechanical properties and degradation behavior was developed. Both PEGDA and PEI have long been used various biomedical applications with proven biocompatibility; PEGDA hydrogels prepared by radical polymerization are commonly utilized in drug delivery and tissue engineering, while polycationic PEI has been a popular choice for

non-viral gene delivery system via electrostatic nanocomplex formation. [12, 68-70] Herein, however, these two polymers were combined to produce *in situ* crosslinkable hydrogel system by inducing Michael addition between two acrylates in PEGDA and multiple amines in PEI. [65, 71] With the aforementioned popularity and availability of PEGDA and PEI, this PEGDA-PEI hydrogel system has the advantage of cost-effective and efficient production, compared to other types of hydrogels which generally require additional chemical conjugation steps to present the functional groups involved with the crosslinking reaction. The mechanical properties of PEGDA-PEI hydrogels were controlled by changing the crosslinking density through their concentrations and the molecular weight (M_W) of PEGDA. In addition, the degradation of PEGDA-PEI hydrogels via hydrolysis of the ester linkages, under physiological conditions regardless of their mechanical properties, was also explored by controlling the degradation rate with PEGDA and PEI concentrations. These degradation and tunable mechanical properties of the PEGDA-PEI hydrogels were eventually utilized to control the drug release kinetics, in which two different drug release mechanisms occurred in sequence to impart more refined overall release profiles.

3.2 Materials and Methods

3.2.1 Synthesis of poly(ethylene glycol) diacrylate (PEGDA)

Acrylate was conjugated to PEG by the nucleophilic substitution reaction between hydroxyl end groups of PEG and acryloyl chloride. Briefly, poly(ethylene glycol) (PEG, Sigma Aldrich) (M_W 1000, 2000, 3000, and 6000 g mol^{-1}) was first dissolved in dichloromethane at 30 %. 2 molar equivalents of acryloyl chloride and triethylamine (Sigma Aldrich) with respect to the hydroxyl groups of PEG were added to the mixture and stirred for 24 hours at room temperature with dry N_2. After the reaction, the insoluble salt formed was filtered out, and the mixture was condensed via rotary evaporation. A large excess of diethyl ether was added to precipitate the product. The product was washed three times with diethyl ether, and dried under vacuum. The acrylate conjugation was confirmed by ^{1}H-NMR (400MHz, Avance III HD, Bruker) (Figure 3-1).

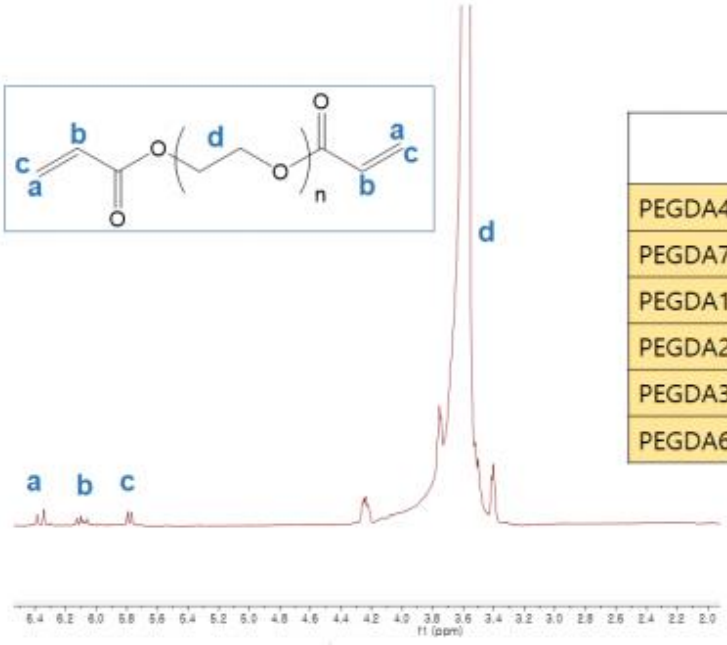

	Acrylate (a, b, c)	Hydroxyethyl (d)
PEGDA400	1	15.6
PEGDA700	1	28.7
PEGDA1K	1	43.5
PEGDA2K	1	95.1
PEGDA3K	1	140.6
PEGDA6K	1	283.5

Figure 3-1. A representative ^{1}H-NMR spectrum of PEGDA. The peak integration ratio between acrylic peaks (a, b, c) and hydroxyethyl peak (d) are listed.

3.2.2 PEGDA-PEI hydrogel fabrication

Stock solutions of 40% PEGDA and 20% PEI (M_W, 2000 g mol^{-1}, Sigma Aldrich) in phosphate buffered saline (PBS, pH 7.4) were mixed in various ratios to prepare a precursor solution. [17, 26, 29] The precursor solution was immediately placed in a custom-made mold having 1 mm spacer, and incubated at 37 °C until hydrogel was formed. Hydrogel disks (8 mm diameter) were punched out, and immersed in PBS until further characterization.

Rheological characterization was performed to analyze the gelation kinetics of PEGDA-PEI hydrogel formation. [72, 73] The PEGDA and PEI solutions were mixed and placed onto a sample holder of a rotating-disk rheometer (Kinexus, Malvern), and the changes in storage moduli (G') and loss moduli (G'') were measured during the crosslinking reaction in a small-amplitude oscillatory shear mode at 37 °C. During the experiment, the frequency and strain of the rotating disk were 1 Hz and 10%, respectively. The gelation time was reported here as the time for the G' and G'' curves to cross over, which represented the point of gelation.

3.2.3 Mechanical properties and degradation of PEGDA-PEI hydrogels

The rigidity of various PEGDA-PEI hydrogels was measured by calculating their elastic moduli obtained from compression experiments. Briefly, the hydrogel disks were subjected to uniaxial compression at the rate of 1 mm min^{-1}, and the strain vs. stress curve was obtained (Model 3343, Instron). The elastic modulus was determined as the slope of the linear region (first 10%) of the curve.

The degradation behavior was analyzed by measuring the change in elastic moduli over time. The PEGDA-PEI hydrogels were incubated in PBS at 37 °C, and their moduli were measured at designated time points. The degradation rate constants (k_d) were obtained by fitting the moduli vs. time curves with the following exponential decay model,

$$\frac{E_t}{E_0} = e^{-k_d \cdot t} \qquad \text{Eq. 3-1}$$

where E_t was the modulus measured at time, t, and E_0 was the initial modulus. [30, 74]

The homogeneity of PEGDA and PEI after the hydrogel formation was assessed by conjugating a fluorophore and monitoring the distribution within the hydrogels. Each PEGDA-PEI hydrogel disk was incubated in fluorescein isothiocyanate (FITC, Sigma Aldrich) solution in PBS (0.1 mg mL^{-1}) for 3 h at room temperature under dark to induce the reaction between amine and FITC. The conjugation was confirmed by the presence of fluorescent color remaining within the hydrogel after extensive washing. The FITC-linked hydrogel was visualized with a fluorescence microscope (XDS-3FL, Optika) to assess the distribution of fluorophores within the hydrogel. The degradation of FITC-linked hydrogel was monitored under the same condition as stated above, and compared with the unmodified hydrogels.

3.2.4 Drug release profiles from PEGDA-PEI hydrogels

Drug release from various PEGDA-PEI hydrogels was measured to evaluate the effect of mechanical properties and degradation behavior. [29, 75] Bovine serum albumin (3 mg mL^{-1}) as a model protein drug was encapsulated into PEGDA-PEI hydrogel by dissolving into the precursor solution prior to hydrogel fabrication. The hydrogel was incubated in PBS at 37 °C, and the released amount was measured at various time points (BCA™ Protein Assay, Thermo Fisher). The cumulative drug release profile was fitted to the following two models,

$$\frac{M_t}{M_\infty} = k_1 \cdot t^n \qquad \text{Eq. 3-2}$$

$$\frac{M_t}{M_\infty} = e^{k_2 \cdot t} \qquad \text{Eq. 3-3}$$

where M_t is the released amount at time, t, M_∞ is the total amount in the hydrogel, k_1 and k_2 are the kinetic rate constants, and n is the exponents related to the release mechanism. [75-77] Eq. 3-2, a power-law release model with fractional time dependence ('Ritger-Peppas model') was used to fit the initial part of the drug release, while Eq. 3-3, an exponential release model, was used to fit the accelerated release which occurred afterwards.

3.3 Results and Discussion

3.3.1 Mechanical properties of PEGDA-PEI hydrogels

PEGDA-PEI hydrogels were fabricated by mixing the stock solutions of PEGDA and PEI at various ratios to control their mechanical properties Figure 3-2). The concentration of PEGDA was controlled at either 10 or 20%, while varying the molecular weight (M_W) of PEGDA from 400 ('PEGDA400') to 6000 ('PEGDA6K') g mol^{-1}. The PEI concentration was also controlled from 3 to 10%. The lower end of this range was chosen as the lowest concentration of PEI resulting in hydrogel formation, while the higher end was chosen at which the mechanical properties began to decrease as well as for the manageable viscosity (i.e. the viscosity of PEI becomes too high beyond 10%, Figure 3-3).

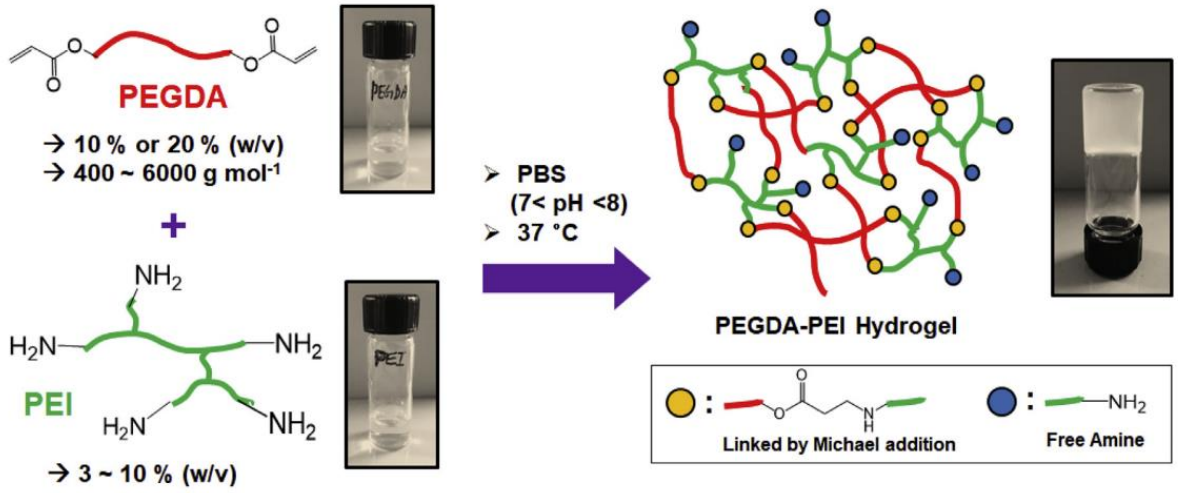

Figure 3-2. Schematic representation of *in situ* crosslinkable PEGDA-PEI hydrogels prepared under physiological condition. The reaction parameters include the concentrations of PEGDA and PEI as well as M_W of PEGDA.

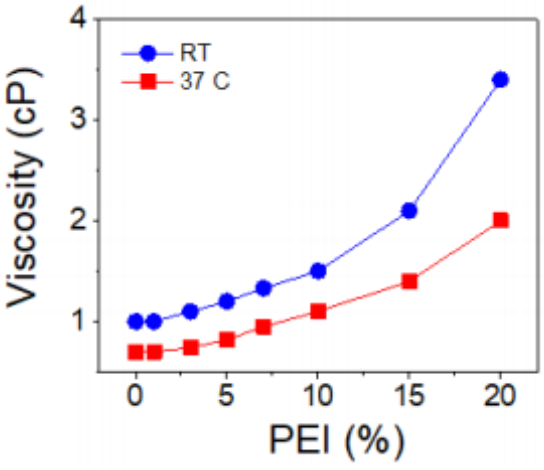

Figure 3-3. The viscosity of PEI at various concentrations, measured at room temperature (RT) or 37 °C.

The homogeneity of PEGDA-PEI hydrogel was assessed by microscopic imaging of fluorophores distributed within the hydrogel. The hydrogel was chemically conjugated with a fluorescent probe (e.g. FITC) via unreacted amine groups of PEI. The consistent fluorescent signals throughout the hydrogel structure indicate that the PEGDA and PEI were homogeneously mixed and distributed within the network (Figure 3-4).

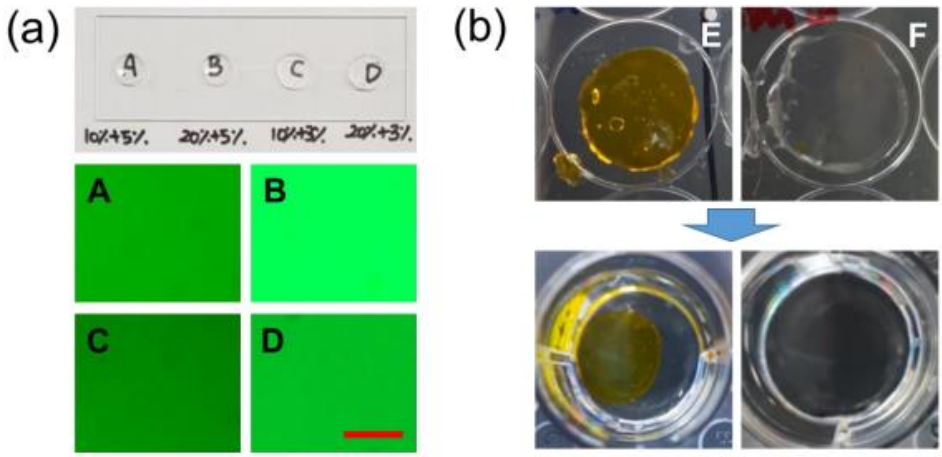

Figure 3-4. (a) Photographic (top) and fluorescent microscopic (bottom) images of PEGDA-PEI hydrogels (scale bar: 100 μm). (A: 10 % PEGDA-5% PEI, B: 20 % PEGDA-5% PEI, C: 10 % PEGDA-3% PEI, D: 20 % PEGDA-3% PEI). (b) (Top) Photographs of PEGDA-PEI hydrogels conjugated with (E) or without (F) FITC after incubation in PBS. Greater swelling was observed for F due to accelerated degradation. (Bottom) After continuous swelling, F disintegrated while E remained intact.

3.3.2 Gelation kinetics

The effects of M_W and concentration of PEGDA and the concentration of PEI on the rate of crosslinking reaction between PEGDA and PEI were evaluated by measuring the changes in viscoelastic properties of the mixture, storage moduli (G', elastic component) and loss moduli (G'', viscous component), over time during the reaction. [72, 73] The rheological characterization was performed at the same strain (10%) and cyclic frequency (1 Hz) for all samples. The gelation time was determined as the time for G' to cross over G'' ('gel point'), which signified the dramatic increase in elastic component by the crosslinking reaction. First, the concentration of PEGDA and PEI were kept at 10% and 5%, respectively while controlling the M_W of PEGDA (Figure 3-5). The gel point was observed up to PEGDA2K (Figure 3-5a-d). However, further increase in M_W of PEGDA (PEGDA3K and PEGDA6K) did not result in G' crossing over G'' at any point during the reaction, showing the gelation did not occur likely due to the number of acrylic groups below the critical number required for gelation under the given concentrations of PEGDA and PEI (Figure 3-6). Increasing the PEGDA concentration to 20% while maintaining 5% PEI, the gelation occurred at all M_W of PEGDA, on account of the increased number of acrylic groups at higher PEGDA concentration (Figure 3-7).

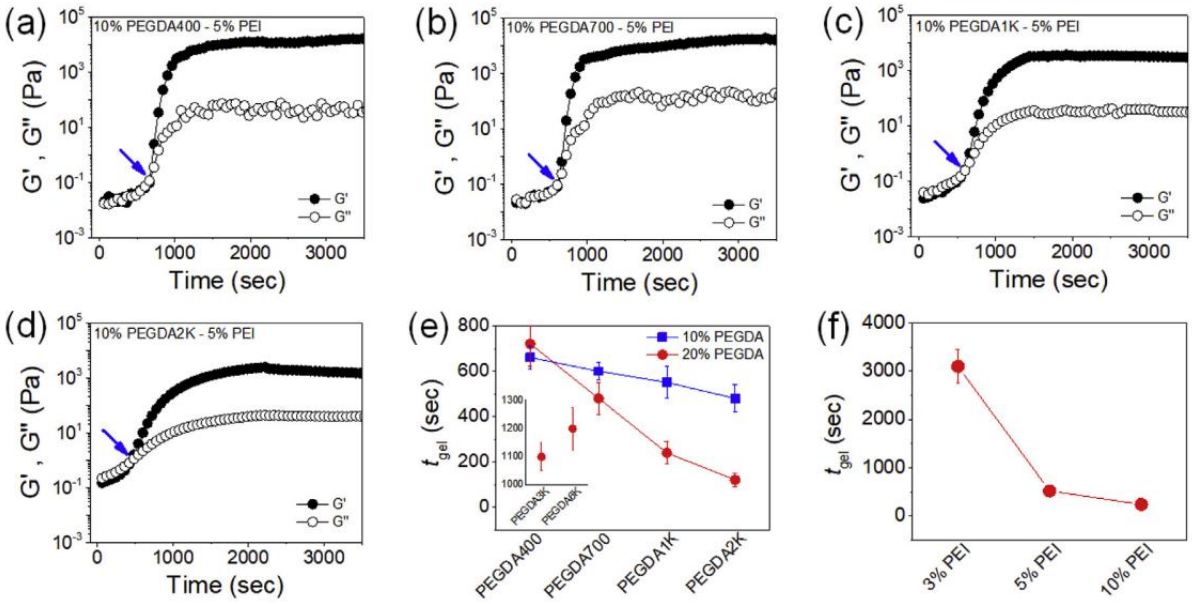

Figure 3-5. Rheological properties of the reaction mixture of 10% PEGDA and 5% PEI, evaluated by the changes in storage (*G′*) and loss (*G″*) moduli measured over time: (a) PEGDA400, (b) PEGDA700, (c) PEGDA1K, and (d) PEGDA2K. The arrows indicate the gel point. (e) The gelation times (t_{gel}) of 10% PEGDA or 20% PEGDA with 5% PEI. (f) t_{gel} values of 20% PEGDA700 with varying concentration of PEI.

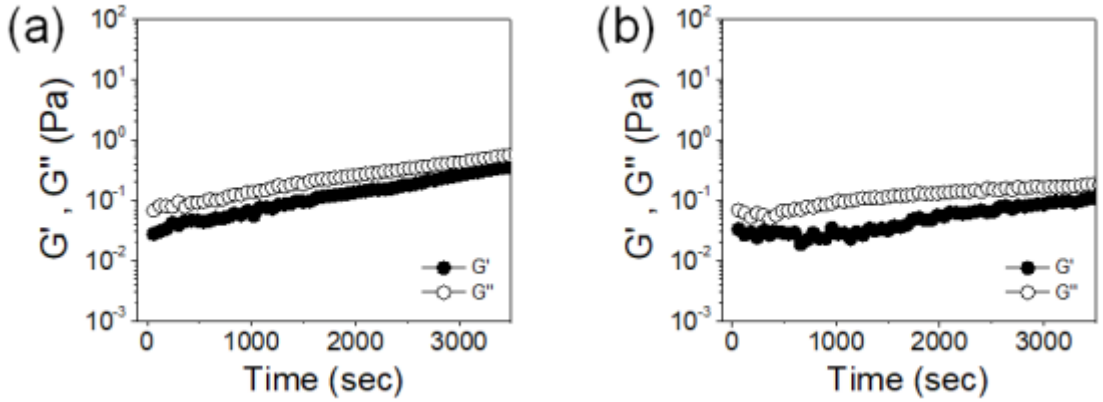

Figure 3-6. Rheological properties of the reaction mixture of 10 % PEGDA and 5 % PEI, evaluated by the changes in storage (*G'*) and loss (*G"*) moduli measured over time: (a) PEGDA3K and (b) PEGDA6K.

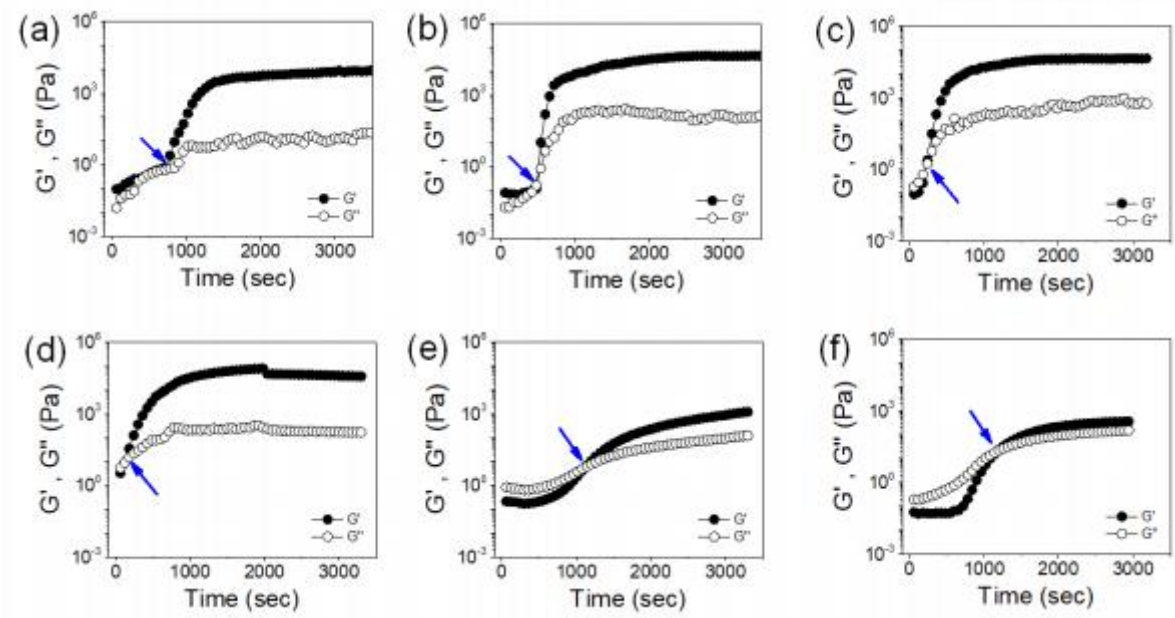

Figure 3-7. Rheological properties of the reaction mixture of 20 % PEGDA and 5 % PEI, evaluated by the changes in storage (*G'*) and loss (*G"*) moduli measured over time: (a) PEGDA400, (b) PEGDA700, (c) PEGDA1K, (d) PEGDA2K, (e) PEGDA3K, and (f) PEGDA6K. The arrows indicate the gel point.

Interestingly, there was a gradual decrease in gelation time (t_{gel}) with increasing M_W of PEGDA for both 10% and 20% PEGDA (Figure 3-5e, Figure 3-7). In addition, the rate of decrease in t_{gel} with M_W of PEGDA was much greater at 20%. This result may be deemed counterintuitive in terms of the concentration effect on reaction kinetics, in which the higher number of acrylates in lower M_W of PEGDA at a given concentration is expected to result in greater reaction rate. This interesting result may have been due to the increased level of hydrophobicity of PEGDA with lower M_W due to the higher number of acrylic groups relative to the hydrophilic ethylene oxide chain, preventing more stable and homogeneous mixing between PEGDA and PEI. [78] As a result, PEGDA with higher M_W having greater hydrophilicity may have had favorable interaction with PEI, driving the initial crosslinking process.

The effect of PEI concentration on t_{gel} was also explored by varying the PEI concentration from 3 to 10% (w/v) reacting with 20% PEGDA700 (Figure 3-5f, Figure 3-8). The t_{gel} values decreased with increasing PEI concentration, which was also against the concentration effect since the number of amine groups available for crosslinking obviously increase with concentration. Since PEI is known to be highly hydrophilic, increased viscosity of PEI at higher concentration likely had the retardation effect on the rate of gelation (Figure 3-3).

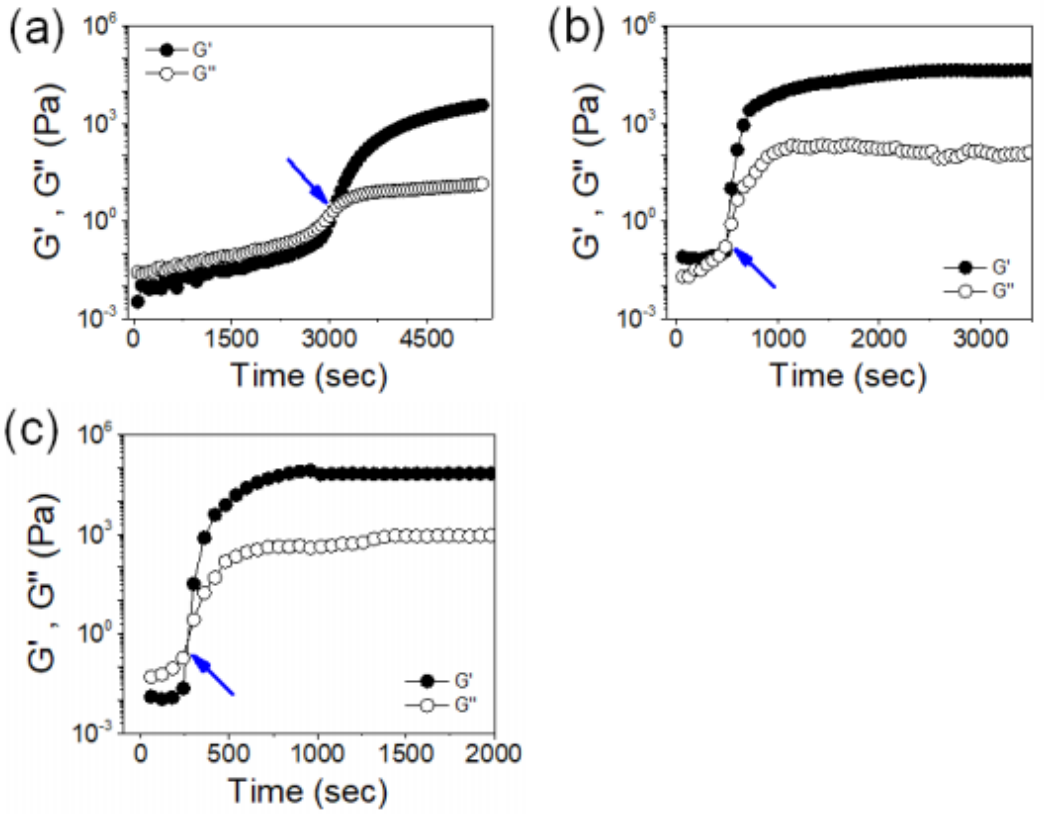

Figure 3-8. Rheological properties of the reaction mixture of 20 % PEGDA700 with (a) 3 % PEI, (b) 5 % PEI, and (c) 10 % PEI. The changes in storage (*G'*) and loss (*G"*) moduli were measured over time. The arrows indicate the gel point.

3.3.3 Rigidity

The trend in gelation kinetics as discussed above may not necessarily correlate with the mechanical properties of the fully-crosslinked hydrogels. With enough time for the completion of crosslinking reaction, it could be reasonably inferred that the hydrogels crosslinked with more reactive functional groups (e.g. higher concentration and lower M_W of PEGDA, and higher concentration of PEI) would result in greater rigidity. Therefore, the rigidity of PEGDA-PEI hydrogels was also assessed by measuring the elastic moduli from uniaxial compression experiments. First, the concentration of PEI was fixed at 5%, while the concentration of PEGDA was controlled at 10% or 20% (Figure 3-9a). The moduli did indeed decrease with M_W of PEGDA, from PEGDA700 to PEGDA2K for 10% PEGDA, and from PEGDA700 to PEGDA6K for 20% PEGDA. However, the modulus of PEGDA400-PEI hydrogel was in fact significantly lower than that of PEGDA700-PEI hydrogel. This result may have been due to the greater hydrophobicity imparted by the high number of acrylic groups of PEGDA400 compared to PEGDA700, in which increased hydrophobicity of PEGDA400 may have prevented homogeneous mixing with hydrophilic PEI, resulting in the diminished degree of crosslinking reaction. [78]

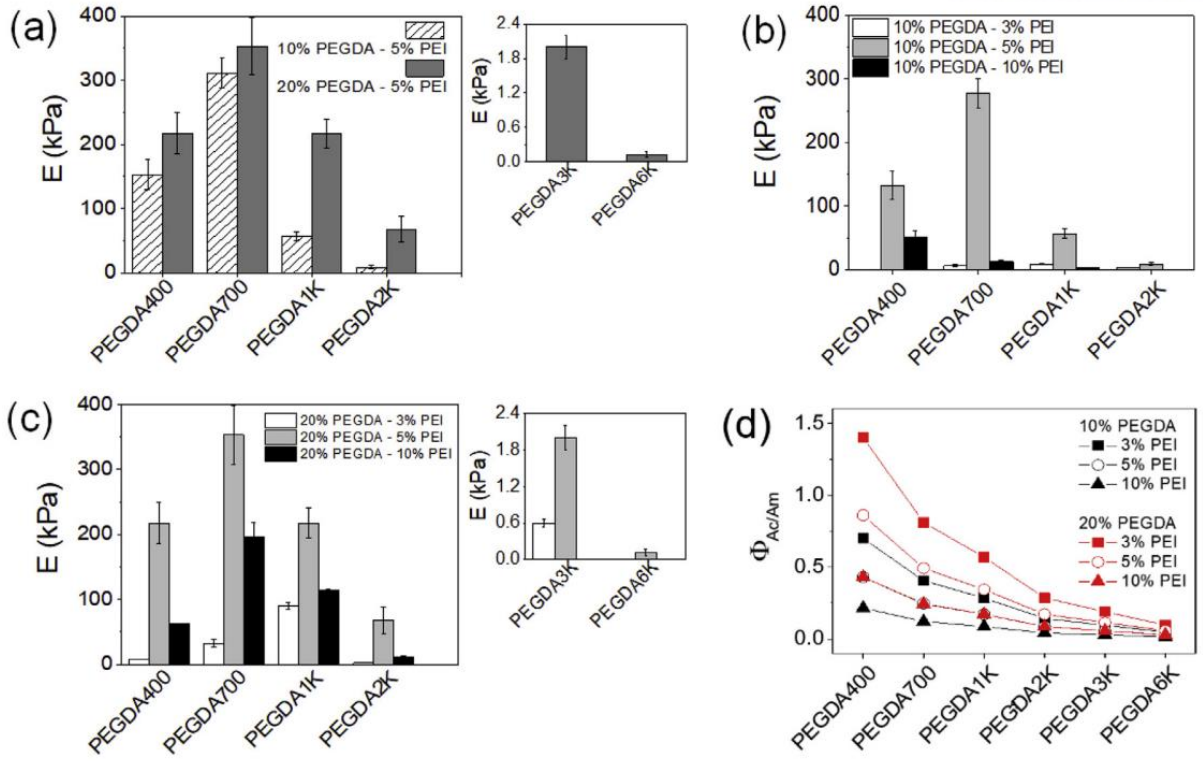

Figure 3-9. Elastic moduli (*E*) of PEGDA-PEI hydrogels: (a) 10% or 20% PEGDA with 5% PEI at varying M_W of PEGDA, (b,c) 10% PEGDA or 20% PEGDA with varying PEI concentration and M_W of PEGDA. (d) The ratio of the number densities of acrylate in PEGDA and amine in PEI ($\Phi_{Ac/Am}$) for varying M_W of PEGDA at different PEI concentrations.

Since the crosslinking reaction occurs via stoichiometric reaction between acrylate and amine, greater crosslinking density would be achieved with the stoichiometric ratio close to unity under a given polymer concentration. To assess the effect of the stoichiometry of acrylate and amine on the mechanical properties of the PEGDA-PEI hydrogels, theoretical number density ratios of acrylate to amine ($\Phi_{Ac/Am}$) were calculated (Figure 3-9d, Table 3-1). As expected, $\Phi_{Ac/Am}$ decreases with M_W of PEGDA at a given PEGDA concentration, thus the hydrogel rigidity decreased with a result of deviation from the stoichiometric unity and reduced crosslinking density. At 20% PEGDA400 in which the number of acrylate at the same concentration was the highest, the highest rigidity was shown for 5% PEI likely due to the $\Phi_{Ac/Am}$ close to unity (0.86) than other conditions (e.g. $\Phi_{Ac/Am} = 0.43$ for 3% PEI, $\Phi_{Ac/Am} = 1.4$ for 10% PEI).

(a)

	PEGDA400	PEGDA700	PEGDA1K	PEGDA2K	PEGDA3K	PEGDA6K
10% PEGDA	5×10^{-4}	2.86×10^{-4}	2×10^{-4}	1×10^{-4}	6.67×10^{-5}	3.33×10^{-5}
20% PEGDA	1×10^{-3}	5.71×10^{-4}	4×10^{-4}	2×10^{-4}	1.33×10^{-4}	6.67×10^{-5}

(b)

3% PEI	5% PEI	10% PEI
7×10^{-4}	1.16×10^{-3}	2.33×10^{-3}

Table 3-1. The number densities (mol mL^{-1}) of (a) acrylate in PEGDA and (b) amine in PEI at different concentrations.

Next, the effect of PEI content on the rigidity was explored by varying the PEI concentration from 3 to 10%, while keeping the PEGDA concentration (Figure 3-9b and c). As expected, the hydrogels with 20% PEGDA generally had greater moduli than those with 10% PEGDA at all M_W of PEGDA. The range of M_W of PEGDA resulting in hydrogel formation at a given PEI concentration was also greater at 20% PEGDA. For example, at 3% PEI, the highest M_W of PEGDA for gelation was PEGDA2K for 10% PEGDA, while it was PEGDA3K for 20% PEGDA. Similarly, at 10% PEI, the highest M_W of PEGDA for gelation was PEGDA1K for 10% PEGDA, while it was PEGDA2K for 20% PEGDA.

The overall trend in moduli with M_W of PEGDA was similar to that shown in Figure 3-9a at all PEI concentrations regardless of the PEGDA concentrations; the biphasic trend with the increase in moduli from PEGDA400 to PEGDA700, followed by the decrease in moduli from PEGDA700 to PEGDA3K. As expected, the moduli of hydrogels with 3% PEI was much lower than those with 5% PEI, due to lower amine content. However, with the increase in PEI concentration to 10%, the moduli decreased significantly for all M_W of PEGDA. The number of acrylic groups of PEGDA at the given concentration and M_W was likely all consumed by the amine groups of PEI at 5% that the further increase in PEI concentration resulted in significant stoichiometric excess of PEI molecules, leading to a limiting effect on the crosslinking reaction (i.e. the presence of excess reactants acted as a hindrance). This also helps explain the fact that the highest M_W of PEGDA for gelation was higher for 3% PEI (PEGDA3K) than 10% PEI (PEGDA2K), even though the moduli of hydrogels with 10% PEI were generally larger than those with 3% PEI; that is, a critically large excess of PEI at 10% PEI at the lowest number of acrylate at 10% PEI prevented hydrogel formation by limiting the crosslinking reaction.

The rigidity of the hydrogels was also evaluated by the G' values under cyclic shear condition after

complete gelation as shown in Figure 3-5 and Figure 3-6 to Figure 3-8 (Figure 3-10). For the hydrogels with 10% PEGDA and 5% PEI, the trend in G' was similar to that of elastic moduli (Figure 3-10a). However, when the PEGDA concentration was increased to 20%, G' values continuously increased with M_W of PEGDA up to PEGDA2K. Since the hydrogels crosslinked with higher M_W PEGDA were more resilient, though lower in rigidity, they were able to maintain their structural integrity under shear conditions. On the other hand, the hydrogels crosslinked with lower M_W PEGDA had much higher elastic moduli, but were also much more brittle. Thus, there was extensive fracture occurred for these hydrogels during the cyclic shear measurements, resulting in diminished G' values. Similar results were shown for the hydrogels with varying PEI concentrations while maintaining the concentration and M_W of PEGDA (Figure 3-10b). With 10% PEGDA700, the trend in G' was similar to that of elastic moduli shown in Figure 3-9b. However, with 20% PEGDA700, the G' at 5% PEI was lower than 3% and 10% PEI even though the elastic modulus was higher than the other conditions, which was also attributed to the significant brittleness.

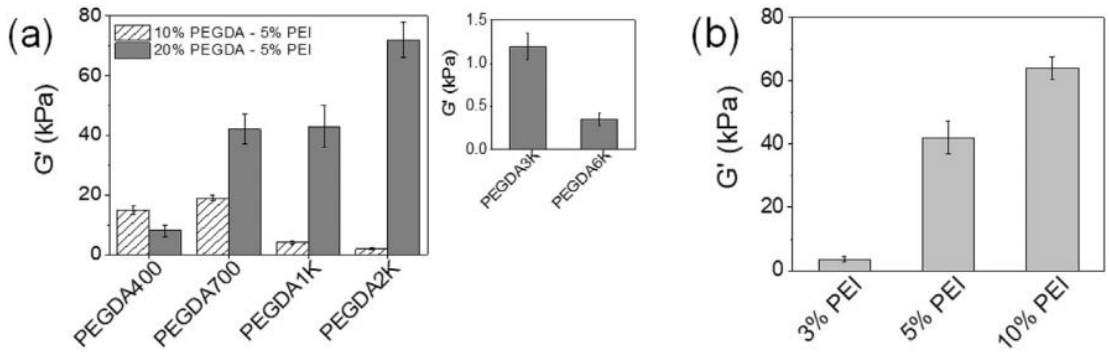

Figure 3-10. Storage moduli (G') of PEGDA-PEI hydrogels, taken from the highest G' values after gelation from the rheological experiments. (a) 10% or 20% PEGDA with 5% PEI at varying M_W of PEGDA and (b) 20% PEGDA700 with varying PEI concentration.

3.3.4 Degradation of PEGDA-PEI hydrogels

It was expected that there would remain a considerable number of unreacted amine groups in the PEGDA-PEI hydrogels since it is unlikely that all the amines in a PEI chain would react with the acrylate in PEGDA; due to the decreasing conformational and translational mobility of polymer chain as the crosslinking reaction proceeds, leading to diminished reactivity. [79] With the PEGDA-PEI hydrogels linked via ester bonds, the unreacted amine groups would facilitate the hydrogel degradation via direct nucleophilic attack or the hydrolysis stemming from the increased hydroxide content with the protonation of amine groups (Figure 3-11a). Similar degradation behavior of hydrogels with hydrolysable linkages crosslinked with polyamine have previously been reported. [65, 71]

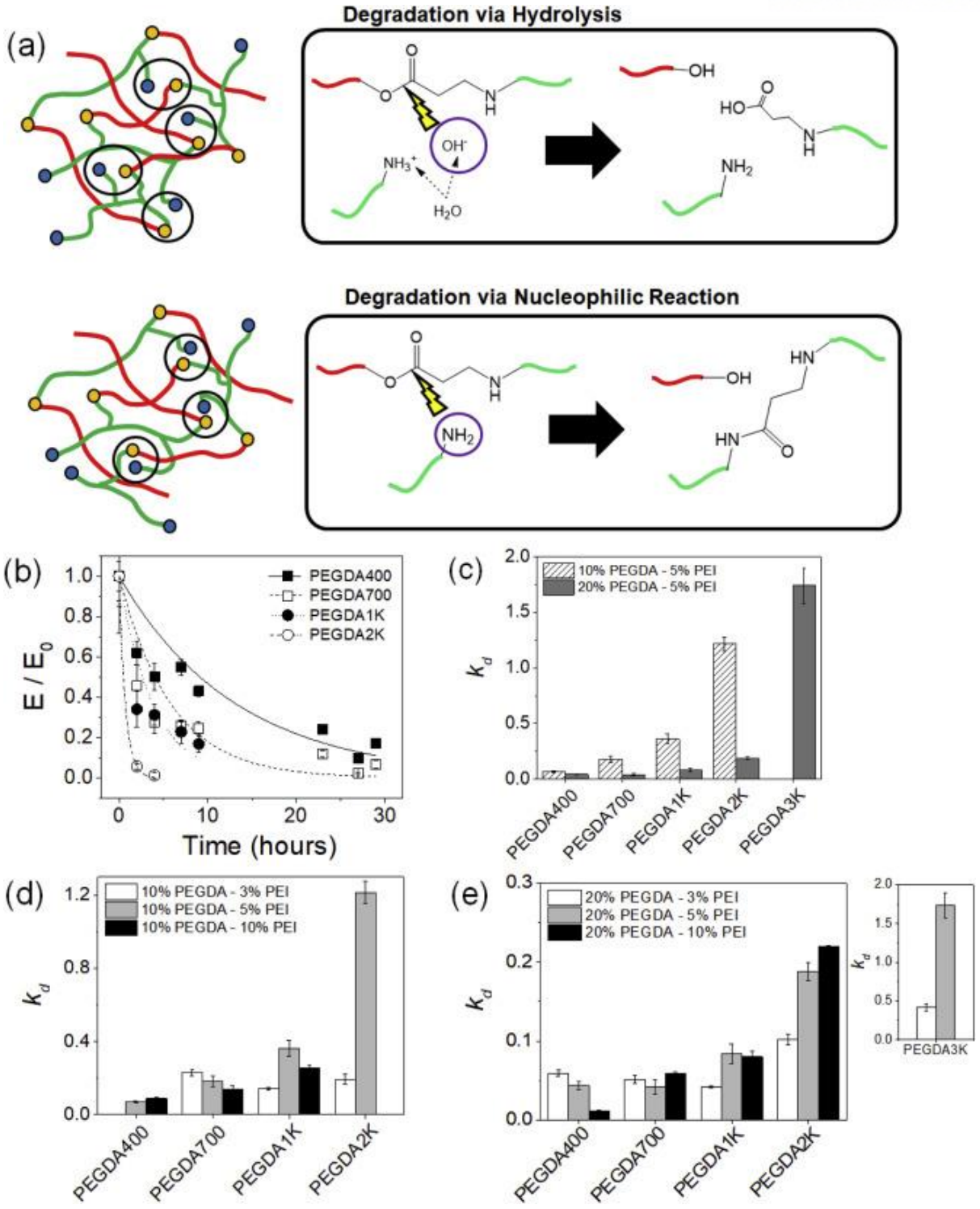

Figure 3-11. (a) Degradation mechanism of PEGDA-PEI hydrogels; hydrolysis of ester bonds by increased local hydroxide ions and/or direct nucleophilic attack on ester bonds by unreacted amine groups. (b) The change in normalized elastic moduli (E/E_0) of 10% PEGDA-5% PEI hydrogels with varying M_W of PEGDA plotted over time. (c) The degradation rate constants (k_d) obtained by fitting (b) with Eq. 3-1. The k_d values for (d) 10% PEGDA and (e) 20% PEGDA linked with varying concentrations of PEI.

To demonstrate their degradation behavior, the hydrogels were immersed in a physiological buffer (i.e. PBS) and the changes in elastic moduli were evaluated over time. As predicted, the PEGDA-PEI hydrogels at all conditions demonstrated complete structural disintegration, though at varying rates. The fractional change in moduli (E/E_0) vs. time (t) profiles were then fitted to an exponential decay model (Eq**.** 3-1) to obtain the degradation rate constant (k_d). First, the concentration of PEI was fixed at 5% while changing the M_W and concentration of PEGDA (Figure 3-11b and c, Figure 3-12). For both 10% and 20% PEGDA, the degradation rate was significantly influenced by the M_W of PEGDA, with k_d values generally increasing with M_W of PEGDA. This result indicated that the hydrogels with lower degree of crosslinking showed faster degradation, which was expected since there are less ester linkages in the hydrogels need to be broken for degradation and larger osmotic pressure within the hydrogels having higher degree of swelling at higher M_W of PEGDA.

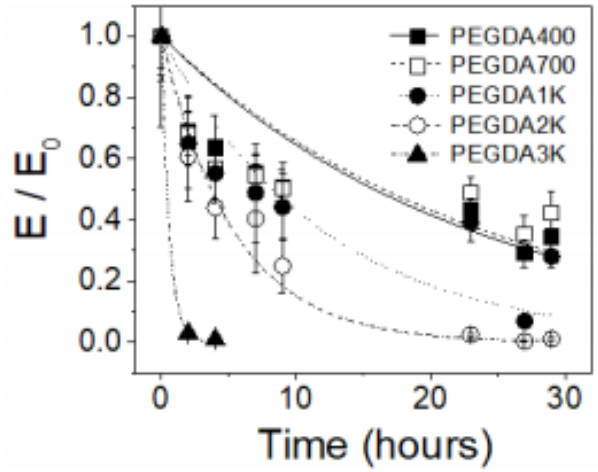

Figure 3-12. The change in normalized elastic moduli (E/E_0) of 20 % PEGDA-5 % PEI hydrogels with varying M_W of PEGDA plotted over time. The plots were fitted with Eq. 3-1 to obtain the degradation rate constants (k_d) which are shown in Figure 3-11.

The degradation was also monitored for the PEGDA-PEI hydrogels with varying PEI concentration (Figure 3-11d and e). Generally, the k_d values increased with M_W of PEGDA regardless of the PEI concentration for both 10% and 20% PEGDA, highlighting the dominant effect of the number of hydrolysable ester groups. Interestingly, for the highest M_W PEGDA (i.e. 10% PEGDA2K and 20% PEGDA3K), the k_d value was markedly higher at 5% PEI than 3% PEI, even though the modulus was much higher at 5% PEI. In addition, the change in k_d with M_W of 10% PEGDA with 3% PEI was significantly lower than those with 5% PEI (Figure 3-11d). Similarly, at 20% PEGDA, the increase in k_d with M_W of PEGDA became more prominent with the concentration of PEI (Figure 3-11e). Taken together, it could be concluded that the greater amount of unreacted amine groups at higher concentration of PEI likely facilitated the degradation process, irrespective of the difference in the initial rigidity of the hydrogels.

In situ crosslinkable PEGDA-PEI hydrogels developed in this study undergo degradation via hydrolysis of ester groups. If a potential application requires *in situ* crosslinkable hydrogel to be non-degradable, one could utilize a different conjugation chemistry which does not result in hydrolysis. For example, PEGDA crosslinked *in situ* with a thiol-based crosslinker (e.g. Thiocure®) to form hydrogels did not show any meaningful degradation for several months. [80] Alternatively, PEG with aldehyde end groups was crosslinked with a multi-amine polymer, poly (vinyl amine), via Schiff base formation, which only showed accelerated degradation at acidic conditions. [81] In addition, "click" chemistry, an orthogonal reaction between azide and alkyne functional groups has been utilized to develop *in situ* crosslinkable hydrogels. [63, 82]

The effect of unreacted amine groups on the degradation via hydrolysis was further confirmed by eliminating the amine groups in the hydrogel by chemical reaction. The unreacted amine groups in PEGDA-PEI hydrogels were conjugated with FITC, as stated above. These hydrogels were expected to remain stable in a physiological condition since the free amine groups were all consumed, as compared with unmodified hydrogels which were all shown to undergo degradation. As expected, the FITC-linked hydrogels remained stable in PBS while the unmodified hydrogel became fully disintegrated, which demonstrated that the unreacted amine groups in the PEGDA-PEI hydrogels were responsible for the hydrogel degradation (Figure 3-4).

3.3.5 Degradation of PEGDA-PEI hydrogels

Tunable mechanical properties, combined with the degradation behavior, of *in situ* crosslinkable PEGDA-PEI hydrogels could be an ideal form of injectable delivery applications. Therefore, the release of BSA as a model drug from PEGDA-PEI hydrogels was measured over time and the cumulative drug release vs. time (t) profiles were obtained and analyzed (Figure 3-13, Figure 3-14). The overall release profiles of PEGDA-PEI hydrogels at all M_W of PEGDA interestingly consisted of two different phases occurring in sequence: (1) initial power law curve with fractional time dependence ($\sim t^n$, $0 < n < 1$), followed by (2) an exponential curve which showed the rapid rise in release rate before reaching the endpoint (Figure 3-13a, Figure 3-14a). This result signified that the initial drug release was governed by the swelling behavior of the hydrogels, which stems from the combination Fickian diffusion and chain relaxation of the polymeric network, while the later drug release was further facilitated by the degradation of the hydrogels (Figure 3-13a). [75-77]

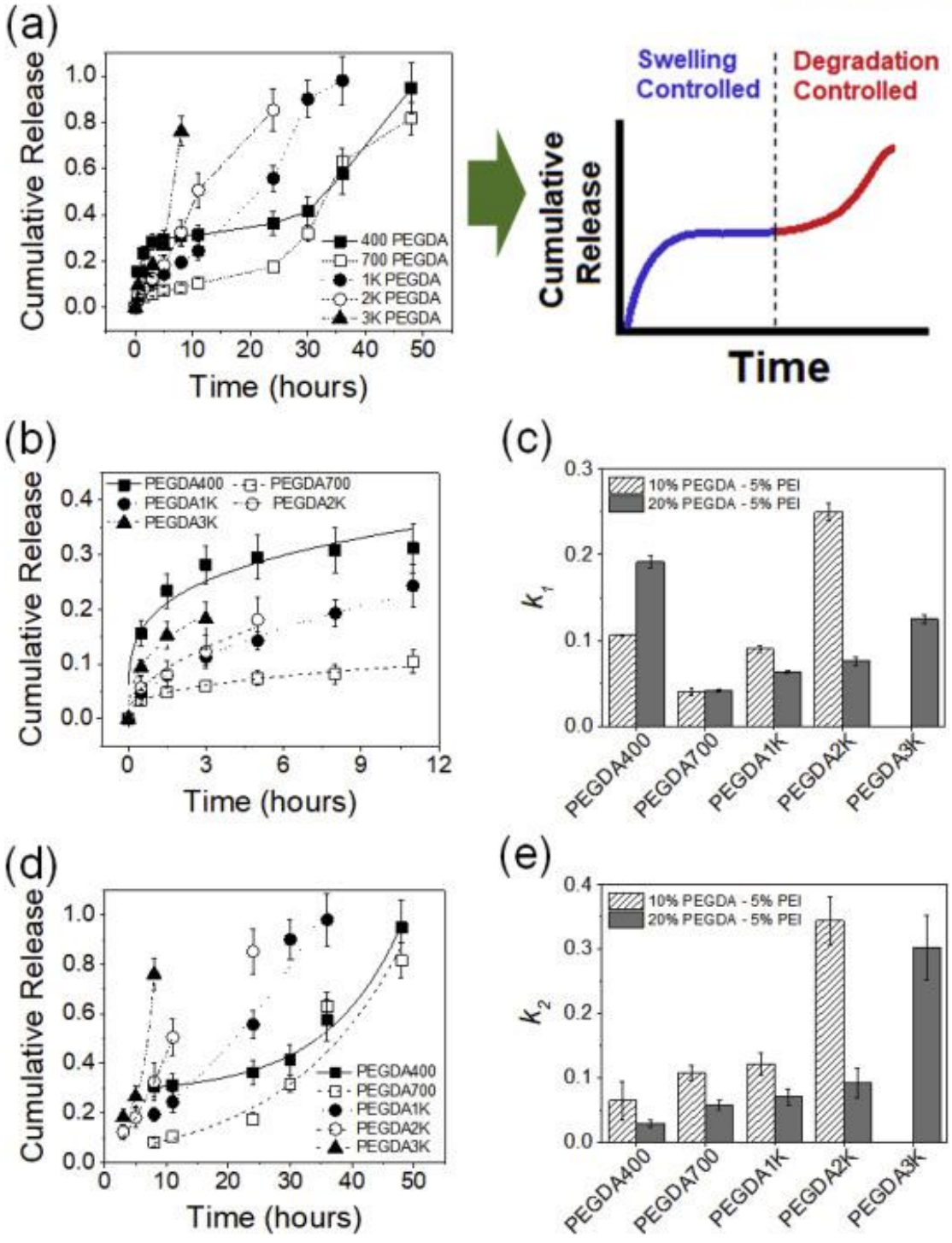

Figure 3-13. (A) The drug release profiles of PEGDA-PEI hydrogels (10% PEGDA with 5% PEI). The profiles consisted of two separate modes of release occurring in sequence; initial swelling-controlled mechanism, followed by degradation-controlled mechanism. (b) The initial drug release profiles were fitted with Eq. 3-2 and (c) the kinetic rate constants (k_1) were obtained. (d) The latter drug release profiles were fitted with Eq. 3-3 and (e) the kinetic rate constants (k_2) were obtained.

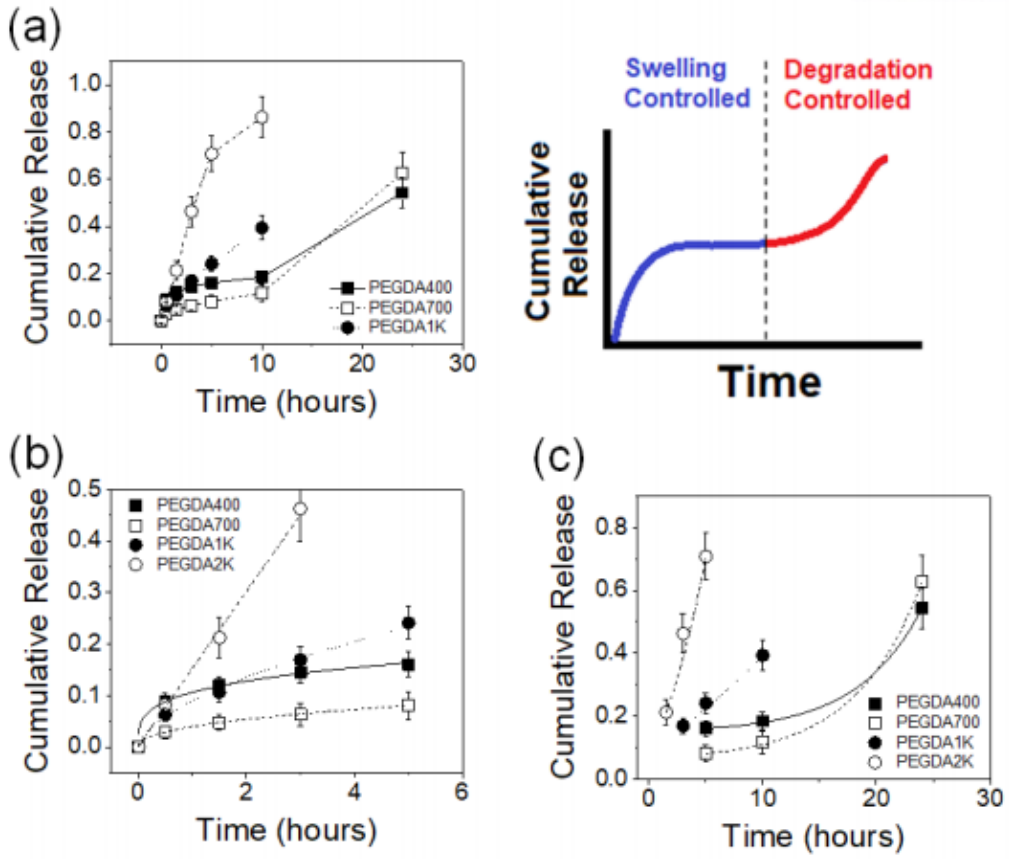

Figure 3-14. (a) The drug release profiles of PEGDA-PEI hydrogels (20 % PEGDA, 5 % PEI). The profiles consisted of two separate modes of release occurring in sequence; initial swelling-controlled mechanism, followed by degradation-controlled mechanism. (b) The initial drug release profiles were fitted with Eq. 3-2, and (c) the latter drug release profiles were fitted with Eq. 3-3. The k_1 and k_2 values obtained from (b) and (c) are shown in Figure 3-13.

The drug release profiles for the first 12 h were first fitted with Ritger-Peppas model (Eq. 3-2) (Figure 3-13b and c, Figure 3-14b). As expected, the kinetic rate constants (k_1) values increased with M_W of PEGDA, from PEGDA700 to PEGDA3K for 20% PEGDA and from PEGDA700 to PEGDA2K for 10% PEGDA, since the release is generally faster from hydrogels with less crosslinking density. The release rate from PEGDA400-PEI hydrogel was surprisingly much higher than any other condition despite having the highest crosslinking density, suggesting the highly elevated hydrophobicity at the lowest M_W PEGDA (i.e. aforementioned high acrylate/ethylene oxide ratio in lower M_W PEGDA) had driven the hydrophilic molecules out of the hydrogels more readily than other conditions.

The subsequent drug release profiles which showed a rapid increase in release rates were then fitted with an exponential drug release model (Eq. 3-3) to account for the drug release governed by the hydrogel degradation and obtain the kinetic release rate constants (k_2) (Figure 3-13d–e, Figure 3-14c). Similar to the trend for degradation kinetics (k_d) in Figure 3-11, the k_2 values increased with M_W of PEGDA for both 10% and 20% PEGDA, thus confirming that the release kinetics following the initial

swelling-controlled mechanism were largely governed by the hydrogel degradation.

This sequential drug release profiles were also demonstrated in the hydrogels crosslinked by varying PEI concentrations for both 10% and 20% PEGDA (Figure 3-15). The trends k_1 values for both 10% and 20% PEGDA were generally inversely related to the mechanical strength of the hydrogels as shown in Figure 3-9, as expected, indicating the initial drug release was mostly governed by the hydrogel diffusion (Figure 3-15a and c). The increase in k_2 values with M_W of PEGDA was more prominent at higher PEI concentrations, pointing to the effect of higher degradation rate at higher PEI concentration on the accelerated drug release (Figure 3-15b and d). Especially, the k_2 value for 10% PEGDA1K-10% PEI was significantly higher than any other condition, which likely stemmed from the combination of weak mechanical strength, as identified by the low elastic modulus shown in Figure 3-9, and the high content of unreacted amine groups facilitating the hydrogel degradation (Figure 3-15b). At lower PEI concentrations, the trend in k_2 values with M_W of PEGDA at 10% followed more closely to that of their mechanical strength, suggesting greater influence of diffusion than degradation on the drug release. Interestingly at 20% PEGDA, the dependence of k_2 values on the hydrogel degradation was more evident, as their trends closely followed those of k_d values in Figure 3-13 (Figure 3-15d). This suggested that for hydrogels with higher crosslinking density having greater mechanical strength and lower diffusion, the effect of degradation on the drug release was much more significant than that of diffusion. These results clearly highlighted that this dual-mode drug release behavior is a unique characteristic of this PEGDA-PEI hydrogel system regardless of the reaction conditions.

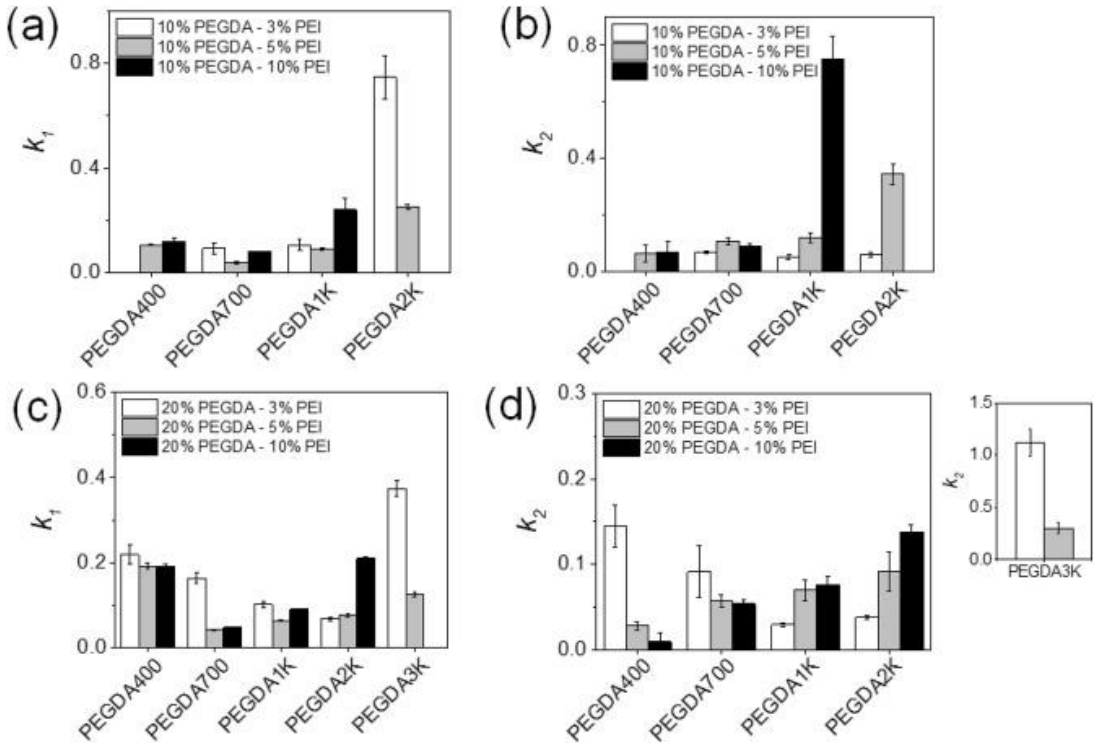

Figure 3-15. k_1 and k_2 values obtained from drug release profiles of PEGDA-PEI hydrogels. (a,b) 10% PEGDA and (c,d) 20% PEGDA linked with varying concentrations of PEI.

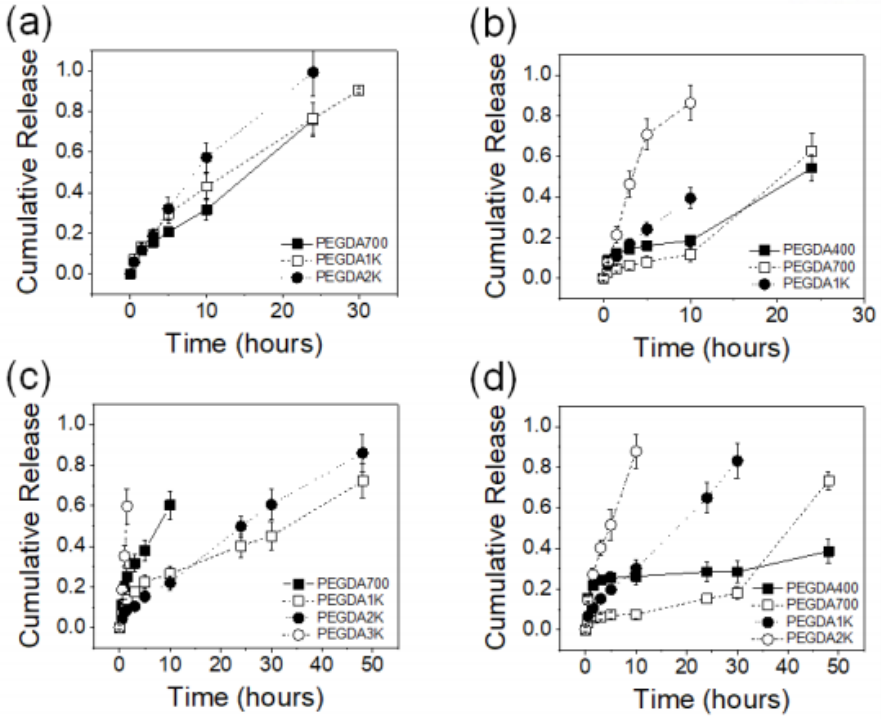

Figure 3-16. The drug release profiles of PEGDA-PEI hydrogels. (a) 10 % PEGDA with 3 % PEI, (b) 10 % PEGDA with 10 % PEI, (c) 20 % PEGDA with 3% PEI, (d) 20 % PEGDA with 10% PEI.

3.4 Conclusion

In this study, mechanical properties and degradation behavior of PEGDA-PEI hydrogels prepared by *in situ* crosslinking between PEGDA and PEI via Michael addition were explored. The abundance of free amine groups in PEI, as well as tunable number of acrylic groups of PEGDA via variable M_W and concentration, allowed for facile crosslinking reaction to form hydrogels under mild, physiological conditions without the need of a catalyst. Mechanical properties of the PEGDA-PEI hydrogels could be controlled in a wide range by varying the concentrations of PEGDA and PEI, as well as the M_W of PEGDA. Interestingly, the hydrogels all underwent complete degradation, likely due to the unreacted amine groups responsible for the hydrolysis via local basic environment or the direct nucleophilic attack on the ester linkages. This combination of tunable mechanical properties and degradation behavior of the PEGDA-PEI hydrogels was highly effective in modulating the rate and mode of drug release by sequential swelling- and degradation-controlled mechanisms. Taken together, this *in situ* crosslinkable hydrogel system with tunable physical properties as well as injectability is expected provide an efficient and effective platform for biomedical applications.

CHAPTER 4. In situ facile-forming chitosan hydrogels with tunable physicomechanical and tissue adhesive properties by polymer graft architecture

4.1 Introduction

Hydrogels have become an indispensable part of biomedical engineering, as carriers of biologically-relevant therapeutic molecules (e.g. drugs, proteins, DNA) for drug delivery and artificial extracellular matrices (ECM) for tissue engineering. [15, 49, 83] With increasing awareness of importance of cellular microenvironment, hydrogels are growingly utilized as cell-culture platform for fundamental biological investigation. [84-86] In addition, the hydrogels are increasingly translated into commercial products in personal care and medical markets, such as wound dressing, adhesives, and cosmetics. [2] Hydrogels, unlike other types of materials commonly used in biomedical applications such as nanofibers and elastomers, possess a unique blend of controllable elasticity and hydrophilicity (i.e. high water content) that allow for broad applicability.

Most hydrogels are generated by employing chemical reactions to crosslink hydrophilic monomers or macromers. For example, radical polymerization is commonly adopted for unsaturated compounds for fast reaction rate and wide range of materials; in addition to small molecules, such as acrylamide, acrylic acid, methyl methacrylate, and 2-hydroxyethyl methacrylate, macromers devoid of radically active functional groups can be easily rendered as such by simple chemical reactions, such as poly(ethylene glycol) diacrylate, methacrylate-conjugated gelatin and alginate. [54, 87] The radical polymerization requires the use of initiators, which often becomes problematic for bioencapsulation due to possible toxicity. Even for those deemed biocompatible (e.g. Irgacure2959, lithium phenyl-2,4,6-trimethylbenzoylphosphinate ('Li-TPO'), and 2,2'-azobis[2-methyl-N-(2-hydroxyethyl)propionamide] ('VA-086') [88, 89], it is still difficult to keep the initiator concentration low enough to maintain the biocompatibility while allowing enough chemical reactions to form hydrogels.

The hydrogels formed by spontaneous chemical reaction between two macromers have gained significant research interest over the last two decades. Broadly termed as "*in situ* forming" hydrogels, they have the advantage of biocompatible fabrication as they can be formed by mild chemical reactions without the use of cytotoxic initiators under physiologically-relevant conditions (e.g. ambient temperature, neutral pH. [5, 90, 91] For example, Hubbell and co-workers were one of the first to report the hydrogel fabrication under mild conditions via Michael addition reaction between thiol and vinyl groups and biocompatible cell encapsulation. [67, 92] Schiff base, an imine linkage formed by the addition between amine and carbonyl groups followed by dehydration, similarly has been utilized to

generate hydrogels. [93-96] Due to this mode of hydrogel fabrication, the *in situ* forming hydrogels have been considered especially attractive as a tissue injectable and implantable form for biomedical applications, allowing spontaneous hydrogel formation upon delivery. [91, 97-99]

One of the major challenges of *in situ* forming hydrogel is the control of mechanical properties in a wide range while appropriately maintaining the rate of crosslinking reaction, at least within a manageable range for practical handling. Since the mechanical properties are governed by the crosslinking density which also controls the rate of gelation (i.e. the hydrogel forms faster at higher crosslinking density, and slower at lower crosslinking density). As a result, the hydrogel with low mechanical strength may be too slow to form, while it may form too fast to allow handling and processing for the hydrogel with greater mechanical strength. For radical polymerization, on the other hand, the rate of hydrogel formation is largely determined at initiation and can be effectively controlled by the initiation parameters, such as initiator concentration and degree of activation (e.g. heat, light, and amount of co-initiator). [16, 100]

In this study, physical properties of gel-forming polymer were varied to control the mechanical properties of *in situ* forming hydrogels, while effectively maintaining the gelation kinetics. Chitosan was chosen as the gel-forming polymer, widely used in biomedical applications for its innate anti-microbial properties as well as biocompatibility and abundant natural source. [96, 101-104] More significantly, an extensive number of amine groups on chitosan, one on each saccharide monomer, provides ample avenue for chemical modifications, including various nucleophilic reactions for *in situ* forming hydrogels. Here, hydrophilic poly(ethylene glycol) (PEG) chains were conjugated onto the chitosan backbone with varying graft length and density ('PEG-*g*-*Cs*'), and their effect on the mechanical properties of the resulting hydrogels crosslinked via Schiff base formation were evaluated (Figure 4-1). The chitosan with PEG graft architecture not only served to control the physicomechanical properties of hydrogels, it also allowed the chitosan to be readily dissolved in neutral aqueous solutions, by removing some of the amine groups in chitosan (i.e. native polycationic chitosan only dissolves in acidic conditions). [105, 106] In addition, the physical dimension (i.e. chain length) of the crosslinker, PEG-dialdehyde, was also varied to further control the gel mechanics by modulating the interaction with polymer grafts. To further illustrate their potential application as tissue sealant, the adhesive properties of the *in situ* forming Cs-PEG hydrogels on biological tissues were examined both *ex vivo* and *in vivo*.

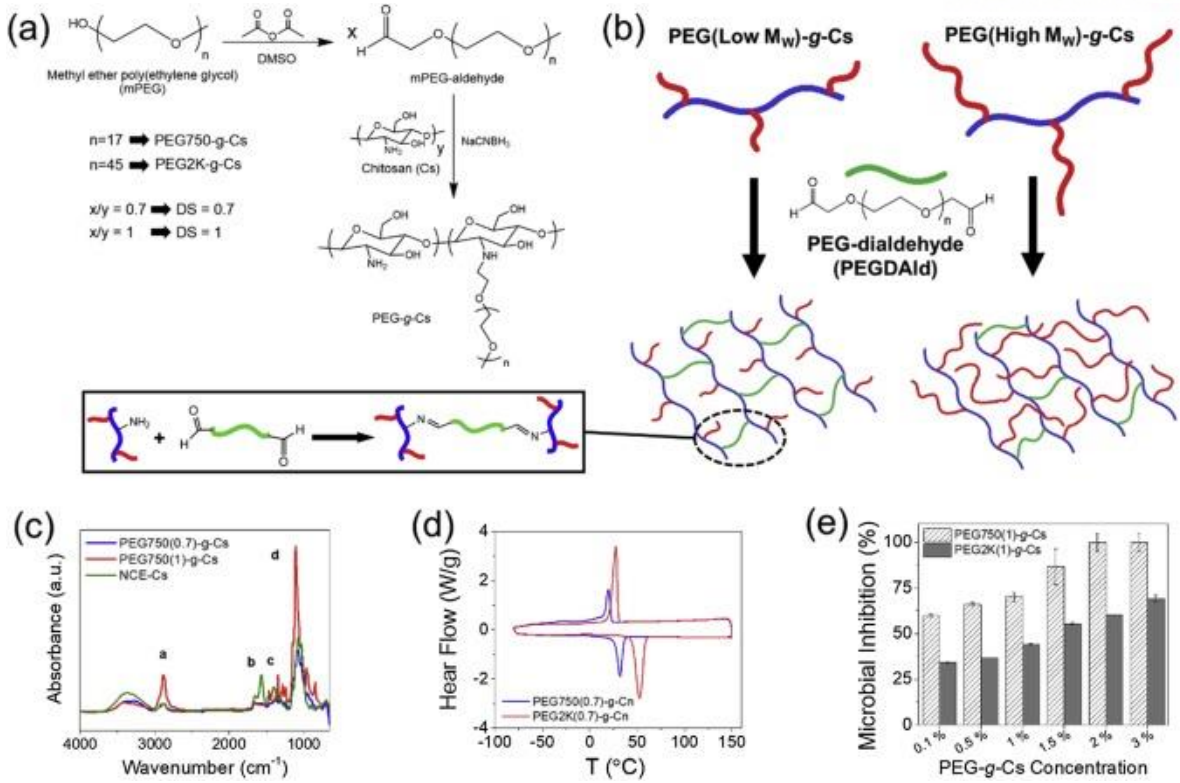

Figure 4-1. (a) PEG grafting of chitosan (PEG-*g*-Cs). mPEG was first oxidized to present aldehyde groups (mPEG-aldehyde), which was then reacted with chitosan via Schiff base formation. Sodium cyanoborohydride was used to irreversibly reduce the Schiff base into secondary amine. (b) Schematic representation of *in situ* forming PEG-*g*-Cs hydrogel, with PEG-dialdehyde (PEGDAld) as a crosslinker. (c) FT-IR spectra of PEG750-*g*-Cs (a: ν_s(C-H), b: ν_s(C-O-O)(anti) (carboxylic acid salt), c: ν_s(C-N), d: ν_s(C-O-C)(anti)). (d) DSC curves of PEG750(0.7)-*g*-Cs and PEG2K(0.7)-*g*-Cs. (e) The microbial inhibition rates of PEG750(1)-*g*-Cs and PEG750(1)-*g*-Cs.

4.2 Materials and Methods

4.2.1 Synthesis of PEG-grafted chitosan ('PEG-g-Cs') and PEG-dialdehyde

Chitosan conjugated with poly(ethylene glycol) (PEG) with varying lengths and density was synthesized by a two-step process: (1) the synthesis of methyl ether PEG (mPEG)-aldehyde and (2) the conjugation of mPEG-aldehyde onto the chitosan. [107, 108]

First, PEG with an aldehyde end group was synthesized by the oxidation of methyl ether PEG (mPEG). mPEG (M_W of 750 or 2000 g mol^{-1}, mPEG, Sigma Aldrich) was first dissolved in dimethyl sulfoxide (DMSO)/chloroform (8:2 volume ratio, Samchun Chemicals, Korea) at 20 wt%. DMSO/chloroform was treated with dry molecular sieve (3 Å, Sigma Aldrich) to remove residual water and sonicated for 30 minutes for degassing. Acetic anhydride (Sigma Aldrich) was added to the mixture and continuously

stirred at room temperature for 24 hours under dry N_2. The molar ratio of mPEG to acetic anhydride was 1:3. The mixture was precipitated and washed twice with excess diethyl ether, and then dried under vacuum to obtain mPEG-aldehyde.

Chitosan was reacted with mPEG-aldehyde via Schiff base reaction to develop PEGylated chitosan (PEG-*g*-Cs). Briefly, 1 g chitosan (Cat#448869, low M_W, 75-85 % deacetylation, Sigma Aldrich) was dissolved in a mixture of 40 mL acetic acid solution (2 wt%, Samchun Chemicals, Korea) and 20 mL methanol (Samchun Chemicals, Korea). mPEG-aldehyde, as synthesize above, was added to the mixture and stirred for 30 min. Two different grafting densities (DS) of mPEG on chitosan, defined by the feed molar ratio of mPEG-aldehyde to saccharide groups in chitosan, were prepared; 0.7 and 1. Then, the pH of the mixture was adjusted to 6 with a slow addition of 1 M NaOH and stirred for 1 hour. In this step, ultrasonication was applied (VCX130, Sonic) in a pulse mode (output power: 65 W, frequency: 70 kHz, pulse: 30 seconds on, 10 seconds off) until the aggregation disappeared. Sodium cyanoborohydride (0.7 molar equivalent of added mPEG-aldehyde, Sigma Aldrich) was added and continuously stirred for 24 hours to reduce the Schiff base to irreversible secondary amine. The entire process was done at room temperature. The mixture was extensively dialyzed against deionized (DI) water and the product was obtained by lyophilization. The PEG grafting density and length were evaluated by FT-IR spectroscopy (Cary 670, Agilent), ^{1}H-NMR spectroscopy (400 MHz, Avance III, Bruker), and differential scanning calorimetry (Q200, TA Instruments).

The degree of substitution (DS_{PEG}), defined as the percentage of amine groups substituted with PEG grafts, was determined indirectly by measuring the amount of remaining amine groups via 2,4,6-trinitrobenzenesulphonic acid (TNBS) assay. Briefly, 0.05 mL of PEG-*g*-Cs sample in DI water and 0.05 mL of TNBS working solution (0.1 % TNBS, 4 % NaHCO3, pH 8.5) were mixed and incubated in 37 °C for 2 hours. Afterwards, 0.05 mL of 10 % sodium dodecyl sulfate and 0.05 mL of 1 M HCl. The absorbance at 335 nm (Abs_{335}) was measured using a spectrophotometer (Synergy HTX, BioTek). DS_{PEG} was calculated using the following equation,

$$\mathrm{DS_{PEG}} = \frac{Abs_{335}(\mathrm{Cs}) - Abs_{335}(\mathrm{PEG\text{-}g\text{-}Cs})}{Abs_{335}(\mathrm{Cs})} \times 100 \qquad \text{Eq. 4-1}$$

where Abs_{335}(Cs) and Abs_{335}(PEG-*g*-Cs) were the absorbance values at 335 nm for unmodified chitosan and PEG-*g*-Cs, respectively. The grafting efficiency (GE_{PEG}), defined as the percentage of mPEG-aldehyde reacted with chitosan, was calculated as the percentage of experimental DS_{PEG} from theoretical DS_{PEG}. (Table 4-1).

Samples	DS_{PEG} (%)
PEG750(0.7)-g-Cs	26.5 ± 0.8
PEG2K(0.7)-g-Cs	30.7 ± 1.6
PEG750(1)-g-Cs	35.8 ± 0.7
PEG2K(1)-g-Cs	36.2 ± 1.2

Table 4-1. DS_{PEG} of various PEG-*g*-Cs

PEG-dialdehyde as the crosslinker for PEG-*g*-Cs was synthesized by acetic anhydride/DMSO oxidation of PEG, as similarly done for mPEG-aldehyde. Instead of mPEG, PEG having hydroxyl groups on both ends was used. Briefly, PEG was first dissolved in DMSO/chloroform (8:2) at 20 wt%, followed by the addition of acetic anhydride. The molar ratio of hydroxyl groups of PEG to acetic anhydride was 1:3. The mixture was continuously stirred at room temperature for 24 hours. The product was obtained by precipitation in excess diethyl ether. Three different M_Ws of PEG, 2000, 3400, and 6000, were used (Sigma Aldrich).

4.2.2 Fabrication of Cs-PEG hydrogels

Stock solutions of PEG-*g*-Cs (8 % for PEG750-*g*-Cs, 10 % for PEG2K-*g*-Cs) and PEG-dialdehyde (60 %) were prepared in DI water. The solutions were thoroughly mixed, placed between two glass plates (1 mm spacer), and incubated at 37 °C to allow Cs-PEG hydrogel formation. Hydrogel disks (8 mm diameter) were punched out and kept in phosphate buffered saline (PBS, pH 7.4) before characterization. The range of concentrations of PEG-*g*-Cs was 3-8 %, while that of PEG-dialdehyde was 5-20 %. At a given PEG-*g*-Cs concentration, only the M_W of PEG-dialdehyde was varied while keeping the concentration. For measuring adhesive properties, the stock solutions were placed in separate containers of a dual syringe (Nordson EFD), and extruded out of the single outlet of the syringe together, and onto a biological tissue sample. The two solutions joined prior to exiting the syringe, and the mixture became a clear, homogeneous solution without apparent phase separation, as they passed through the narrow outlet.

4.2.3 Mechanical and rheological properties of Cs-PEG hydrogels

The mechanical properties of Cs-PEG hydrogel were measured by uniaxial compression experiments (Model 3343, Instron). [94, 95, 109] Each hydrogel disk was compressed at the rate of 1 mm min^{-1} and a stress-strain curve was obtained. The elastic modulus was calculated as the slope of the stress-strain curve at the first 10 % strain. For each condition, the mean and standard deviation values were reported ($n = 6$).

Gelation kinetics of Cs-PEG hydrogel was evaluated using a rotating-disk rheometer (Kinexus,

Malvern). [72, 94] The storage moduli (G') and loss moduli (G'') of the mixture of PEG-*g*-Cs and PEG-dialdehyde solutions were measured over time at 37 °C in a small-amplitude oscillatory shear mode. The frequency and strain of the rotating disk were 1 Hz and 10 %, respectively. The gelation time was determined by the time at which G' crossed over and exceeded the G''.

4.2.4 Diffusional properties of Cs-PEG hydrogels

The diffusional properties of Cs-PEG hydrogels were evaluated by measuring their swelling ratios and drug release profiles. The weight of a fully swollen hydrogel, obtained by incubating in PBS at 37 °C for 24 hours, and that of a dried gel mesh, obtained by lyophilization, were measured. The swelling ratio was calculated as the weight ratio of swollen hydrogel to dry gel mesh. Drug release characteristic from Cs-PEG hydrogels were evaluated using bovine serum albumin (BSA, Sigma Aldrich) as a model protein drug. BSA (5 mg mL^{-1}) was encapsulated into Cs-PEG hydrogel by dissolving in the PEG-*g*-Cs stock solution prior to hydrogel fabrication. Each hydrogel disk was incubated in 0.5 mL PBS at 37 °C and the BSA released to the medium was analyzed using BCA™ Protein Assay kit (Thermo Fisher), following the manufacturer's instructions. The cumulative drug release profile was fitted to the following Ritger-Peppas equation,

$$\frac{M_t}{M_\infty} = k \cdot t^n \qquad \text{Eq. 4-2}$$

M_t is the amount of drug released at a time, t, M_∞ is the total amount of drug in the hydrogel, k is the kinetic rate constant, and n is the exponent related to the release mechanism. [43, 93, 95]

4.2.5 Tissue adhesive properties of Cs-PEG hydrogels

Ex vivo lap-shear test. The adhesive properties of Cs-PEG hydrogel were measured based on a standard method for strength properties of tissue adhesives in lap-shear by tension loading (ASTM F2255-05). [103, 110-112] The measurements were performed using porcine skin (purchased from Biozoa Biological Supply Co., Korea). The skin specimens (15 × 25 mm each) were first washed by immersing in PBS at 37 °C for 1 hour, and each glued to an acrylic fixture using cyanoacrylate glue. Afterwards, Cs-PEG mixture (100 μL) was spread on the surface of one skin specimen, immediately covered with another specimen, and incubated at 37 °C to allow hydrogel formation. After curing, the set-up was loaded onto the universal testing machine (Model 3343, Instron) via the acrylic fixture on tensile grips, and then uniaxially elongated at the rate of 10 mm min-1 until the hydrogel broke and the two skin specimens separated.

From the stress-strain curve obtained, several parameters for adhesive properties were obtained. The shear modulus was calculated as the slope at the first 10 % strain. The adhesive strength was calculated by dividing the maximum load by the bond area. The fracture energy was calculated by dividing the

integral of the force-elongation curve by the adhesion area until the adhesion failed. For each condition, the mean and standard deviation values were reported (n = 12).

Ex vivo burst pressure test. The adhesive properties of Cs-PEG hydrogel were alternatively measured by applying hydraulic pressure to Cs-PEG hydrogel attached to the porcine skin tissue to measure burst pressure, based on an ASTM standard test (ASTM F2392-04). [111, 113, 114] The burst pressure experiments were performed using a custom-built device consisting of an electronic pump (Legato100, KD Scientific), a pressure gauge (P421 series, Wise Control Inc., Korea), and a cylindrical fluid chamber (2 cm diameter, 5 cm height, open top), all connected via plastic tubing. The sample was first prepared by applying Cs-PEG mixture (150 u L) to a hole (5 mm diameter) in a porcine skin specimen. After gelation, the skin specimen was attached on top of the fluid chamber and firmly fastened with a cable tie to prevent fluid leakage. Then, PBS was injected into the fluid chamber via the electronic pump at 3 mL min^{-1} until the adhesive broke and visible fluid leaked. The burst pressure was reported as the maximum pressure recorded during the measurement. For each condition, the mean and standard deviation values were reported (n = 12).

In vivo skin wound closure test. To investigate the *in vivo* biocompatibility and skin wound closure properties of Cs-PEG hydrogel as tissue sealant, a rat skin incision model was used with the approval from Institutional Animal Care and Use Committee (#UNISTIACUC-18-22) of Ulsan National Institute of Science and Technology (UNIST). [110, 115] Normal Sprague Dawley (SD) rats (Male, 3 weeks, 50 g, Hyochang Science, Korea) were anesthetized using isoflurane (liquid for inhalation, TerrellTM) and shaved off their backs. 20 mm long incision was made on the rat's back. Then, 300 μL of a tissue sealant was evenly applied along the incised area using a custom-made syringe (0.75 mm thickness, 8 mm wide). Untreated and sutured samples were used as control groups. After 1 day to allow the incised tissue to close, the hydrogel adhesive was removed.

The wound recovery process was monitored up to five days with photography and optical coherence tomography (OCT) imaging. The detailed specifications of the OCT device used in this study are provided in the Supplementary Information. The OCT enabled non-invasive 3D imaging and monitoring morphological changes of deep tissue with high resolution. [116, 117] Using this technology, the skin tissue down to hypodermal layer surrounding the wound area covered by tissue sealant was imaged and analyzed in real-time throughout the experiment.

On day 3, the animals, one from each condition, were sacrificed and the tissue sections around the wound site were harvested for histological evaluation. A standard hematoxylin and eosin (H&E) staining was performed on the tissue sections, and visualized with an inverted optical microscope (CKX53, Olympus). All the *ex vivo* and *in vivo* adhesion tests were performed with a commercially available fibrin hydrogel adhesive, Beriplast® P (CSL Behring GmbH, Germany), as a control group.

4.2.6 Anti-microbial properties of PEG-g-Cs

The anti-microbial properties of PEG-*g*-Cs were evaluated by a standard broth dilution method.[118, 119] Briefly, a small piece of colony of *E. coli* on agar plate was transferred to a saline solution (0.9 wt% NaCl) and mixed well with vortexing. McFarland diluent (0.05mL of 0.005 % $BaCl_2$ and 0.995 % H_2SO_4 in DI water) was added until the absorbance at 600 nm becomes 0.25~0.3 (i.e. McFarland standard). A sample solution was prepared by mixing 100 μL of PEG-*g*-Cs solution with 50 μL Mueller-Hinton Broth medium (MHB, Sigma Aldrich) and 50 μL McFarland standard, and placed in a well of a 96-well plate. The plate was incubated at 37 °C with gentle shaking, and the absorbance at 600 nm was measured at different times up to 12 hours using a spectrophotometer (Multiskan GO, Thermo Fisher). Pure MHB solution (200 μL of MHB) was used as a negative control, and bacteria solution (150 μL of MHB and 50μL of McFarland standard) as a positive control.

Alternatively, the anti-microbial properties of PEG-*g*-Cs hydrogels were determined. Briefly, 5 % PEG-*g*-Cs and 20 % PEGDAld in LB medium with varying M_W were mixed together and placed into 24-well plates. After Cs-PEG hydrogels were formed, each hydrogel surface was inoculated with 50 μL of *E. coli* solution by streaking across the hydrogel surface. After 16 hours of culture at 37 °C, the bacterial growth on the hydrogel surface was visualized by staining with MTT solution (3-(4,5-dimethylthiazol-2-yl)-2,5-diphenyltetrazolium bromide, Sigma Aldrich), which turned live bacteria brown-purple. A standard LB agar plate was used as a control.

4.2.7 Swept-Source Optical Coherence Tomography (SS-OCT)

The swept source laser (Axsun Technologies, Inc., US) integrated into the SS-OCT system has 1,310 nm center wavelength and 110 nm tuning range with a sweep rate of 20 mW and axial resolution of ~ 8 μm in tissue. The light emitted from the swept source laser moved along the fiber optics based on Mach-Zehnder interferometry and it split into sample arm and reference arm following fiber coupler and a circulator. The sample arm responsible for imaging of the skin sample was composed of a collimator, two-axis galvanometer scanner, and objective lens providing lateral resolution of ~ 15 μm in tissue. Reflected light from the sample and reference arm were combined and these interference signals converted to an electrical signal by a balanced photodetector (PDB450C, Thorlabs Inc., US). The electrical signals digitized by a digitizer (ATS9350, AlazarTech Inc., Canada), and then an intensity-based image was generated. The intensity-based 1D arrays called A-line images were accumulated using a galvanometer scanner in the sample arm to reconstruct a 2D OCT image which is the cross-sectional image of the sample. Also, a 3D OCT image which has volumetric information of the skin can be obtained by an accumulation of the 2D OCT images using the scanner.

4.3 Results and Discussion

4.3.1 Synthesis and physical properties of PEG-g-Cs

Chitosan is a highly unique cationic polysaccharide biopolymer, obtained by deacetylation of N-acetylglucosamine units of naturally-occurring chitin to generate a significant amount of secondary amine-containing N-glucosamine units. [96, 101, 102, 120] In addition to biocompatibility, this highly polycationic nature renders chitosan natural anti-microbial properties (i.e. polycations are known to disrupt bacterial cell walls). Hydrogels made from chitosan have been extensively investigated not only in biomedical applications such as drug delivery, tissue scaffolds, and wound dressings, but also in environmental applications, mostly for removing toxin via adsorption. However, there are several issues that need to be addressed for more complete biomedical utilization of chitosan. First, the polycationic nature only allows dissolution in acidic aqueous conditions, preventing biocompatible encapsulation of biological molecules (e.g. proteins and DNAs) and cells. Second, it is difficult to control the mechanical properties of chitosan hydrogels, with high viscosity of chitosan limiting the range of concentration. Third, since chitosan hydrogels are commonly fabricated by anionic crosslinkers such as glycerophosphate and tripolyphosphate, there is a possibility of losing their long term stability with ion leaching.

To overcome these limitations, *in situ* forming chitosan hydrogels with varying mechanical properties were developed. Chitosan was first conjugated with hydrophilic PEG chains with varying length and density, PEG-*g*-Cs (Figure 4-1a). This PEG-graft architecture of chitosan served two purposes; eliminate some of the amine groups and increase the hydrophilicity to allow dissolution in neutral aqueous conditions, and control the mechanical properties of resulting hydrogels by modulating the physical interaction with crosslinking molecule, PEG-dialehdyde (PEGDAld). *In situ* forming mechanism also has the advantage of biocompatible hydrogel formation without the need for potentially toxic initiators, and more scalable mechanics and structural durability over ionic crosslinking.

The length of PEG graft on PEG-*g*-Cs was controlled; 750 (‘PEG750’) and 2000 (PEG2K) g mol^{-1}, while the grafting density was also controlled; 0.7 and 1 feed molar equivalents of saccharide groups in chitosan. They are designated as PEG750(0.7)-*g*-Cs, PEG750(1)-*g*-Cs, PEG2K(0.7)-*g*-Cs, and PEG2K(1)-*g*-Cs. The degree of substitution of PEG grafts, experimentally determined via TNBS assay, indeed showed greater grafting density for PEG(1)-*g*-Cs than PEG(0.7)-*g*-Cs (Table 4-1). Unlike unmodified chitosan, PEG-*g*-Cs also showed very high aqueous solubility at neutral pH, with maximum aqueous solubility of 8 % and 10 % for PEG750-*g*-Cs and PEG2K-*g*-Cs, compared to 6 % for NCE-Cs. This further demonstrated that the hydrophilic PEG grafts could facilitate greater water solvation, and longer PEG grafts allowed greater separation between chitosan chains.

Spectroscopic and calorimetric characterizations of PEG-g-Cs. The PEGylation was confirmed with NMR, FT-IR, and DSC analyses, with N-carboxyethyl chitosan (NCE-Cs), a widely-investigated form of substituted chitosan for neutral buffer solubility, serving as a control group. [73, 121, 122] ^{1}H-NMR and FT-IR spectra both showed peaks corresponding to PEG grafts for PEG-*g*-Cs, confirming the presence of PEG grafts (Figure 4-1c, Figure 4-2**,** and Figure 4-3).

DSC thermograms of PEG750-*g*-Cs and PEG2K-*g*-Cs showed characteristic endothermic peaks at 34 °C and 54 °C, respectively, which corresponded to T_m and ΔH of PEG grafts on chitosan (Figure 4-1d, Figure 4-4). In addition, ΔH of PEG grafts for PEG2K-*g*-Cs was much higher than that of PEG750-*g*-Cs. Furthermore, ΔH of PEG grafts increased with graft density, more so for PEG2K-*g*-Cs. These findings demonstrated that the PEG grafts on chitosan allowed their crystallization, and the degrees of crystallinity increased with the graft length and density. [123] On the other hand, NCE-Cs, devoid of PEG grafts, did not show such melting phenomena at the same temperature. Overall, these analyses all confirmed the controlled PEG graft length and density of PEG-*g*-Cs.

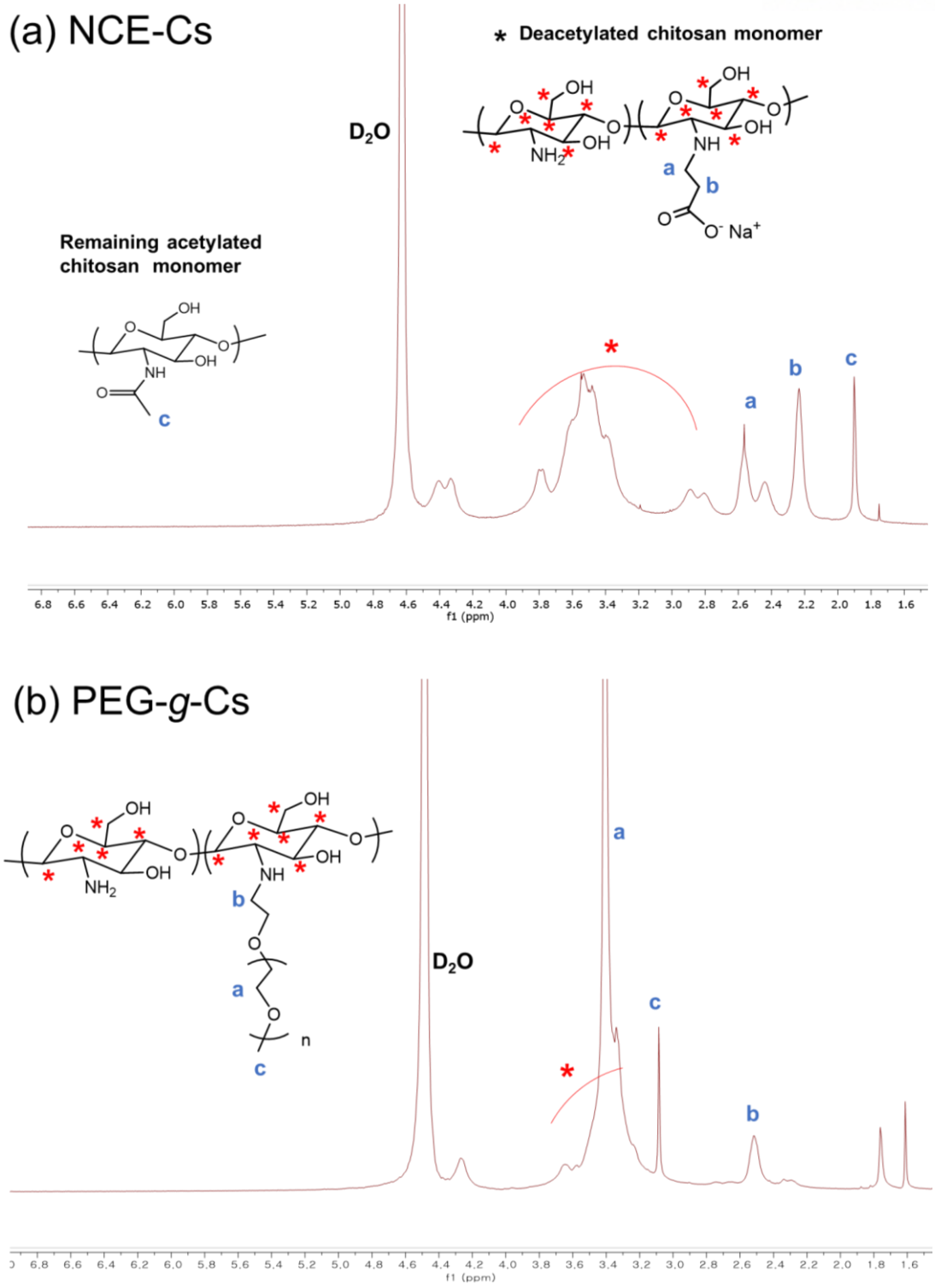

Figure 4-2. Representative ^{1}H-NMR spectra of (a) N-carboxyethyl chitosan (NCE-Cs) and (b) PEG-*g*-Cs. Characteristic peaks corresponding to N-carboxyethyl and PEG are assigned.

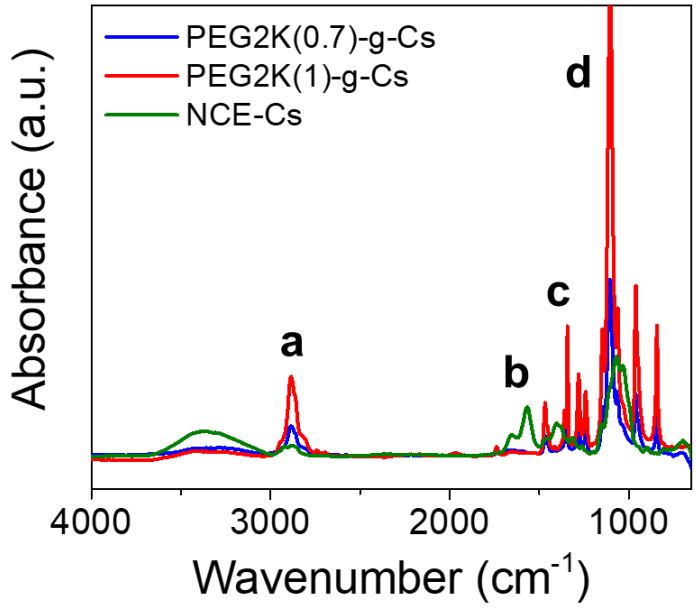

Figure 4-3. FT-IR spectra of PEG2K-*g*-Cs. a: ν_s(C-H), b: ν_s(C-O-O)(anti) (carboxylic acid salt), c: ν_s(C-N), d: ν_s(C-O-C)(anti)

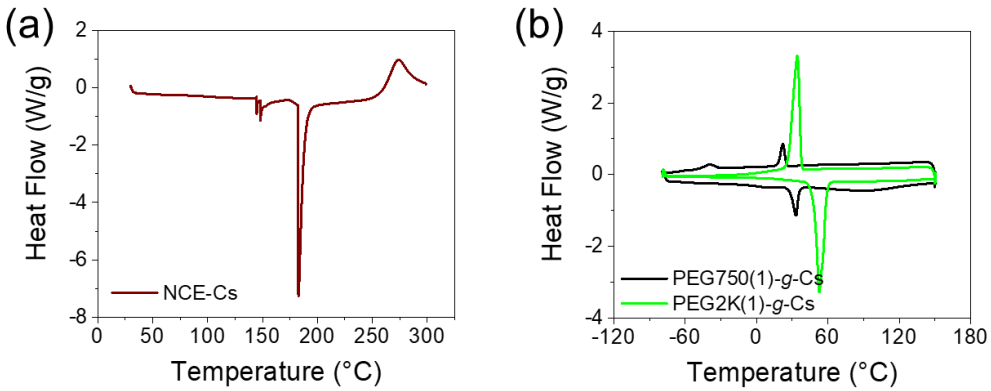

(c)

	T_m (PEG) (°C)	ΔH (J/g)
PEG750(0.7)-*g*-Cs	34.6 ± 1.7	6.2 ± 2.7
PEG750(1)-*g*-Cs	33.8 ± 2.3	15.8 ± 3.2
PEG2K(0.7)-*g*-Cs	54.1 ± 2.5	89.6 ± 4.2
PEG2K(1)-*g*-Cs	53.4 ± 1.6	124.9 ± 11.4

Figure 4-4. Representative DSC curves of (a) N-carboxyethyl chitosan (NCE-Cs) and (b) PEG-*g*-Cs. (c) T_m and ΔH of PEG chains obtained from the peaks corresponding to the melting of PEG chains on Cs.

Anti-microbial activity of PEG-g-Cs. One of the hallmarks of chitosan is the natural anti-microbial activity, owing to its polycationic nature. Since many of the amine groups were converted to PEG grafts, it was plausible that the anti-microbial activity could have been reduced as a result. Therefore, anti-bacterial activity was evaluated by measuring the viability of *E. coli* in response to varying concentrations of PEG750(1)-*g*-Cs and PEG750(1)-*g*-Cs up to 3 % (Figure 4-5) after 12 hours of exposure, and the microbial inhibition, defined as the percentage of decrease in microbial growth from the positive control (no treatment), was calculated (Figure 4-1e). For PEG750(1)-*g*-Cs, there was almost a complete microbial growth arrest at 2 % and above, and with gradual decrease in anti-microbial activity with decreasing concentrations. Even at the lowest concentration at 0.1 %, the microbial activity was inhibited by 65 %, demonstrating significant anti-microbial effect. For PEG2K(1)-*g*-Cs, on the other hand, the anti-microbial activity was reduced, likely due to the increased portion of PEG relative to chitosan. Nonetheless, significant microbial inhibition was demonstrated at various concentrations of PEG2K(1)-*g*-Cs; 70 % inhibition at 3 %, 64 % inhibition at 2 %, and 55 % inhibition at 1.5 %. It should be noted that after initial growth inhibition, there is a gradual microbial growth over time, likely due to the small amount of remaining bacteria growing in the culture media.

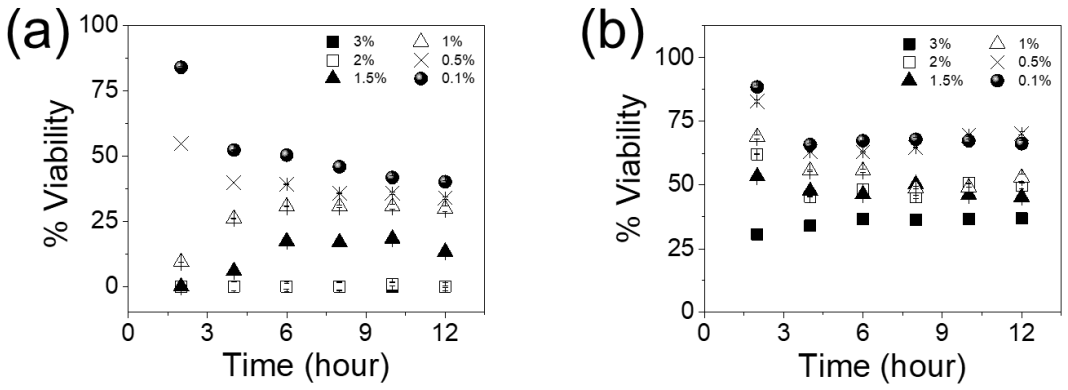

Figure 4-5. Anti-bacterial properties of (a) PEG750(1)-*g*-Cs and (b) PEG2K(1)-*g*-Cs at various concentrations by measuring the viability of *E. coli* over time.

4.3.2 Mechanical properties of Cs-PEG hydrogels

In order to fabricate hydrogels by *in situ* chemical reaction, PEGDAld was used as a crosslinker which is able to undergo Schiff base reaction with amine groups of PEG-*g*-Cs. The M_W of PEGDAld was varied, 2000 ('2K'), 3400 ('3.4 K') and 6000 ('6K') g mol^{-1}, to control the mechanical properties of the resulting "Cs-PEG" hydrogels by varying the number of reactive functional groups; PEGDAld with higher M_W would have less reactive functional groups at the same concentration. Furthermore, the chain length of the polymeric crosslinker could influence the physical interaction with PEG-*g*-Cs, especially with regards to varying PEG graft length and density.

First, for a PEG-*g*-Cs with given concentration and PEG grafting density at 0.7, the M_W of the PEGDAld was varied while keeping the concentration at 20 % to develop Cs-PEG hydrogels. At 3 %

PEG750(0.7)-*g*-Cs, the elastic modulus (*E*) was the highest at intermediate M_W of PEGDAld (PEGDAld3.4 K), and the lowest at low M_W PEGDAld2K, suggesting there is an optimal chain length for maximal crosslinking reaction (Figure 4-6a). It is especially interesting that the hydrogel crosslinked with PEGDAld2K, which had the most reactive functional groups, had the lowest *E*, which further highlighted the importance of proper physical interaction between two polymers. It was possibly due to the difficulty of shorter PEGDAld to crosslink PEG-*g*-Cs chains with steric hindrance by surrounding PEG grafts (Figure 4-6e). [124-126] On the other hand, further reduced number of reactive groups for high M_W PEGDAld also likely caused the decrease in *E* even with greater accessibility. When the concentration was increased to 5 % PEG750(0.7)-*g*-Cs, *E* increased at all M_W of PEGDAld, as expected. But the *E* increased with the M_W of PEGDAld, with the maximum value at PEGDAld6K, rather than the intermediate PEGDAld3.4 K. It is speculated that at higher concentration, with greater steric hindrance by PEG grafts on chitosan for PEGDAld to overcome, it was more difficult for low and intermediate M_W PEGDAld to undergo crosslinking reaction.

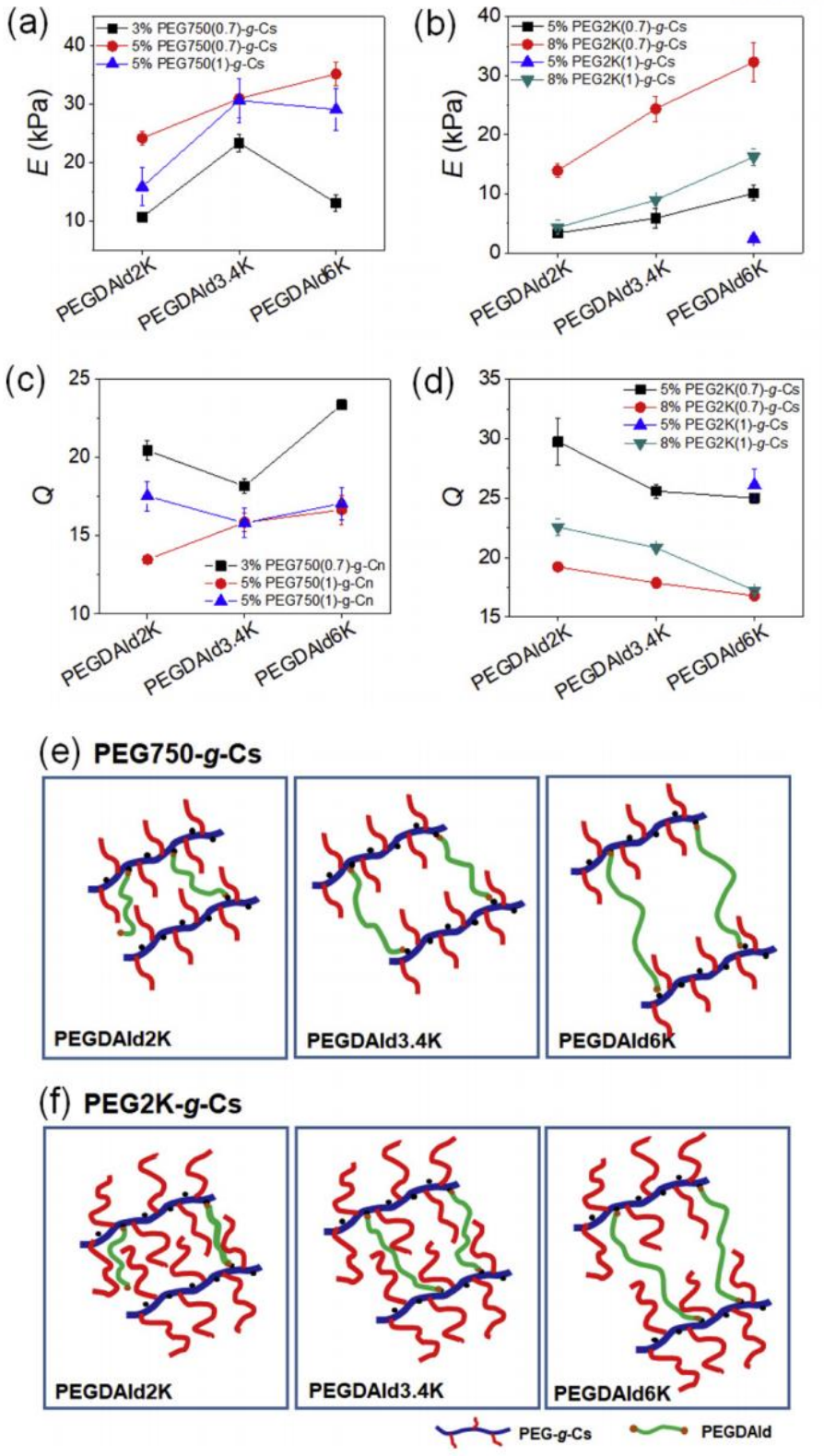

Figure 4-6. Elastic moduli (*E*) and swelling ratios (*Q*) of Cs-PEG hydrogels. (a, c) PEG750-*g*-Cs, (b, d) PEG2K-*g*-Cs. PEG-*g*-Cs was crosslinked by 20 % PEGDAld with varying M_W. The PEG graft density and length, and the concentration of PEG-*g*-Cs were controlled. Possible physical interaction mechanisms between varying M_W of PEGDAld with (e) PEG750-*g*-Cs and (f) PEG2K-*g*-Cs.

When the PEG graft density was increased, 3 % PEG750(1)-*g*-Cs did not form hydrogel with any PEGDAld at the same concentration, but the hydrogels formed at all PEGDAld and the *E* showed the same biphasic dependence on M_W of PEGDAld at higher concentration of 5 % PEG750(1)-*g*-Cs. At higher graft density, the reduced number of amine groups coupled with the increased steric hindrance by PEG grafts contributed to insufficient crosslinking, requiring higher concentration of PEG750(1)-*g*-Cs for gelation.

For PEG2K-*g*-Cs, the hydrogels did not form at 3 % with any PEGDAld. At 5 %, PEG2K(0.7)-*g*-Cs did form hydrogels with all PEGDAld, but the moduli were much lower than PEG750(0.7)-*g*-Cs at the same concentration (Figure 4-6b). The range of E for PEG2K-*g*-Cs became similar to that for 5 % PEG750-*g*-Cs when the concentration was increased to 8 %. These results indicated that higher graft length rendered PEG2K-*g*-Cs more limiting towards physical interaction with PEGDAld due to much greater steric hindrance, leading to insufficient crosslinking and hydrogels with lower mechanical properties (Figure 4-6f). In addition, the E increased with M_W of PEGDAld at all conditions, rather than showing a maximum at intermediate M_W of PEGDAld, which also indicated that shorter PEGDAld had greater difficulty of accessing amine groups of chitosan by increased steric hindrance of PEG2K grafts.

In addition, when the graft density was increased, PEG2K(1)-*g*-Cs only formed a stable hydrogel with PEGDAld6K. Those crosslinked with PEGDAld2K and PEGDAld3.4 K quickly dissolved in buffered media, likely due to the critically low number of crosslinks being broken under highly hydrated environment, since Schiff base formation is a reversible equilibrium reaction which could revert back via hydrolysis. [81, 127] It should be noted that the hydrogels reported here in Figure 4-6 were all stable under neutral aqueous conditions because their degrees of crosslinking were significant enough to withstand possible hydrolysis.

The effect of concentration of PEGDAld was also explored while keeping the PEG grafting constant (Figure 4-7). The hydrogels were successfully formed at a wide range of PEGDAld concentrations, as low as 5 %, for both PEG750(0.7)-*g*-Cs and PEG2K(0.7)-*g*-Cs, and the moduli were dependent on the crosslinker concentration. In addition, there was a gradual increase in moduli with M_W of PEGDAld, which became more noticeable with increasing PEGDAld concentration. With increasing PEGDAld concentration, the effect of increased chain length of PEGDAld, which likely enhanced the crosslinking efficiency by overcoming the steric hindrance of PEG grafts, was more significantly demonstrated.

For comparison, 3 % NCE-Cs was also crosslinked with varying M_W of PEGDAld, and their moduli were measured. Compared to PEG750(0.7)-*g*-Cs at the same concentration, the moduli were significantly lower at all M_W of PEGDAld (Figure 4-8a). Moreover, unlike PEG-*g*-Cs which showed either biphasic dependence or increased with M_W of PEGDAld, the moduli decreased with M_W of PEGDAld, in line with a more typical hydrogel system whose mechanics and crosslinking density are inversely related. This result further suggested that the PEG grafts on chitosan could significantly

improve the mechanical properties of Cs-PEG hydrogels by physical interaction (i.e. van der Waals force, chain entanglement) with PEGDAld crosslinkers (Figure 4-8b).

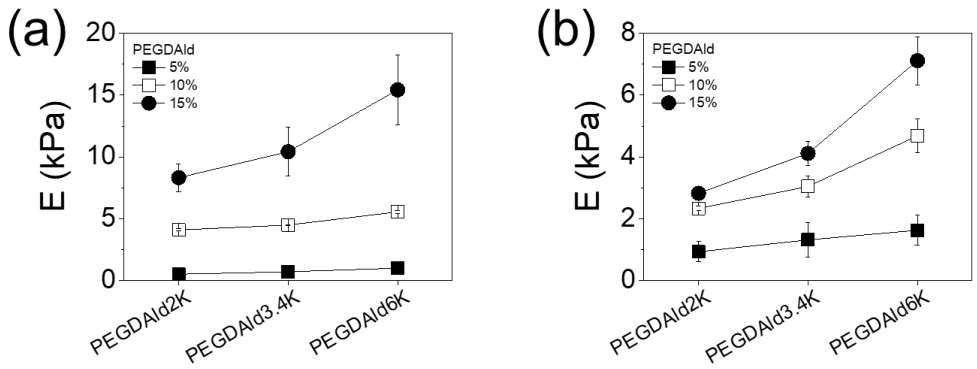

Figure 4-7. Elastic moduli (*E*) of Cs-PEG hydrogels. (a) 5 % PEG750(0.7)-*g*-Cs and (b) PEG2K(0.7)-*g*-Cs crosslinked by PEGDAld with varying M_W and concentration.

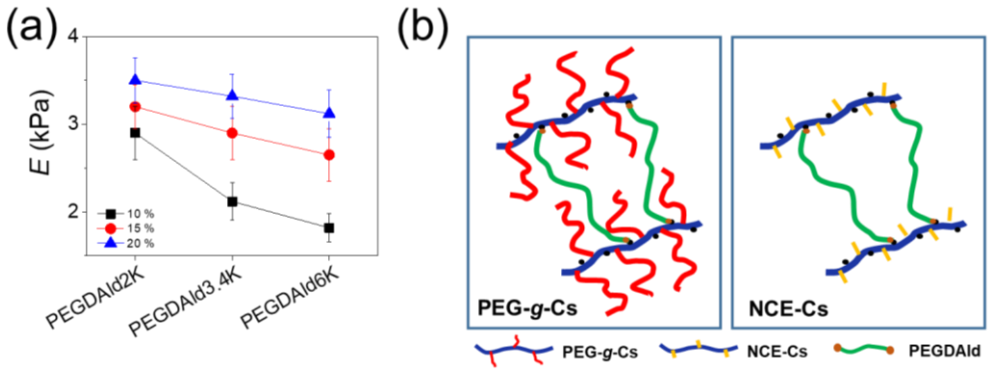

Figure 4-8. (a) Elastic moduli (*E*) of Cs-PEG hydrogels made by crosslinking NCE-Cs with varying M_W of PEGDAld. (b) Possible mechanisms of PEGDAld interaction with PEG-*g*-Cs and NCE-Cs.

4.3.3 Diffusional properties of Cs-PEG hydrogels

With the ability to alter physicomechanical characteristics via PEGDAld crosslinking and PEG grafting, the diffusional properties of Cs-PEG hydrogels were expected to be tuned concurrently. To demonstrate the control of diffusional properties, the swelling ratios (*Q*) of the Cs-PEG hydrogels were first measured in conjunction with *E* shown in Figure 4-6a and b. *Q* and *E* generally demonstrated the typical inverse relationship, which was expected for an elastic network whose *E* and *Q* are governed by crosslinking density (ξ) (i.e. $\zeta \propto E$ and $\zeta \propto Q^{-1/3}$) (Figure 4-6c and d). [16, 30, 128] This result indicated that the Cs-PEG hydrogels are highly elastic, and their diffusional properties could be controlled by both M_W of PEGDAld and PEG grafting of PEG-*g*-Cs. However, for 5 % PEG750(0.7)-*g*-Cs, which showed greater degree of crosslinking by PEGDAld with higher M_W, the *E* and *Q* both showed increase with M_W of PEGDAld. It is inferred that the increased crosslinking efficiency by PEGDAld with higher M_W resulted in increased *E*. At the same time, higher hydrophilicity and chain

length possibly allowed greater influx of water into the hydrogel, leading to increased *Q*. The porosity of Cs-PEG hydrogels was further evaluated by SEM (Figure 4-9a). At the given 5 % PEG750(0.7)-*g*-Cs, the pore size generally increased with M_W of PEGDAld. In addition, the pore size as substantially increased by increasing PEG graft length, PEG2K(0.7)-*g*-Cs. Overall, the pore size, as expected, coincided with *Q*.

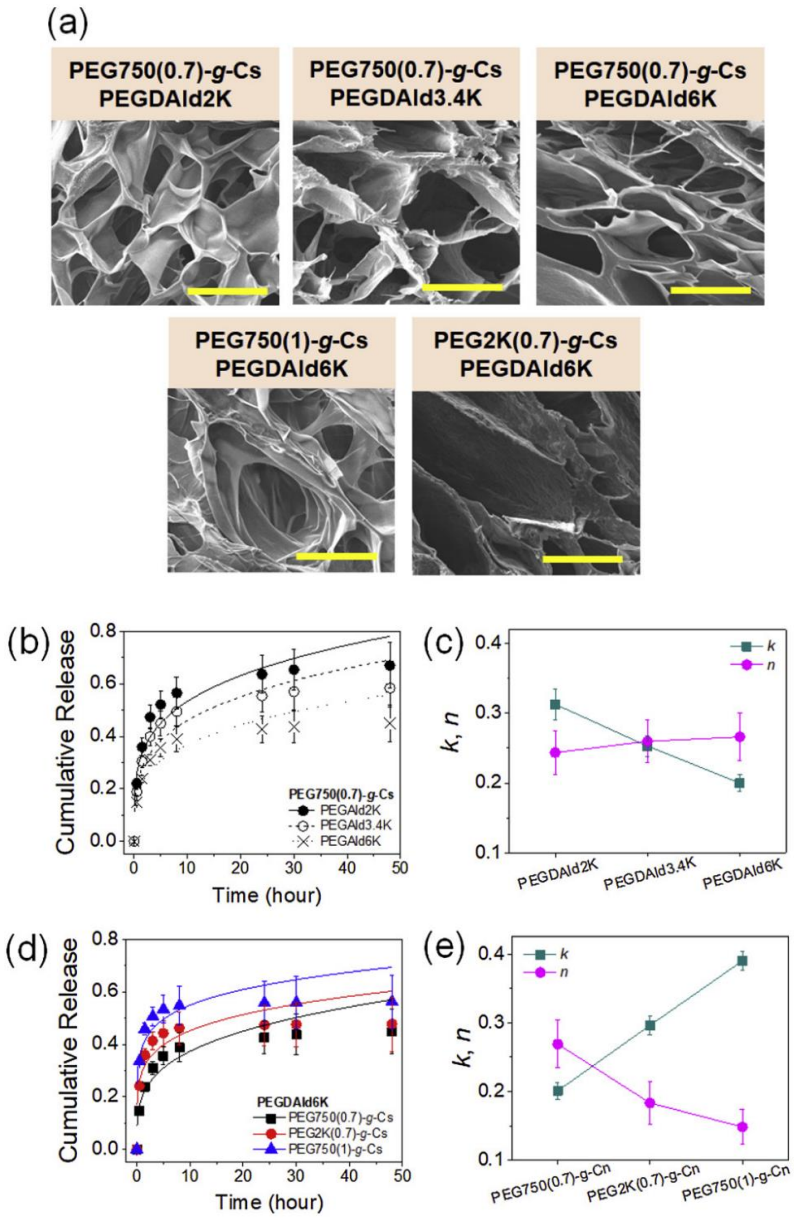

Figure 4-9. (a) Scanning electron microscopic visualization of pore networks of Cs-PEG hydrogels (scale bar: 50 μm). (b-e) Cumulative amount of BSA release profiles from Cs-PEG hydrogels, and kinetic constants (*k*) and exponents (*n*) obtained by fitting the profiles with a mathematical model (Eq. 4-2); (b, c) PEG750(0.7)-*g*-Cs crosslinked with varying M_W of PEGDAld, (d, e) different types of PEG-*g*-Cs crosslinked with PEGDAld6K.

One critical advantage of hydrogel over other forms, such as films and textile, is the ability to safely encapsulate sensitive and bioactive therapeutic molecules and control their release kinetics through hydrogel mechanics. [7] Therefore, to assess the applicability of Cs-PEG hydrogels as a drug delivery system, drug release characteristics for Cs-PEG hydrogels were measured, using bovine serum albumin (BSA) as a model drug. The cumulative release profiles over time were measured, and they were fitted with a Ritger-Peppas model to obtain kinetic constants (k), which represent release rates, and exponents (n), which are related to release mechanisms (Figure 4-9). [43, 93, 95] First, when the M_W of PEGDAld was controlled, while keeping the concentration at 20 %, to crosslink 5 % PEG750(0.7)-*g*-Cs, the release rates decreased with M_W of PEGDAld, as expected, correlating inversely with the E values shown in Figure 4-6; lower release rates for highly crosslinked hydrogels (Figure 4-9b and c). It should be noted that the release rates decreased despite having higher Q values. Since the drug release rates obtained with the Ritger-Peppas model are largely determined by the initial rate, they were more heavily influenced by the degree of crosslinking than swelling which was determined later at equilibrium state. Increasing PEG graft length and density, which showed much lower E, resulted in increased release rates (Figure 4-9d and e). n values were not significantly affected by the M_W of PEGDAld, and all in between 0.2 and 0.3, which was below 0.5 expected for pure Fickian diffusion. This "pseudo" Fickian diffusion suggested that the release was more expedited than simple diffusion, possibly due to the presence of PEG chains known for anti-fouling effect, combined with hydrophilic chitosan, facilitated the BSA release.

4.3.4 Anti-microbial properties of Cs-PEG hydrogels

In addition to the anti-microbial activities of PEG-*g*-Cs, as shown in Figure. 1e, those of Cs-PEG hydrogels were also evaluated by inoculating *E. coil* on the hydrogel surfaces. Agarose hydrogel surface, widely used to culture bacteria, was used as a positive control (Figure 4-10). The extensive *E. coli* growth on the agarose hydrogel was obviously evident. On the other hand, Cs-PEG hydrogels all showed much reduced bacterial growth, demonstrating their antimicrobial activities. At the same 5 % PEG750(0.7)-*g*-Cs, increasing M_W of PEGDAld resulted in greater bacterial reduction. In addition, at the same M_W of PEGDAld6K, increasing PEG graft length and density further diminished the bacterial growth on the hydrogels. These results demonstrated that the presence of PEG in the hydrogels, in the form of grafting or crosslinker, synergistically enhanced the anti-microbial activity likely due to the hydrophilicity and anti-fouling effect of PEG. [129]

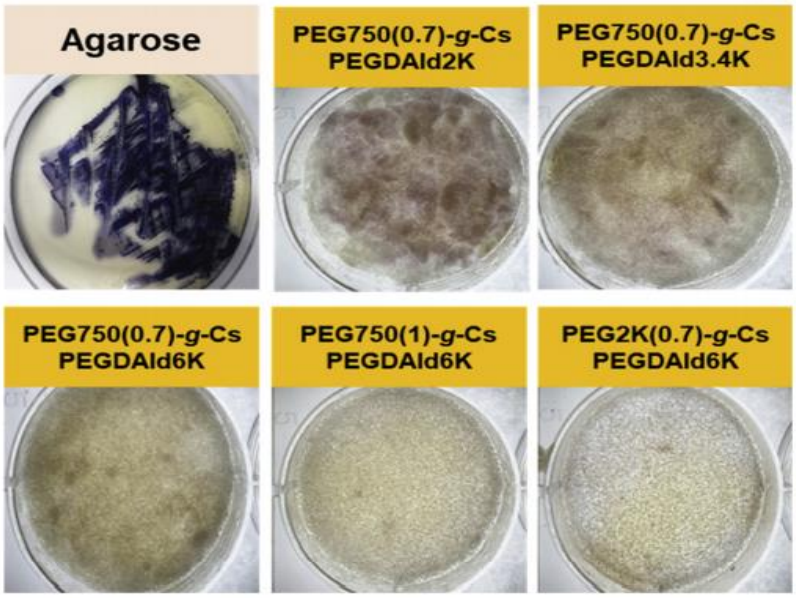

Figure 4-10. *E. coli* growth on various Cs-PEG hydrogel surfaces, visualized by staining with MTT, which turns live bacterial cells brown-purple. LB agarose hydrogel was used as a control.

4.3.5 Gelation kinetics of Cs-PEG hydrogels

The effects of M_W and concentration of PEGDAld and the PEG graft length and density on the gelation kinetics to form Cs-PEG hydrogels were assessed by measuring rheological properties of the gel precursor solution of PEG-*g*-Cs and PEGDAld during the crosslinking reaction. The storage modulus (*G'*) and loss modulus (*G"*) were measured over time to account for the elastic and viscous components, respectively. The gelation time, defined as the time for *G'* and *G"* to cross, due to the increase in elasticity and the decrease in viscosity during gelation.

At the PEG grafting density of 0.7, the gelation kinetics were not significantly affected regardless of PEG graft length and MW of PEGDAld, the gelation times were all within 60 seconds, especially considering the wide range of E of resulting Cs-PEG hydrogels from 3 to 35 kPa (Figure 4-11a, b and e). Since the concentrations of PEG-*g*-Cs and PEGDAld were the same, only changing the M_W of PEGDAld did not significantly alter the number of reactive functional groups, as compared to changing the concentration, so the rate of crosslinking reaction was not significantly affected, especially with lower PEG grafting density allowing sufficiently facile physical interaction between PEG-*g*-Cs and PEGDAld. On the other hand, when the PEG grafting density was increased, there was a substantial difference in gelation time with the same PEGDAld (Figure 4-11c, d and f). This demonstrated that the physical interaction between PEG-*g*-Cs and PEGDAld became more restricted by increased graft length and density, leading to much further delayed crosslinking reaction. Taken together, barring the physically restrictive condition at the highest PEG grafting density the mechanical properties of Cs-PEG hydrogels could be controlled in a wide range by M_W of PEGDAld, while minimally affecting facile gelation kinetics.

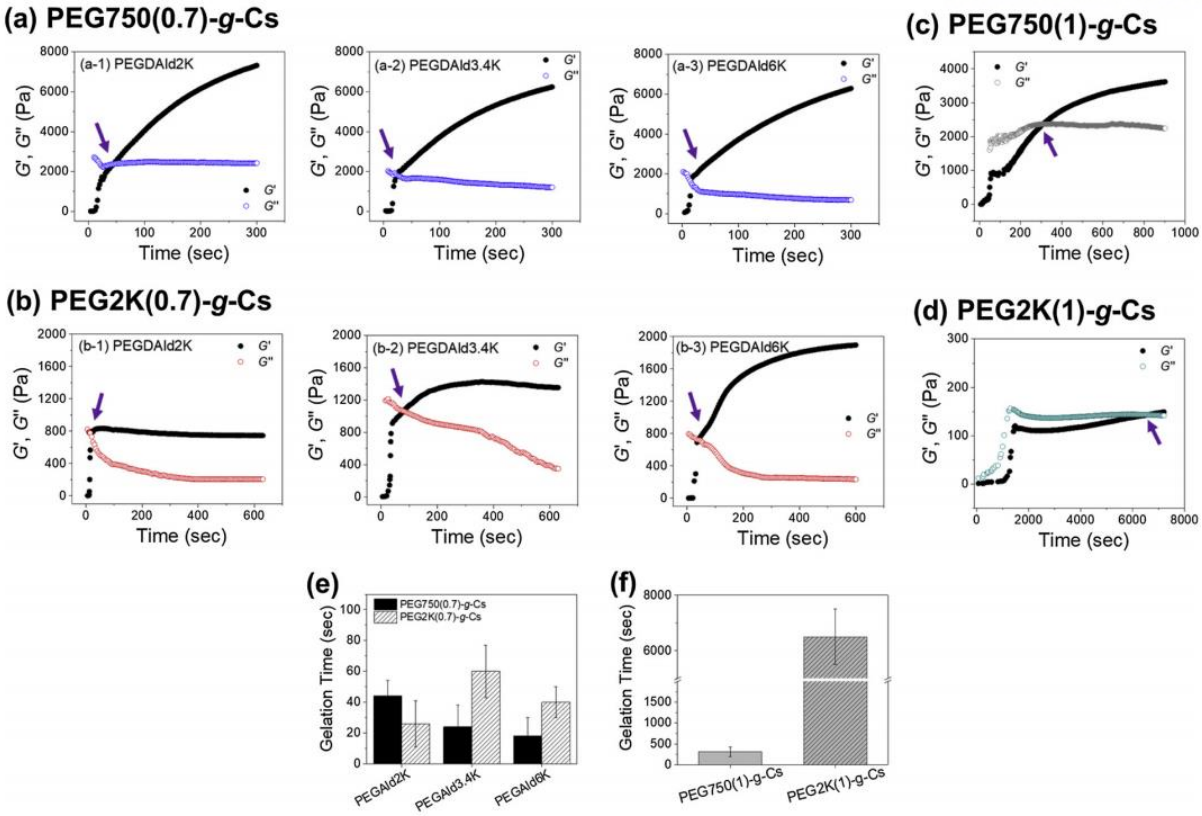

Figure 4-11. Rheological characterization of PEG-*g*-Cs and PEGDAld during gelation by measuring storage (*G'*) and loss (*G"*): (a) PEG750(0.7)-*g*-Cs, (b) PEG2K(0.7)-*g*-Cs, (c) PEG750(1)-*g*-Cs, and (d) PEG2K(1)-*g*-Cs. In (c) and (d), PEGDAld6K was used. Gelation time for (e) PEG750-*g*-Cs and (f) PEG2K-*g*-Cs, determined by the time for *G'* and *G"* curves to cross (identified with arrows).

4.3.6 Tissue adhesive properties of Cs-PEG hydrogels

Chitosan based materials have been widely investigated in topical wound care, combining biocompatibility, cost-effectiveness, mechanical durability, and anti-microbial activity, with several products already in the market. [105, 120, 130] *In situ* forming Cs-PEG hydrogels, with their ability to form in a biocompatible and timely manner, would ideally serve as sealants for wound closure applications. To allow stable adhesion to biological tissue, it is desirable to tune the physical properties of hydrogels for optimal interaction, which could be accomplished by varying the physical properties of PEG-g-Cs and PEGDAld. In addition, the Schiff base formation used to fabricate Cs-PEG hydrogels could further aid in tissue adhesion, as the proteins make up ECM contain abundance of amine groups that could participate in the crosslinking reaction.

To demonstrate the tissue adhesion properties of Cs-PEG hydrogels, lap shear tests using porcine skin tissue were first performed; Cs-PEG hydrogel was fabricated between two porcine skin tissue sections, which were then laterally pulled apart until the tissues were completely separated, and adhesion parameters, namely adhesive strength (σ_{max}) and adhesive energy (J_A), were measured (Figure

4-12a). At a given PEG750(0.7)-*g*-Cs or PEG2K(0.7)-*g*-Cs, both parameters showed gradual increase with M_W of PEGDAld, coinciding with the compressive mechanical properties (Figure 4-12c and d). This highlighted that the increased mechanical rigidity of Cs-PEG hydrogels by greater extent of crosslinking generally enhanced their adhesion to biological tissues. Interestingly, increasing PEG graft length, from PEG750(0.7)-*g*-Cs to PEG2K(0.7)-*g*-Cs, had opposite effect on σ_{max} and J_A. More rigid PEG750(0.7)-*g*-Cs detached at higher stress than PEG2K-*g*-Cs hydrogels, and as a result σ_{max} values of PEG750(0.7)-*g*-Cs hydrogels were generally higher than those of PEG2K-*g*-Cs hydrogels. However, since more rigid PEG750(0.7)-g-Cs hydrogels were also less resistant to deformation, they detached from the tissues at lower strain during lap shear conditions than PEG2K(0.7)-*g*-Cs hydrogels, resulting in lower overall adhesive energy (J_A). In addition, there was more noticeable increase at PEGDAld6K, more so for J_A than σ_{max}, which coincided with the increase in modulus as shown in Figure 4-6a, demonstrating again that the increased mechanical strength of Cs-PEG hydrogels at the highest M_W of PEGDAld contributed to stronger adhesion to biological tissue. At higher grafting density, varying the graft length from PEG750(1)-*g*-Cs to PEG2K(1)-*g*-Cs resulted in much greater reduction for both σ_{max} and J_A, also highlighting the difference in mechanical strength (Figure 4-12f-g).

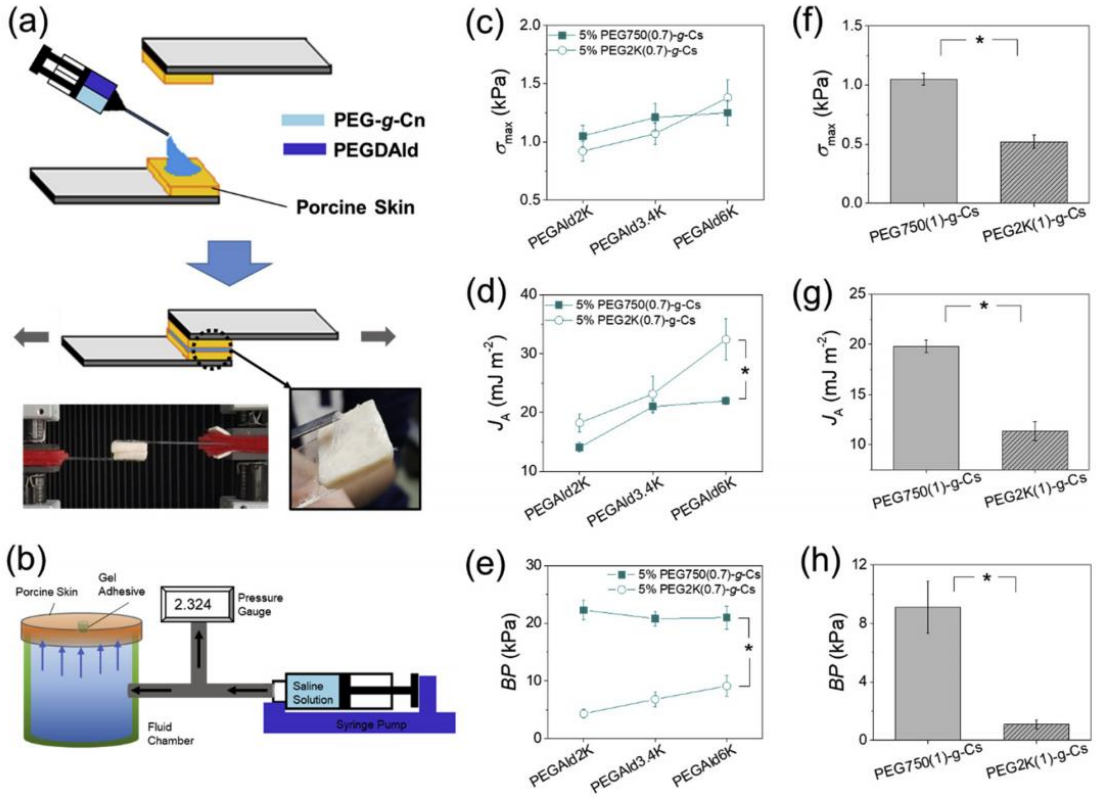

Figure 4-12. (a) Schematic illustrations of (a) a lap shear test and (b) a burst pressure test. Adhesive strength (σ_{max}), adhesive energy (J_A), and burst pressure (*BP*) of CsPEG hydrogels: (c, d, e) PEG750(0.7)-*g*-Cs and PEG2K(0.7)-*g*-Cs crosslinked with varying M_W of PEGDAld, (f, g, h) PEG750(1)-*g*-Cs and PEG2K(1)-*g*-Cs crosslinked with PEGDAld6K. (*$p < 0.05$, $n = 12$).

The adhesive properties of Cs-PEG hydrogels were alternatively evaluated by burst pressure measurements, in which fluid pressure was applied to the Cs-PEG hydrogel attached to a tissue sample until the hydrogel became detached, and the maximum fluid pressure was measured ('burst pressure (*BP*)') (Figure 4-12b). Interestingly, unlike σ_{max} and J_A, *BP* was not significantly affected by the M_W of PEGDAld, rather more substantially by the PEG graft length; *BP* values for PEG750(0.7)-*g*-Cs were much greater than those for PEG2K(0.7)-*g*-Cs at all M_W of PEGDAld by as high as 4.4-fold (Figure 4-12e). It is possible that the extended drag during the lap shear testing diminished the difference in adhesive strength (i.e. the drag between tissues and adhesives continues to occur even after initial detachment), whereas it became more evident in the instantaneous burst condition. Similar to σ_{max} and J_A, at higher grafting density, increasing the graft length PEG750(1)-*g*-Cs to PEG2K(1)-*g*-Cs resulted in significant reduction in *BP* (Figure 4-12h). Taken together, the adhesive strength of Cs-PEG hydrogels was strongly correlated with their mechanical properties, and there was a significant reduction at the highest PEG grafting density and length of PEG-*g*-Cs.

The adhesive properties of a commercially available hydrogel-based tissue adhesive, Beriplast-P, was measured for comparison. Beriplast-P is a fibrin hydrogel prepared by crosslinking fibrinogen with thrombin. [131] *E*, σ_{max} and J_A for Beriplast-P from lap-shear tests were 17.3 (± 2.3) kPa, 1.73 (± 0.4) kPa, and 33.5 (± 4.1) mJ m^{-2}, respectively. These values were comparable to the Cs-PEG hydrogel made with PEG750-*g*-Cs and PEGDAld6K, as shown in Figure 4-11. *BP* for Beriplast-P was measured at 8.4 (± 1.4) kPa, which was much lower than all Cs-PEG hydrogels with PEG750(0.7)-*g*-Cs, and comparable with that of PEG750(1)-*g*-Cs crosslinked with PEGDAld6K. These further highlighted the potential effectiveness of Cs-PEG hydrogels for clinical applications.

4.3.7 In vivo evaluation of Cs-PEG hydrogel as tissue sealant

The potential clinical application of Cs-PEG hydrogel as a tissue sealant was further evaluated using an *in vivo* skin wound model. A lateral incision was made on the skin of a SD rat, and Cs-PEG hydrogel was applied to close the wound via a syringe (Figure 4-13a). The Cs-PEG gel was readily formed and well attached to the skin. Three different Cs-PEG hydrogels were tested; (1) PEG750(0.7)-*g*-Cs, (2) PEG2K(0.7)-*g*-Cs, and (3) PEG2K(0.7)-*g*-Cs encapsulated with epidermal growth factor (EGF). EGF, a well-known promoter for wound healing, was included in the Cs-PEG hydrogel to demonstrate the advantage of hydrogel-based tissue sealant for the delivery of therapeutic biomolecules for accelerated wound healing. [132] Untreated, sutured, and Beriplast-P treated conditions were also tested as control groups. In addition to macroscopic visualization, the wound healing process was monitored in detail by OCT imaging (Figure 4-13b and c, Figure 4-15). The OCT imaging technology allows non-invasive *in situ* visualization of detailed skin tissue structure around the wound area with micrometer-scale resolution down to hypodermis. The wound dimensions, width and depth, were also quantified from the OCT images (Figure 4-13d and e).

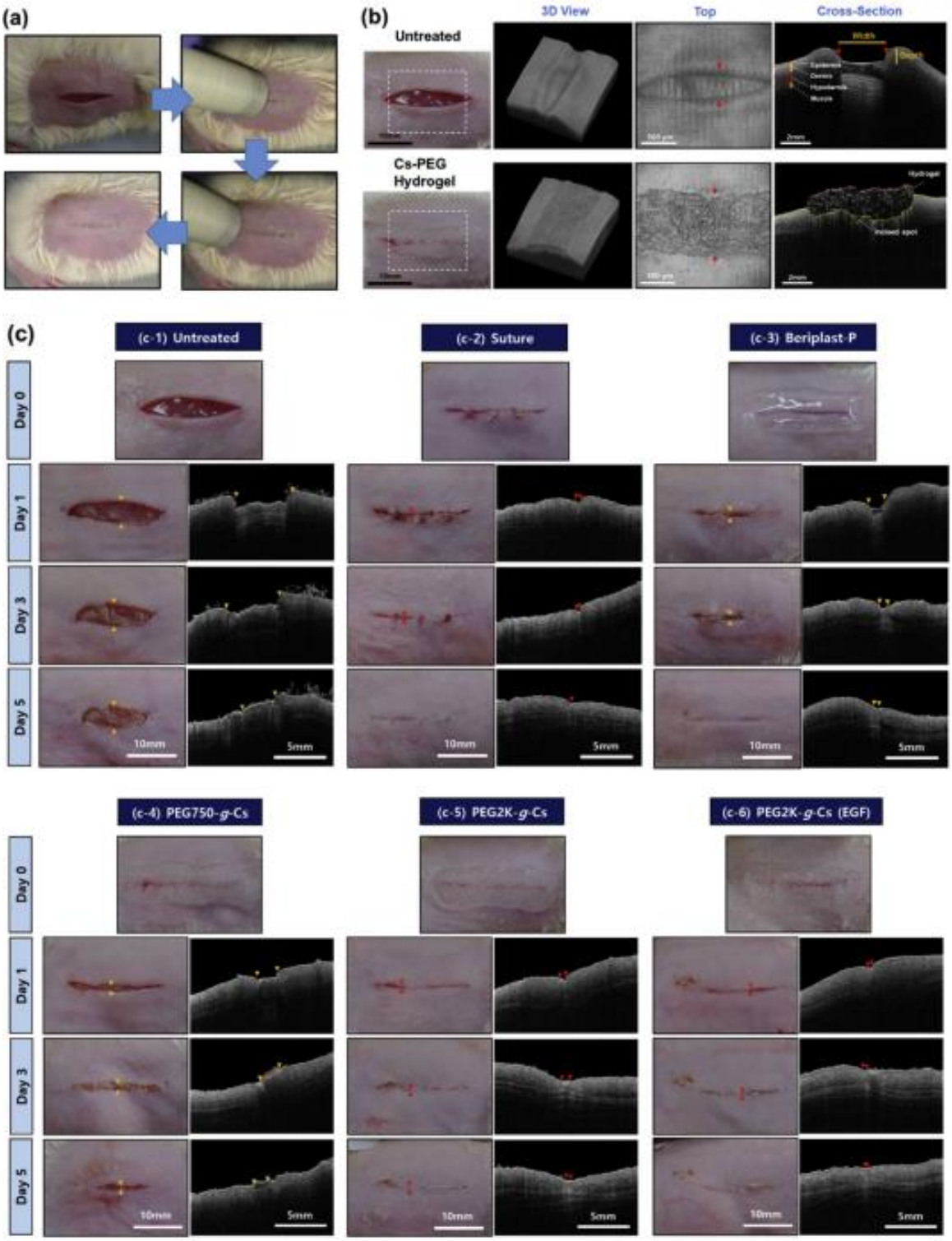

Figure 4-13. (a) Cs-PEG hydrogel was applied to a rat skin wound model via syringe to close the wound gap. (b) OCT imaging was used to visualize the detailed skin tissue around the wound area. (c) After applying tissue sealants, the wound closure and subsequent healing process was monitored over time up to 5 days: (c-1) untreated, (c-2) suture, (c-3) Beriplast-P, (c-4) PEG750-*g*-Cs hydrogel, (c-5) PEG2K-*g*-Cs hydrogel, (c-6) PEG2K-*g*-Cs hydrogel encapsulated with EGF. The markers on OCT images identify the wound area.

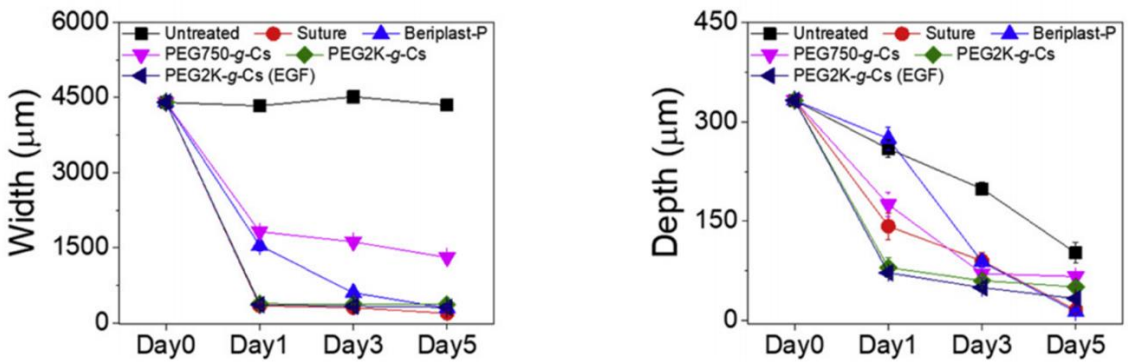

Figure 4-14. The wound dimensions, width and depth, measured from the OCT images (marked with arrows in Figure 4-13)

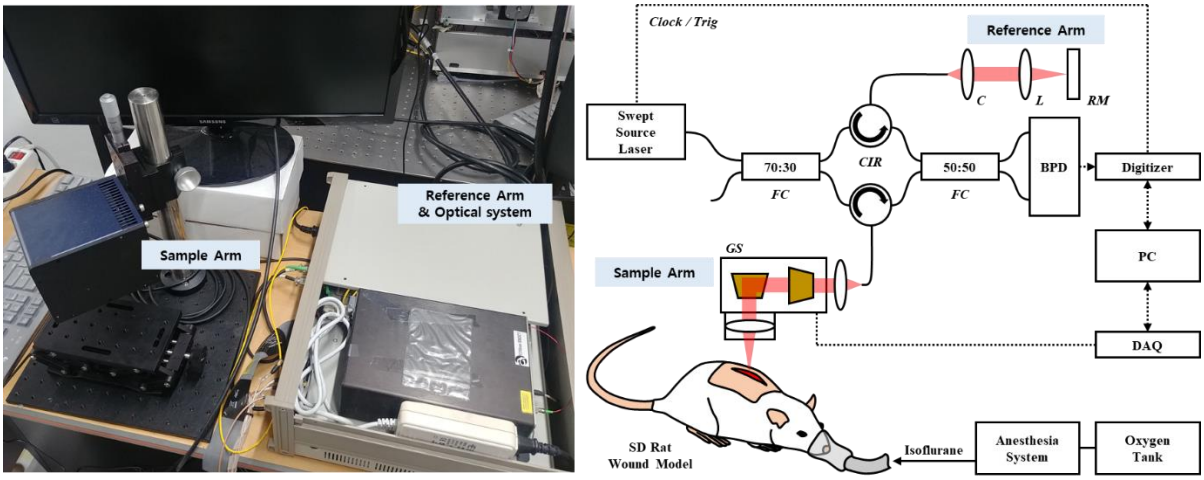

Figure 4-15. Detailed schematics of Swept-Source Optical Coherence Tomography (SS-OCT) imaging apparatus to visualized skin tissue; C: Collimator, L: Lens, RM: Reference mirror, FC: Fiber coupler, CIR: Circulator, BPD: Balanced photo-detector, GS: Galvanometer scanner.

Without any sealant ('untreated'), the wound gap was wide enough that it did not close naturally, and the scab formed on the wound area, with erythema surrounding the area, as expected. The suture allowed the gap to close tightly, and significant wound healing took place by day 3, though suture scar remained up to 5 days. Beriplast-P as a hydrogel tissue sealant also helped close the wound gap, but there was some inflammation surrounding the wound site, as identified by erythema and swelling which eventually subsided and healed by day 5. The OCT image clearly visualized the difference in tissue texture underneath the wound site; higher reflection signals caused by denser tissue structure, compared to normal tissue. Since OCT utilize the scattering contrast for imaging, higher reflection signal of OCT image presenting bright regions indicated higher tissue density, likely fibrotic tissue. The early inflammation of fibrin-based Beriplast-P has been associated with the immunological response stemming from allogenic source. [131] But the biological effect of fibrin, a protagonist for wound healing, likely expedited the process.

For PEG750-*g*-Cs, the initial wound gap closure was similar to Beriplast-P, but there was less inflammation, while the wound healing was slower. More remarkably, there was a greater degree of wound closure and less inflammation after day 1 was shown for PEG2K-*g*-Cs, more so than Beriplast-P and PEG750-*g*-Cs. One critical difference of PEG2K-*g*-Cs from PEG750-*g*-Cs was more sustained water retention, since PEG2K-*g*-Cs hydrogel has higher degree of swelling. Therefore, it was inferred that continued presence of moisture provided by PEG2K-*g*-Cs hydrogel substantially reduced the inflammation. [133] PEG750-*g*-Cs, on the other hand, more quickly dried out over the same time period.

To further illustrate the advantage of Cs-PEG hydrogel as a drug delivery system, epidermal growth factor (EGF), a growth factor involved with wound healing process, was encapsulated to be released to the wound area, expediting the wound healing process. The macroscopic view of the wound area was similar to that without EGF. But the OCT image showed less signal intensity at the wound site, suggesting there was less fibrotic tissue formed by the action of released EGF.

Detailed tissue morphology during the wound healing process after tissue sealant application was further histologically evaluated (Figure 4-16). The H&E stained histological tissue images largely confirmed the inflammation and fibrotic tissue formation by OCT imaging. Untreated and Beriplast-P treated tissues showed the highest degree of fibrosis. PEG750-*g*-Cs and PEG2K-*g*-Cs treated tissues showed less fibrosis than Beriplast-P. Moreover, EGF encapsulated PEG2K-*g*-Cs treated tissue showed the least amount of fibrosis. Taken together, these results highlighted that the Cs-PEG hydrogel, coupled with controlled release of a therapeutic agent, highly effective as a tissue sealant.

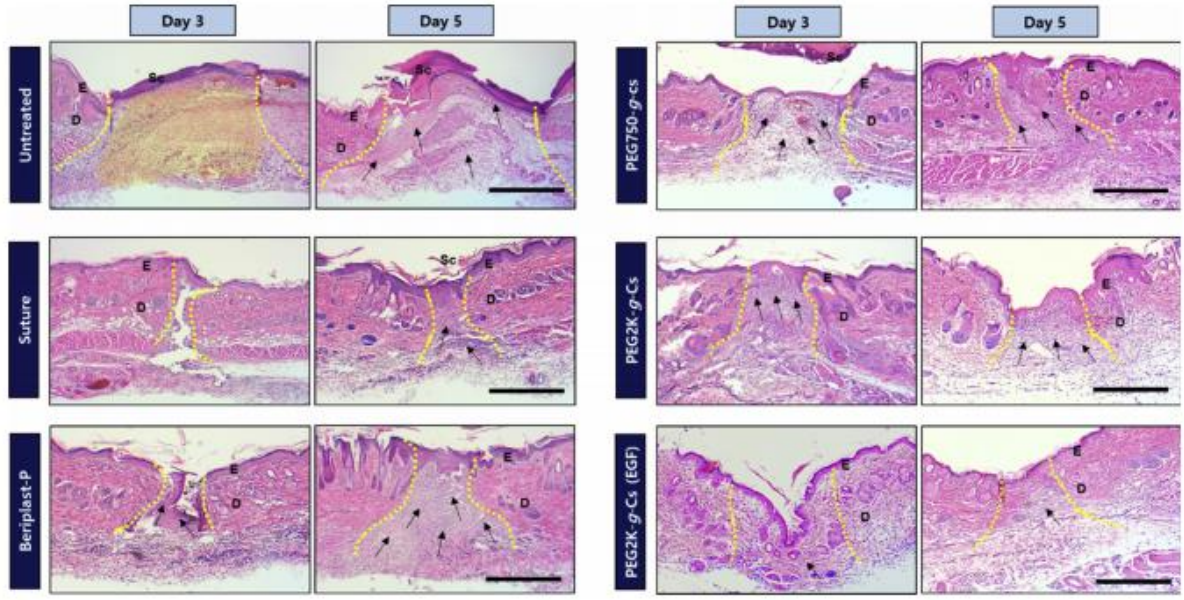

Figure 4-16. Histological evaluation of the skin wound tissues after tissue sealant treatment. The tissues harvested at day 3 and 5 were stained with hematoxylin & eosin (scale bar: 500 μm). E: epidermis, D: dermis, Sc: scab, arrows and highlighted area: fibrotic tissue.

4.4 Conclusion

In this study, *in situ* forming chitosan hydrogel, via Schiff base formation, capable of controlling mechanical properties in a wide range without compromising gelation kinetics was developed. Chitosan was conjugated with PEG grafts with controlled length and density (PEG-*g*-Cs) not only to allow aqueous solubility at physiological pH, but more importantly to modulate physical interaction with varying M_W of polymeric crosslinker, PEG-dialdehyde (PEGDAld), which directly influenced the mechanical outcome of the resulting Cs-PEG hydrogels. The gelation kinetics, determined from rheological evaluation, showed that all hydrogels, except at the highest PEG graft length and density, were readily formed (within a minute). The adhesive properties of Cs-PEG hydrogels evaluated by *ex vivo* lap shear and burst pressure tests were generally in line with the mechanical properties, and were similar to a commercial hydrogel-based tissue sealant. The clinical potential of Cs-PEG hydrogels as a tissue adhesive was demonstrated with an *in vivo* rat skin wound model, which showed wound closure with minimal inflammation. More significantly, controlled release of EGF from Cs-PEG hydrogel significantly reduced the inflammation, effectively demonstrating an important advantage of therapeutic delivery for hydrogel-based tissue sealant.

CHAPTER 5. In situ facile-forming chitosan hydrogels with tunable physicomechanical and tissue adhesive properties by polymer graft architecture

5.1 Introduction

Controlling mechanical properties is a major research focus in the field of biomaterials. The materials used in various biomedical applications, including tissue engineering, drug delivery, biosensors, and actuators, must possess sufficient structural integrity and durability throughout their intended lifetimes in order to maintain their performance. In addition, it is well established that physicomechanical signals imparted by the extracellular matrices influence important biological functions of many different types of cells; thus, it is of significant importance that biomaterials as cell culture platforms should have tunable mechanical properties. [134-138] Mechanical properties are also directly connected to permeability, which controls the diffusion of soluble factors through the biomaterials, which is an important parameter for controlled drug delivery and 3D cell culture applications. [57, 134, 135]

Polymers with multivalent reactive functional groups, often called macromers, have been considered highly effective cross-linkers to develop materials with variable mechanical properties over conventional small molecular cross-linkers. [30, 93, 109, 136, 137] Small molecules can only have a few functional groups and often show limited solubility in various solvents, limiting their controllable range. On the other hand, polymers that have functional groups throughout their repeating units serving as sites for chemical reactions can present more reactive functional groups than small molecules, further increasing the range of control per concentration. In addition, adding reactive functional groups to a long polymer chain usually does not impact the overall solubility. The macromers having self-reacting moieties such as (meth)acrylate that undergo radical cross-linking and can cross-link by themselves to form structures above threshold concentrations without the need for additional cross-linkers. Conversely, macromers can easily hybridize with one another, provided their physicochemical miscibility and mutual reactivity.

Polysuccinimide (PSI), commonly synthesized by one-step polycondensation of aspartic acid, has been shown to be a good precursor system for conjugating various functional groups. [138-141] Specifically, amine-based nucleophiles react with succinimidyl groups of PSI via ring-opening addition, resulting in polyaspartamide. Previous studies have demonstrated that polyaspartamide can be utilized as a gel-forming polymer and cross-linker by presenting reactive functional groups such as amine, thiol, and methacrylate. [93, 142-145] Furthermore, convenient control of the degree of substitution allows the control of cross-linking density in addition to changing the concentration.

In our previous work, it was demonstrated that polyaspartamide presenting amine or hydrazide groups could form hydrogels having controllable mechanical properties by Schiff base formation or Michael addition, based on the degree of substitution. [93] However, the influence of physical properties of polyaspartamide on the hydrogel mechanics has not been explored. Therefore, herein, the grafting parameters, graft density, and length of reactive functional groups of polyaspartamide cross-linkers were modulated in order to control the mechanical properties of resulting hydrogels. Polyaspartamide presenting primary amine groups was developed by reacting PSI with diamine with poly(ethylene glycol) (PEG) linkers having varying lengths. PEG-diamine with varying molecular weights were synthesized and used to present amine groups on the polyaspartamide backbone. The resulting poly(2-hydroxyethyl aspartamide)-*g*-amino-poly(ethylene glycol) (PHEA–PEGAm) was then reacted with aldehyde-presenting alginate via Schiff base to develop hydrogels. The length of PEG linker and the degree of amine substitution were varied to control the mechanical properties of hydrogels. Moreover, the unreacted amine groups on PHEA–PEGAm facilitated the degradation and eventual dissolution of hydrogels via hydrolysis under physiological conditions, and the rate of degradation was also controlled by the grafting parameters. The biomedical potential of this hydrogel as a tissue injectable and degradable delivery system was demonstrated using an *ex vivo* model. To further control the degradation and mechanics, the alginate component of hydrogels was additionally cross-linked with divalent calcium ions.

5.2 Materials and Methods

5.2.1 Synthesis of Polysuccinimide (PSI)

Polysuccinimide (PSI) was prepared by polycondensation of aspartic acid with phosphoric acid as an acidic catalyst. [93, 142-145] l-Aspartic acid (50 g, Samchun Chemicals, Korea) and orthophosphoric acid (1.22 mL, Sigma-Aldrich) were dissolved in sulfolane (130 mL, Junsei Chemical, Japan) and refluxed at 180 °C with mechanical stirring under dry N_2. Water formed during the reaction was continuously removed using a Dean–Stark trap. After 7 h, the red-orange-colored reaction mixture was precipitated with methanol. The precipitate was washed with deionized water several times and dried to obtain the final product.

5.2.2 Synthesis of PEG-Diamine

Poly(ethylene glycol) diamine (PEG-diamine) was synthesized by direct amination of PEG (M_w 200, 600, and 1000, Sigma-Aldrich) via Mitsunobu reaction. [146] Briefly, diisopropyl azodicarboxylate (DIAD, Alfa Aesar) dissolved in 1,4-dioxane was slowly added via syringe to an ice-cooled triphenylphosphine (Ph_3P, Sigma-Aldrich) solution and mixed for 1 h. PEG was dissolved separately

in dry 1,4-dioxane (Samchun Chemicals, Korea) under dry N_2 gas. Then, PEG solution was slowly added to the DIAD/Ph_3P solution and stirred until it became clear. Phthalimide (Sigma-Aldrich) was added to the mixture and stirred overnight at 50 °C under N_2. The molar ratio of PEG/DIAD/TPP/phthalimide was 1:3:3:3.

After the conjugation of phthalimide, hydrazine (Alfa Aesar) was added to the mixture in 15-fold access and refluxed for 3 h to remove the phthalimide and generate amine on PEG. After the reaction, the mixture was completely dried in vacuo 60 °C to obtain the crude product. Subsequently, the crude product was dissolved in ice-cooled water to remove the water-insoluble impurities via filtration. The same procedure was repeated using HCl (5 M). The filtered solution was neutralized using NaOH (5 M), and the final product was obtained by freeze-drying. The chemical structure of PEG-diamine was analyzed with ^{1}H NMR (Figure 5-1). The degree of amination was verified using a colorimetric trinitrobenzenesulfonic acid (TNBS) assay, which measures the amount of amine and related molecular weight (Figure 5-2). [93, 147]

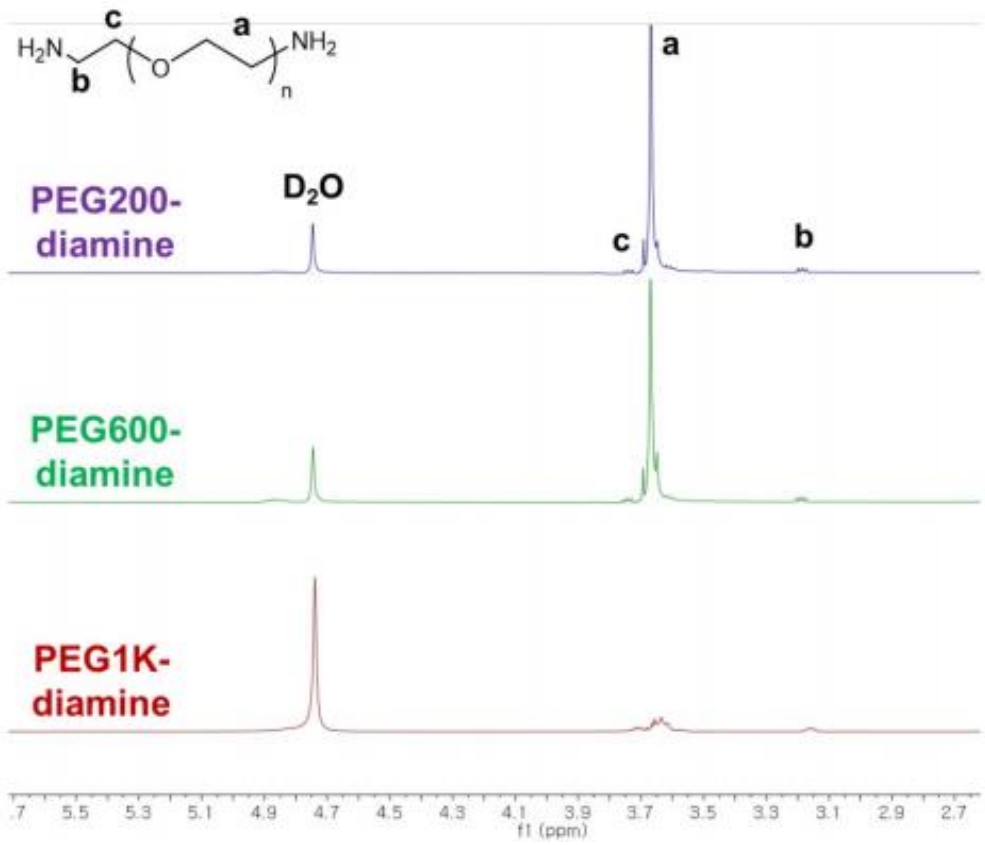

Figure 5-1. ^{1}H-NMR spectra of PEG-diamine with varying molecular weights; 200, 600, 1000 (1K) g mol-1. Characteristic peaks of ethylene oxide repeating are noted (a-c).

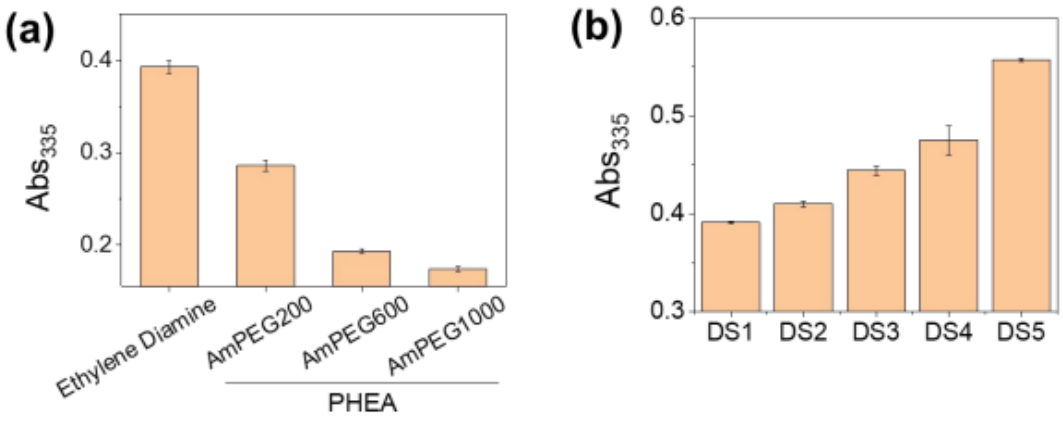

Figure 5-2. The amount of amine in (a) PEG-diamine and (b) PHEA-PEGAm600 with varying DS_{Am} determined by TNBS assay (absorbance at 335 nm).

5.2.3 Synthesis of Poly(2-hydroxyethyl aspartamide)-g-Amino-Poly(ethylene glycol) (PHEA–PEGAm)

PHEA–PEGAm, presenting varying amounts of hydroxyl and amine groups are synthesized by reacting PSI with ethanolamine and PEG-diamine, respectively. [93] First, ethanolamine (Sigma-Aldrich) was added to PSI (1 g) dissolved in 20 mL of dimethyl sulfoxide (DMSO, Samchun Chemicals, Korea) and reacted overnight at 70 °C under dry N_2 gas to synthesize an intermediate polyaspartamide containing hydroxyl and unreacted succinimidyl groups, poly(2-hydroxyethyl aspartamide) (PHEA). Ethanolamine was reacted before PEG-diamine because unreacted PSI with numerous succinimidyl groups can react with both amine groups of PEG-diamine, resulting in cross-linking of PSI chains. The amount of ethanolamine was determined so the number of remaining unreacted succinimidyl groups to be reacted with PEG-diamine was the desired degree of amine substitution. Then, the mixture was slowly added to PEG-diamine dissolved in DMSO and continued to react at 70 °C for 48 h. The 2-fold excess amount of PEG-diamine to that of unreacted succinimidyl groups was used to ensure only one amine group of PEG-diamine reacted with the succinimidyl groups of PHEA, and the other amine group was not reacted. After reaction, the mixture was dialyzed against DI water and lyophilized to obtain product.

PHEA–PEGAm with different degrees of amine substitution (DS_{Am}), defined as the fraction of succinimidyl groups conjugated with amine groups, were obtained by simply varying the PEG-diamine reactant. As a control, PHEA presenting short aminoethyl grafts, PHEA–PEGAm, were also synthesized by using ethylenediamine instead of PEG-diamine. The chemical structure and DSAm of PHEA–PEGAm were analyzed with FT-IR and ^{1}H NMR spectroscopies. As a control system without PEG linker, PHEA presenting aminoethyl groups, PHEA-EtAm, was synthesized following the same procedure as described above, except ethylene diamine (Sigma-Aldrich) was used instead of PEG-diamine. [93]

5.2.4 Trinitrobenzene sulfonic acid (TNBS) assay

0.1 mL of TNBS working solution (0.5 % TNBS, 4 % $NaHCO_3$, pH 8.5) was added to 0.1 mL of sample solution (PEG-diamine or PHEA-PEGAm) and allowed to react for 2 hours at 37 °C. After the reaction, 0.1 mL of 1 M HCl was added. The absorbance of the solution at 335 nm was measured (Multiskan GO, Thermo Fisher Scientific).

5.2.5 Synthesis of oxidized alginate

Sodium alginate (Sigma Aldrich) was dissolved in deionized water at 1 %. 0.43 g sodium periodate was added to the solution and reacted with stirring at room temperature for 24 hours under dark. After quenching the reaction with excess ethylene glycol, the solution was extensively dialyzed against DI water, and freeze-dried to obtain the product. [148, 149]

5.2.6 Fabrication of PHEA–PEGAm Hydrogels

Alg-PHEA hydrogel was fabricated by reacting PHEA–PEGAm with alginate presenting aldehyde groups (Alg-ALD) via Schiff base formation. [148, 149] PHEA–PEGAm and Alg-ALD solutions in 0.1 M sodium phosphate buffer (pH 8.0), were mixed in various ratios. The mixture was immediately placed in between glass plates with 1 mm spacer and incubated at 37 °C to allow hydrogels to form. The hydrogel disks (8 mm diameter, 1 mm thickness) were punched out, and mechanical properties were determined. To induce secondary ionic cross-linking, Alg-PHEA hydrogel was immersed in CaCl2 solution for 1 h with gentle shaking. The concentration of $CaCl_2$ was controlled up to 5 M.

5.2.7 Mechanical and Degradation Properties of Hydrogels

The rigidity of hydrogels was evaluated by calculating elastic moduli obtained from uniaxial compression experiments (Model 3343, Instron). [29, 94, 150] The pressure applied to each hydrogel at the rate of 1 mm min^{-1} and the stain versus stress curve were obtained. The elastic modulus was then determined as the slope of the strain–stress curve at the first 10% strain in the linear curve region (the elastic region).

The degradation behavior was monitored by measuring the change in elastic moduli over time. The hydrogels were incubated in PBS at 37 °C, and their moduli were analyzed at designated time points until the hydrogel were completely dissolved. The degradation rate constant (k_D) was obtained by fitting the fractional change in moduli versus time curve with the following exponential decay model:

$$\frac{E_t}{E_0} = e^{-k_d \cdot t} \qquad \text{Eq. 5-1}$$

where E_t was the modulus measured at time, t, and E_0 was the initial modulus measured immediately

after formation. [74, 94]

5.2.8 Drug Release Kinetics

Drug release kinetics from hydrogels were measured using bovine serum albumin (BSA, Sigma-Aldrich) as a protein drug model. Before the hydrogel fabrication, BSA (5 mg mL^{-1}) was dissolved in the PHEA–PEGAm precursor solution for encapsulation. Then, each hydrogel disk was incubated in PBS (0.8 mL) at 37 °C, and the protein released into the medium was measured at various time points using a BCA Protein Assay kit (Thermo Fisher) according to the manufacturer's instructions. The cumulative drug release profile was fitted to the Ritger-Peppas equation,

$$\frac{M_t}{M_0} = k_R \cdot t^n \qquad \text{Eq. 5-2}$$

where M_t was the amount of protein released at a time, t, M_∞ was the total amount of encapsulated protein, k_R was the release rate constants, and n was the exponent related to the release mechanism. [94, 95, 151]

5.2.9 Rheological Properties of Hydrogels

The gelation kinetics of Alg-PHEA hydrogels were evaluated using a rotating-disk rheometer (Kinexus, Malvern). [72, 73] After mixing Alg-ALD and PHEA–PEGAm solutions, the changes in the storage moduli (G') and loss moduli (G'') of the mixture was performed at the same strain (1%) and cyclic frequency (1 Hz) in a small-amplitude oscillatory shear mode. The gelation time was determined by the time at which G' exceeded the G'' curve (gelation point) due to the elastic component increased rapidly as the cross-linking reaction proceeded.

5.2.10 In Vitro Cytotoxicity

Cytotoxicity of PHEA and Alg-ALD was assessed by measuring the viability of cells exposed to PHEA and Alg-ALD with varying concentrations with MTT assay. Briefly, NIH 3T3 fibroblasts (ATCC) were cultured in a 96-well plate, 2000 cells per well, and incubated at 37 °C for 36 h. The cell culture medium consisted of 10 % fetal bovine serum and 1 % penicillin/streptomycin in Dulbecco's Modified Eagle Medium (DMEM), all purchased from Thermo Fisher Scientific. After the cells reached 50 % confluence, the medium was exchanged with that containing various concentrations of PHEAA and OAlg, and cultured at 37 °C for 36 h. After washing with PBS, the cells were incubated in 100 μL of fresh culture medium added with 10 μL of MTT solution (5 mg mL^{-1}, 3-(4,5-dimethylthiazol-2-yl)-2,5-diphenyltetrazolium bromide (MTT) in PBS) and at 37 °C for 4 h, during which MTT was enzymatically converted to formazan, 1-(4,5-dimethylthiazol-2-yl)-3,5-diphenylformazan, in proportion to the live cells. A total of 100 μL of the stop solution (20 % sodium dodecyl sulfate in

water/dimethylformamide (50:50)) was added to dissolve the formazan. The absorbance of the resulting colored solution at 570 nm was measured (Multiskan GO, Thermo Fisher).

5.2.11 Ex Vivo Evaluation of Degradation Behavior of Hydrogel

The degradation behavior of Alg-PHEA hydrogels injected inside a tissue environment was evaluated *ex vivo* using porcine liver explants (purchased from Biozoa Biological Supply Co., Korea). [152] Briefly, 150 μL of hydrogel precursor solution, prepared by mixing Alg-ALD and PHEA solutions, were injected into the center of a liver specimen (10 mm × 10 mm each) and incubated at 37 °C for 10 min to allow hydrogel formation. Subsequently, the specimens were swollen with 10 % neutral buffered formalin solution for a designated time, and then each specimen was cut in half to take microscopic images of the cross-section and harvested for histological evaluation. Hematoxylin and eosin (H&E) staining was performed on the frozen tissue sections.

5.3 Results and Discussion

5.3.1 Synthesis and Characterization of Amine-Presenting Polyaspartamide with Tunable Graft Architecture

Polysuccinimide is a uniquely structured polymer consisting of a series of succinimidyl ring structures that can undergo ring-opening nucleophilic addition with amine-based nucleophiles, resulting in a stable *β*-polypeptide, termed polyaspartamide. This property allows the conjugation of various functional groups to the polyaspartamide backbone. In this study, polyaspartamides presenting different amounts of amine groups were prepared. Starting from PSI, which was synthesized by polycondensation of aspartic acid, it was first reacted with ethanolamine to present hydroxyl groups, then followed by reaction with poly(ethylene glycol) (PEG) diamine to the remaining succinimidyl groups (Figure 5-3a). PEG-diamine was developed from PEG having hydroxyl end groups via Mitsunobu reaction (Figure 5-1, Figure 5-2a, and Figure 5-3b). The length and density of amine grafts of the resulting poly(2-hydroxylethyl aspartamide)-*g*-amino-poly(ethylene glycol) (PHEA–PEGAm) could be conveniently tuned by PEG-diamine with varying degrees of substitution (DS_{Am}) and molecular weights (Figure 5-3c). Three different molecular weights of PEG-diamine were used: 200, 600, and 1000 g mol^{-1}, which were denoted as PHEA–PEGAm200, PHEA–PEGAm600, and PHEA–PEGAm1K, respectively. It should be noted that PEG-diamine with a higher M_w, 2000 and 6000 g mol^{-1}, was also prepared, but it did not lead to sufficient grafting and subsequent gelation, likely due to low amounts of amine groups under the same concentration.

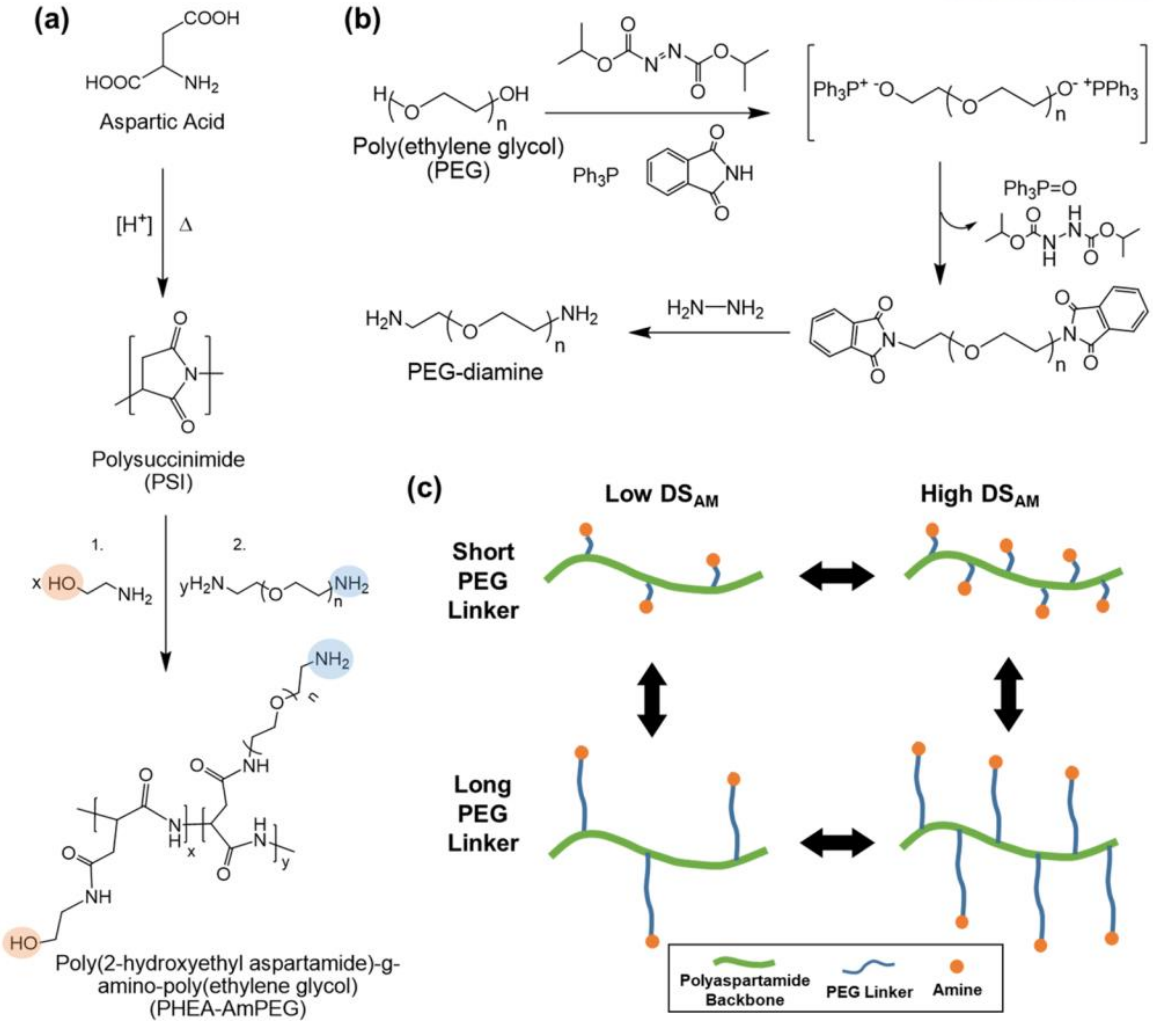

Figure 5-3. (a) Synthesis of poly(2-hydroxylethyl aspartamide)-*g*-amino-poly(ethylene glycol), termed PHEA–PEGAm, via ring-opening addition of polysuccinimide (PSI) with ethanolamine and PEG-diamine. (b) Synthesis of poly(ethylene glycol)(PEG) diamine via Mitsunobu reaction of PEG. (c) Schematic illustration of controlling the length and density of amine grafts of PHEA–PEGAm.

The chemical structures of PHEA–PEGAm with varying DS_{Am} and graft length were analyzed with ^{1}H NMR and FT-IR spectroscopy (Figure 5-4 and Figure 5-5). The peaks corresponding to hydroxyl and amine grafts varied accordingly with the DS_{Am}. TNBS assay, which determines the amount of primary amine groups, was also employed to verify the DS_{Am} (Figure 5-2b). In addition, the different lengths of PEG linker at the same DS_{Am} could also be confirmed with ^{1}H NMR spectroscopy. These results all confirmed the convenient control of graft length and DS_{Am} of PHEA–PEGAm through reaction conditions.

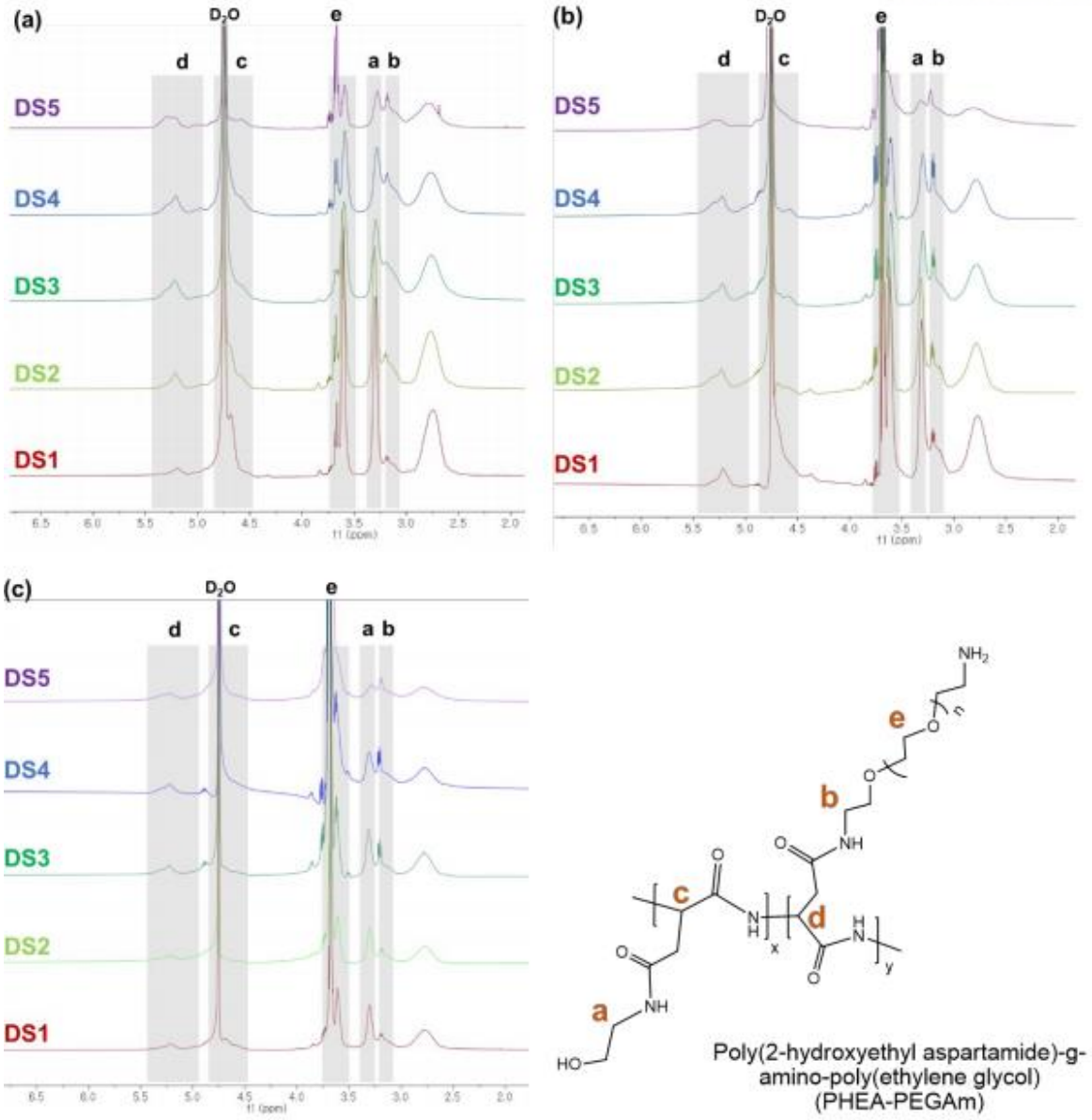

Figure 5-4. ^{1}H-NMR spectra of PHEA-PEGAm with varying DS_{Am}; (a) PHEA-PEGAm200, (b) PHEAPEGAm600 and (c) PHEA-PEGAm1K. Characteristic peaks corresponding to hydroxyl grafts (a, c), amine grafts (b, d) and PEG linkers (e) are noted.

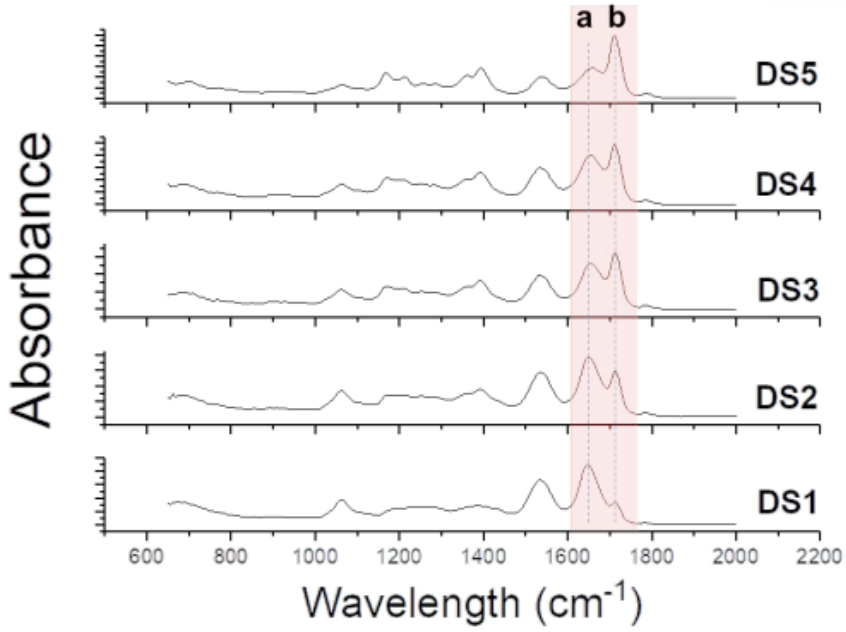

Figure 5-5. Representative FT-IR spectra of PHEA-PEGAm with varying DS_{Am}. Characteristic peaks corresponding to amide vs(C=O) of hydroxyl grafts (a) and amine grafts (b) are noted.

The cytotoxicity of PHEA–PEGAm was assessed *in vitro* by exposing fibroblasts with varying concentrations of PHEA–PEGAm, from the nano to the millimolar range (Figure 5-6). All three PHEA–PEGAm showed significant biocompatibility, with cell viability over 80%, even at a high concentration of 1 mg mL^{-1}. It is interesting to note that, at the highest concentration tested, at 10 mg mL^{-1}, cell viability against PHEA–PEGAm200 was significantly reduced compared to PHEA–PEGAm600 and PHEA–PEGAm1K, indicating the introduction of longer PEG chains, well-known to have high biocompatibility, helped improve the biocompatibility of PHEA–PEGAm. [153]

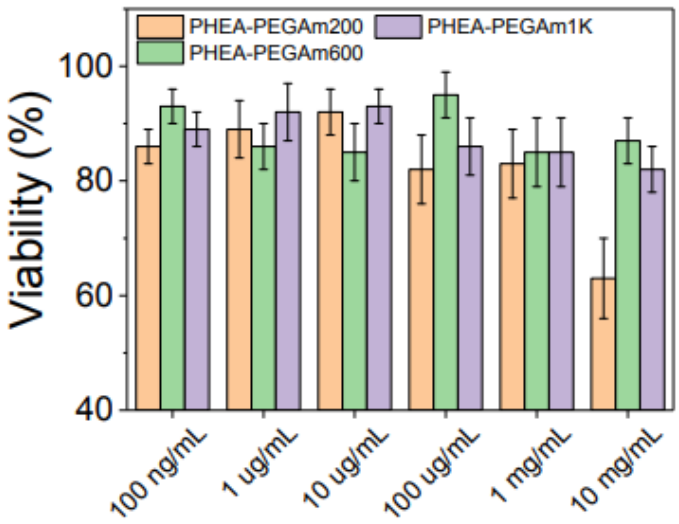

Figure 5-6. Cytotoxicity of PHEA-PEGAm assessed by measuring the viability of cells exposed to various concentrations of PHEA-PEGAm.

5.3.2 Fabrication and Mechanical Properties of PHEA-Linked Hydrogels

To demonstrate the ability of PHEA–PEGAm to react with other polymers to form hydrogels and control their mechanical properties with DS_{Am}, PHEA–PEGAm was reacted with aldehyde-presenting alginate (Alg-ALD) to induce Schiff base formation. The resulting "Alg-PHEA" hydrogels were generated under mild physiological buffered conditions without any additional chemical treatments. Their mechanical properties were evaluated by measuring elastic moduli obtained from uniaxial compression. Hydrogels made with PHEA-EtAm without PEG linker were also evaluated as a control to further delineate the effect of graft length on hydrogel mechanics. The concentration of Alg-ALD was kept at 5%, while PHEA was varied from 10 to 20%.

The hydrogels made with PHEA-EtAm as a control showed increased moduli with increasing concentration at all DS_{Am}, as expected (Figure 5-7a). However, the moduli showed a gradual decrease from DS1 to DS3, despite the increase in DS_{Am}, while a further increase in DS_{Am} from DS3 to DS5 resulted in an expected increase in moduli. This initial decrease in moduli with DS_{Am} may have been due to the conformational change with an initial increase in amine content, possibly chain collapse, before a further increase in amine groups allowed more extensive cross-linking with more amine groups extending outward (Figure 5-8a). This explanation is based on a previous study by Hou et al. demonstrating that a polypeptide consisting of different ratios of amine-presenting lysine and hydroxyl-containing threonine induced conformational changes, in which increasing lysine content increased α-helical and secondary coil structures having amine groups outward. [154]

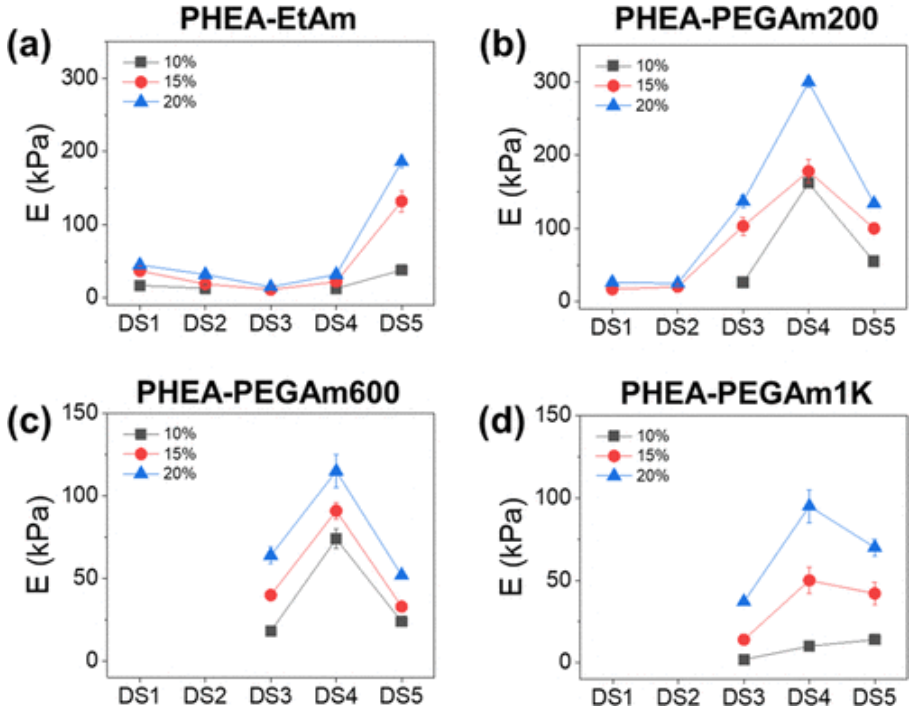

Figure 5-7. Elastic moduli (E) of Alg-PHEA hydrogels controlled with DS_{Am} of PHEA, (a) PHEA-EtAm, (b) PHEA–PEGAm200, (c) PHEA–PEGAm600, and (d) PHEA–PEGAm1K.

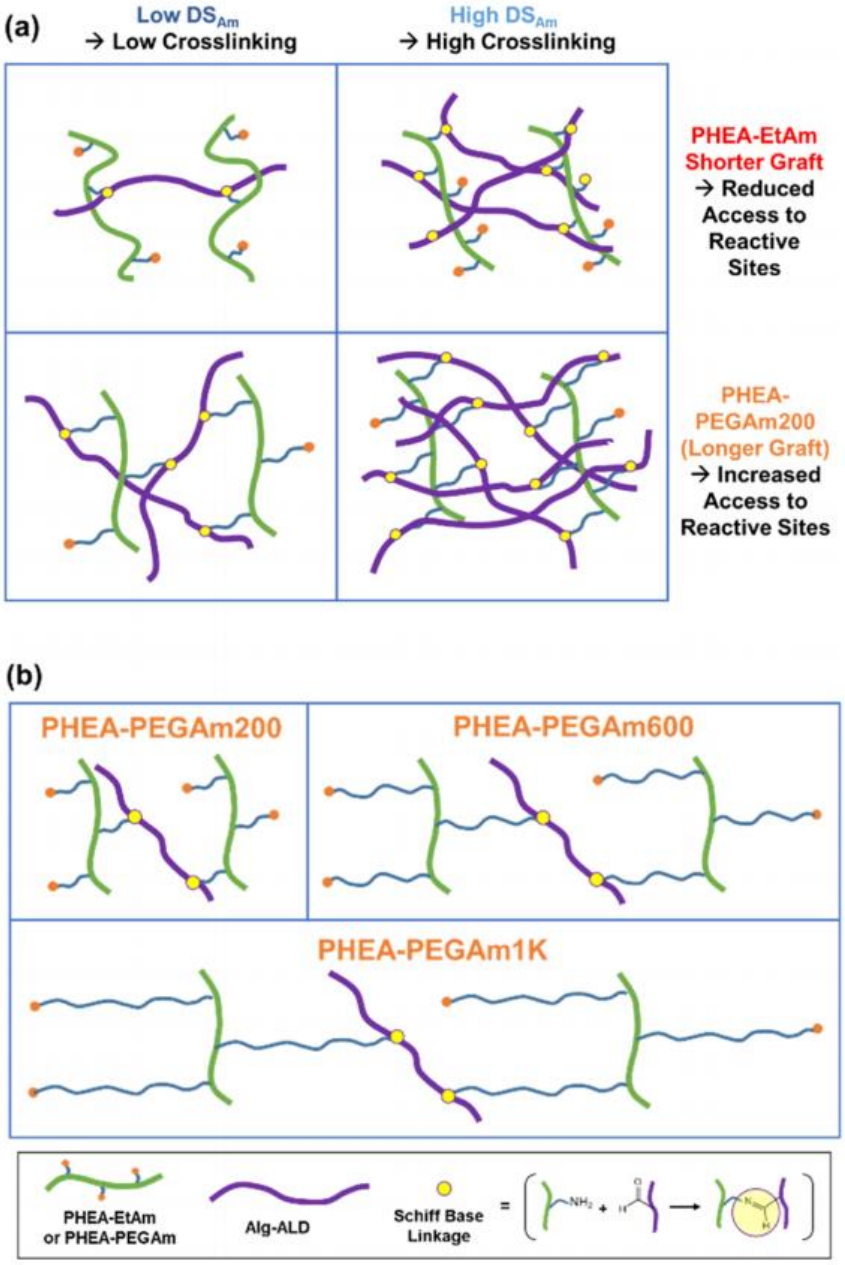

Figure 5-8. Schematic illustration of possible mechanisms of cross-linking reactions: (a) PHEA-EtAm or PHEA–PEGAm200 with varying DS_{Am}; (b) PHEA–PEGAm with varying graft lengths.

On the other hand, the hydrogels made with PHEA–PEGAm200 showed a gradual increase in moduli from DS1 to DS4 at 15 and 20%, and they were much higher than those with PHEA-EtAm at the same concentration and DS_{Am} (Figure 5-7b). This demonstrated that the increased amine graft length likely extended the polymer chains and helped reach the reactive aldehyde on alginate, leading to a greater degree of reactions (Figure 5-8a). Interestingly, however, the hydrogel did not form at the lowest DS_{Am} (DS1 and DS2) at the lowest concentration of 10%. Reduced reactive sites at low DS_{Am} combined with a higher molecular weight between cross-links due to longer graft lengths likely prevented extensive

cross-linking and subsequent hydrogel formation.

Further increase in amine graft length of PHEA–PEGAm resulted in continued decrease in hydrogel rigidity, at all concentrations and DS_{Am} (Figure 5-7c and d). Also, the hydrogel did not form at DS1 and DS2 at all concentrations. These results clearly indicated that increasing graft length significantly hindered the effective cross-linking between Alg-ALD and PHEA–PEGAm. Due to the longer graft pushing the polymer chains farther apart, leading to an insufficient degree of cross-linking for hydrogel formation at lower DS_{Am} or hydrogels with substantially lower mechanical rigidity at higher DS_{Am} (Figure 5-8b). It is also plausible that longer amine grafts have diminished reactivity owing to their reduced mobility and steric hindrance. [71, 155] It should also be noted that the moduli all decreased at the highest DS_{Am} (DS5) for all PHEA–PEGAm, likely due to the stoichiometric access of amine groups reversing the Schiff base formation. Taken together, the graft architecture of PHEA–PEGAm, namely, graft length and degree of substitution of reactive groups, heavily influences the cross-linking reaction between gel-forming polymers, leading to the formation of hydrogels with varying mechanical properties.

The gelation kinetics of Alg-PHEA hydrogels were also assessed by measuring the gelation time (t_{gel}) (Figure 5-9). t_{gel} decreased with DS_{Am} and concentrations of PHEA-EtAm and PHEA–PEGAm, as expected, since having a greater number of reactive functional groups expedites the cross-linking reactions. At the lowest concentration of 10%, t_{gel} was more varied with DS_{Am}, compared to those at higher concentrations of 15 and 20%, in which t_{gel} was more consistent despite the change in DS_{Am} at the same concentration. Increasing graft length also significantly increased t_{gel}, as the decreased conformational mobility due to longer PEG linker reduced the rate of cross-linking reaction. This result suggested that varying DS_{Am} at a given polymer concentration could more effectively keep the gelation kinetics constant while tuning the mechanical properties of hydrogels.

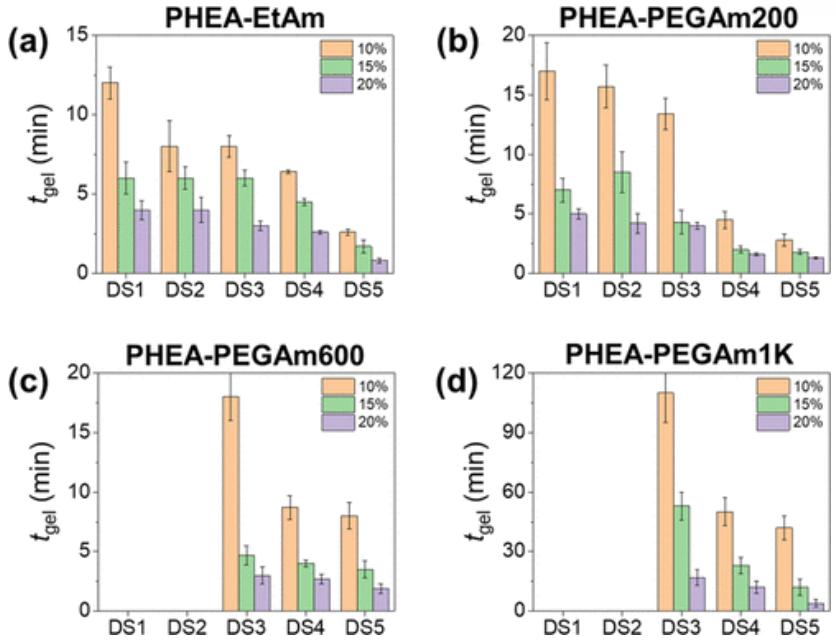

Figure 5-9. Gelation time (t_{gel}) of Alg-PHEA hydrogels controlled with concentration and DS_{Am} of PHEA, (a) PHEA-EtAm, (b) PHEA–PEGAm200, (c) PHEA–PEGAm600, and (d) PHEA–PEGAm1K.

5.3.3 Degradation of PHEA-Linked Hydrogels

Regardless of mechanical properties, all Alg-PHEA hydrogels explored herein underwent facile dissolution in neutral buffered solutions within 10 h. Hydrogels formed via reversible Schiff base formation can undergo reverse dissociation. But since Schiff base is highly favored for hydrogels that are readily formed, they do not generally undergo spontaneous degradation under physiological environment (neutral pH, mild temperature). This highly interesting degradation behavior of PHEA-linked hydrogel system is driven by the remaining unreacted amine groups undergoing nucleophilic attack directly or increasing the basicity of the local environment via protonation, resulting in the reversal of Schiff base linkage, which has been similarly demonstrated in previous studies. [65, 71, 93, 156, 157]

To evaluate the effect of graft length and DS_{Am} on the rate of degradation, the Alg-PHEM hydrogels were incubated in PBS and the change in elastic moduli were measured over time (Figure 5-10a–c). The degradation rate constants (k_D) were obtained by fitting the plots with an exponential decay model (Eq. 5-1; Figure 5-10d–f). For both PHEA–PEGAm200 and PHEA–PEGAm600, the degradation rate generally increased with DS_{Am} and concentration, despite having greater mechanical rigidity, as shown in Figure 5-7. This result showed that the degree of swelling did not directly correlate with the degradation and identified that the degradation was clearly promoted by the amine grafting; having a greater number of amine groups, either by DS_{Am} or concentration, facilitated the degradation. It further corroborated the previous findings that having multiple, unreacted amine groups facilitate the reverse hydrolysis of Schiff base linkage. This decoupled behavior of mechanics and degradation of PHEA-

linked hydrogels does not follow most degradable hydrogel systems via hydrolysis in which the degradation rates correspond with the degree of swelling that expedites the hydrolysis. Therefore, this allows the fabrication of hydrogels with widely controllable mechanics that have comparable degradation rates.

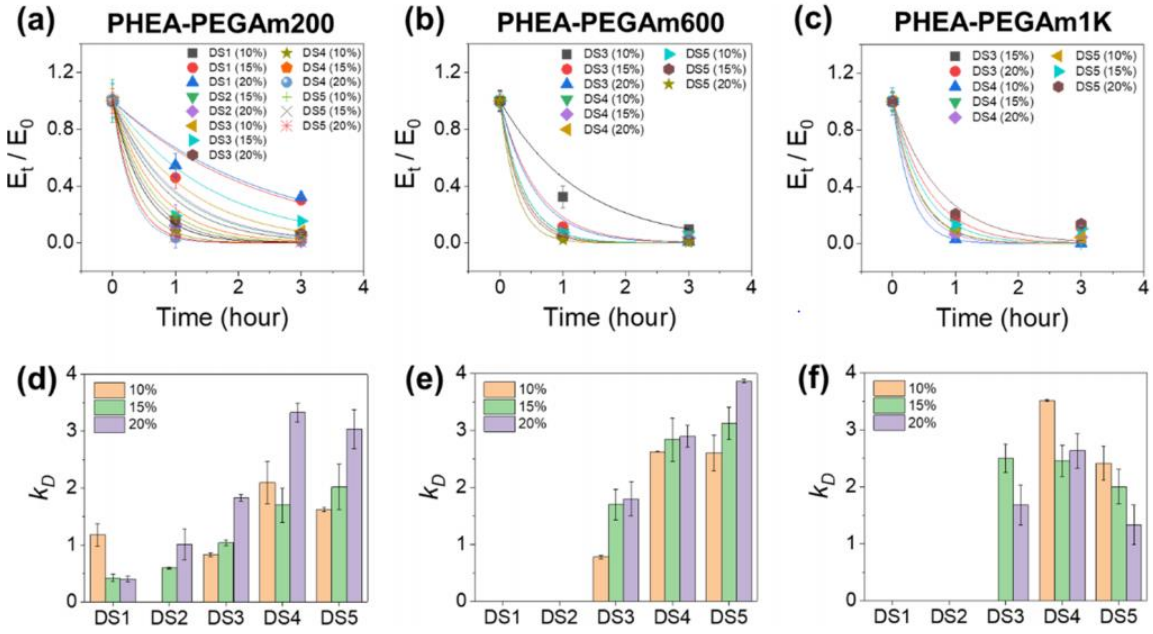

Figure 5-10. Time-resolved fractional change in elastic moduli (E_t/E_0) and degradation rates (k_D) of Alg-PHEA hydrogels: (a, d) PHEA–PEGAm200, (b, e) PHEA–PEGAm600, and (c, f) PHEA–PEGAm1K.

For PHEA–PEGAm1K, on the other hand, the degradation rate decreased with increasing DS_{Am} and concentration. This opposite effect of amine graft could be attributed to the substantially increased portion of PEG buffering the effect of end amine groups expediting the hydrolysis of Schiff base linkage. As a result, the hydrogels with lower mechanical rigidity showed greater rate of degradation. The buffering effect of PEG linkers that delays the amine-induced hydrolysis was further corroborated by the fact that all hydrogels cross-linked with PHEA-EtAm without PEG linkers completely dissolved within 1 h, regardless of concentration and DS_{Am} (data not shown).

It is fascinating to note that, regardless of hydrogel mechanics that varies widely, all PHEA-linked hydrogels underwent complete dissolution in relatively short times, mostly within a few hours. It is believed that the cross-links formed by Schiff base linkage that became extensively reversed by the combination of high water content via swelling and the free amine groups facilitating a nucleophilic attack. [93, 156] In addition, it has been proposed that the amide bonds of the polyaspartamide backbone undergo deamidation by the side chain amine or amide, leading to the main backbone cleavage, which also likely contributed to the facile dissolution of hydrogels. [158, 159]

5.3.4 Drug Release Kinetics of PHEA-Linked Hydrogels

This highly unique hydrogel system that can decouple the mechanical properties and degradation could be viewed as an ideal drug delivery system that allows for both minimally invasive injectability and facile degradation. Therefore, the drug release profiles of Alg-PHEA hydrogels using BSA as a model drug were measured over time (Figure 5-11a–d), and then they were fitted with the Ritger-Peppas model (Eq. 5-2) to obtain drug release rate constants (k_R; Figure 5-11e–h).

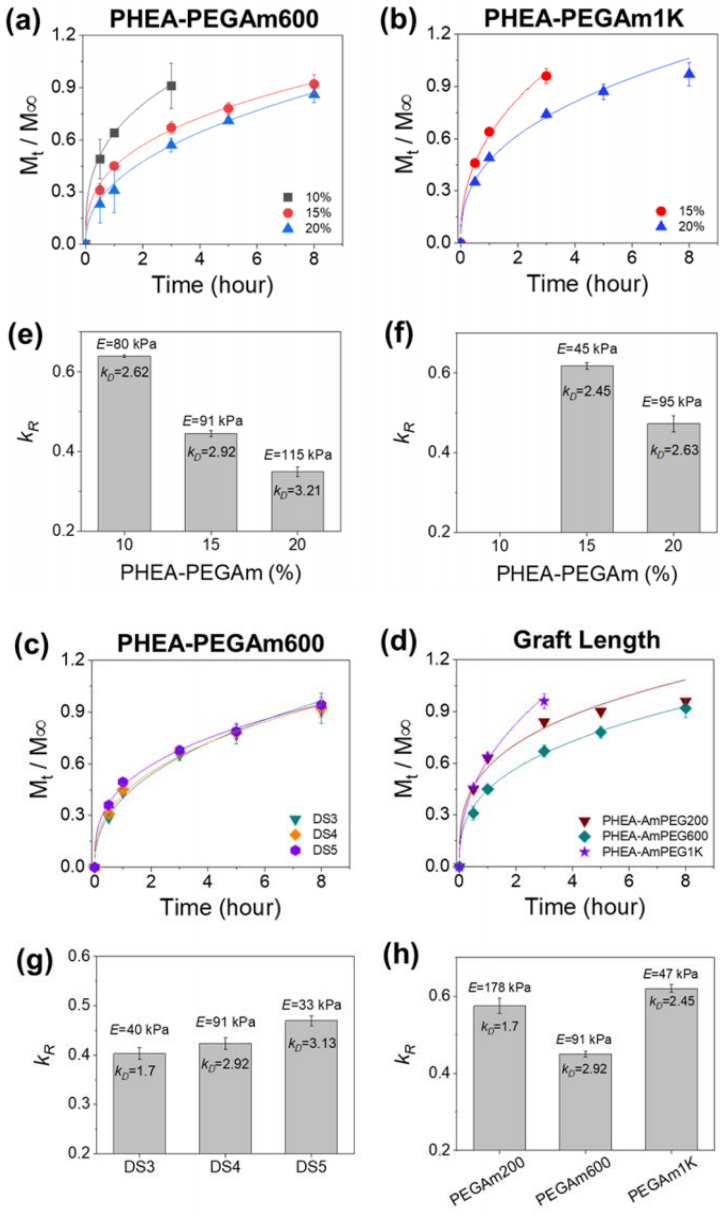

Figure 5-11. Time-resolved fractional drug release profiles (M_t/M_∞) and release rate constants (k_R) of Alg-PHEA hydrogels: (a, e) PHEA–PEGAm600 (DS4), (b, f) PHEA–PEGAm1K (DS4) with varying concentrations, (c, g) 15% PHEA–PEGAm600 with varying DS_{Am}, and (d, h) 15% PHEA–PEGAm (DS4) with varying graft lengths. Elastic modulus (E) and degradation rate constant (k_D) for each condition are noted.

For both PHEA–PEGAm600 and PHEA–PEGAm1K at DS4, k_R decreased with increasing concentration, as expected, since drug release is generally slower in more rigid hydrogels having a higher degree of cross-linking. However, k_R values did not correlate with k_D, in which hydrogels with a faster degradation (higher k_D) are expected to facilitate quicker drug release (higher k_R). In fact, for PHEA–PEGAm600, the trend of k_R was opposite to that of k_D. Since the drug release from hydrogels under aqueous conditions is mostly governed by an initial diffusion, as evidenced by the exponent (n) values obtained from the Ritger-Peppas model all below 0.5, the subsequent degradation did not have a significant effect on the drug release (Figure 5-12). [151]

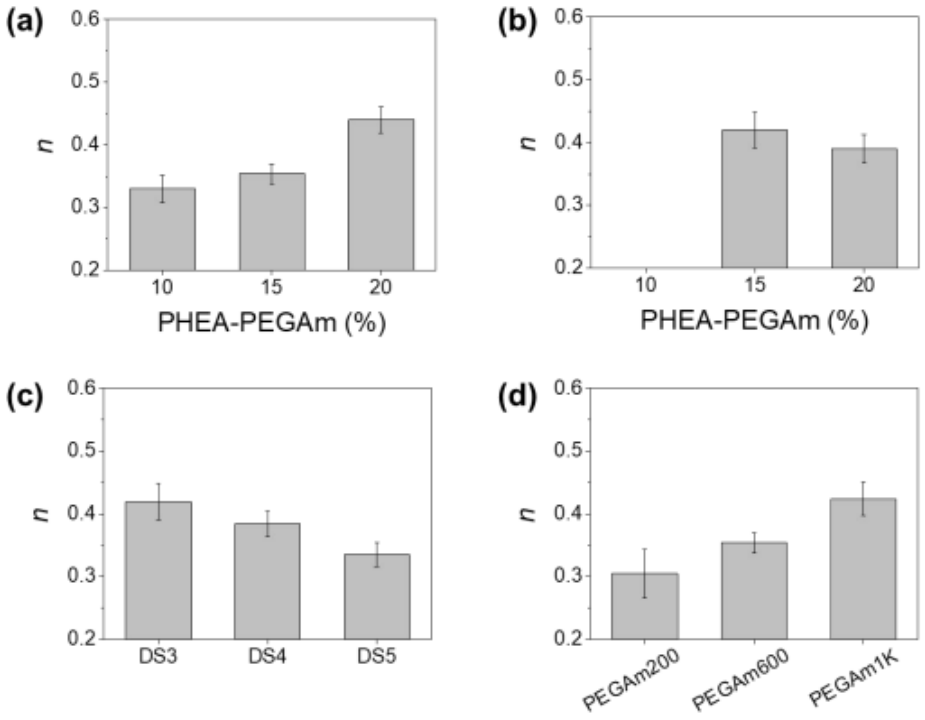

Figure 5-12. Exponent (n) values obtained by fitting the time-resolved drug releases of Alg-PHEA hydrogels with Eq. 5-2 (Ritger-Peppas model): (a) PHEA-PEGAm600 (DS4), (b) PHEA-PEG1K (DS4) with varying concentrations, (c) 15 % PHEA-PEGAm600 with varying DS_{Am}, and (d) 15 % PHEAPEGAm (DS4) with varying graft lengths.

On the other hand, varying the DS_{Am} of Alg-PHEA hydrogels at the same concentration (15%) of PHEA–PEGAm600, k_R indeed increased with k_D and did not correlate with mechanics. Furthermore, at a given DS_{Am} and concentration, increasing from PEGAm600 to PEGAm1K significantly increased k_R, as expected, having lower mechanical properties. But k_R was higher at PEGAm200 having higher mechanical properties and lower degradation rates. It was speculated that having shorter PEG chains could more easily move and change their conformations within the hydrogels, facilitating the protein release. Taken together, these results alluded to the role of amine grafts in facilitating the drug release even against the effect of diffusion and chain relaxation.

5.3.5 Ex Vivo Alg-PHEA Hydrogel Injection and Degradation

The *in situ* forming and fast degrading Alg-PHEA hydrogel system is ideally suited for tissue injectable delivery system. To highlight the injectability and degradability within tissue environment, Alg-PHEA precursor solution was injected into an animal tissue explant model, and *in situ* hydrogel formation and dissolution were monitored (Figure 5-13a).

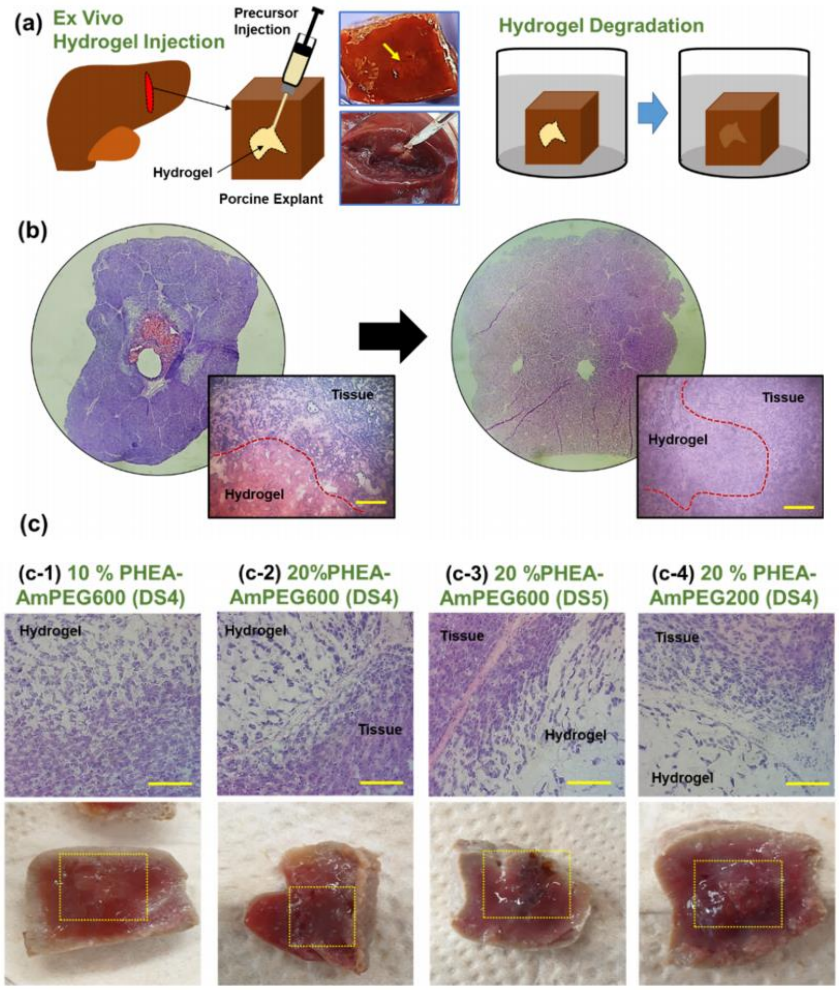

Figure 5-13. (a) Schematic representation of Alg-PHEA hydrogel injection into a tissue explant and subsequent degradation in neutral buffered solution. (b) Representative H&E histological images of Alg-PHEA hydrogel formed within tissue (left) and the same tissue area after hydrogel dissolution in 24 h (right; scale bar: 100 μm). (c) H&E histological images (top) and photographs (bottom) of various Alg-PHEA hydrogels within tissues after 4 h (scale bar: 100 μm). Boxed sections in photographs show embedded hydrogels.

The Alg-PHEA hydrogels did form well within tissue environment upon the injection of precursor solution. The precursor solution did not move away from the injection site, and the hydrogel stayed

within the vicinity (Figure 5-13b). Incubating the tissue explants in neutral buffered solution, the hydrogels eventually all dissolved over time. However, the hydrogels having different mechanics dissolved at different rates. For example, the photographs and histological images taken 4 h after incubation showed that the hydrogel with the lowest rigidity, 10 % PHEA–PEGAm600 (DS4), indeed displayed the most dissolution (Figure 5-13c). The hydrogel with the highest rigidity, 20 % PHEA–PEGAm200 (DS4), on the other hand, still maintained a significant extent of hydrogel structure. Taken together, this *ex vivo* result showed that Alg-PHEA hydrogels can be stably formed upon injection and undergo facile degradation within biological tissue environment, demonstrating the potential for implantable hydrogel delivery system.

5.3.6 Dual Ionic Cross-Linked Alg-PHEA Hydrogels

Alg-PHEA hydrogels have the ability to control mechanical and diffusional properties in a wide range, while maintaining facile dissolution. However, it is often desirable to create hydrogels with a greater range of structural durability and sustained presence. For this purpose, Alg-PHEA hydrogels were further cross-linked ionically using Ca^{2+} with varying concentrations ("Ca-Alg-PHEA"). Alginate has the ability to undergo ionic cross-linking with divalent cations such as Ca^{2+}. [75, 160, 161]

The elastic moduli of Ca-Alg-PHEA hydrogels measured after 1 h of incubation in aqueous buffered solution clearly showed the increase in moduli with Ca^{2+} concentration, (Figure 5-14a). The pore structures visualized with SEM imaging also demonstrated the gradual decrease in porosity with Ca^{2+} concentration (Figure 5-14b). These results effectively verified the additional and increasing degree of ionic cross-linking of Alg-PHEA hydrogels by the concentration of Ca^{2+}.

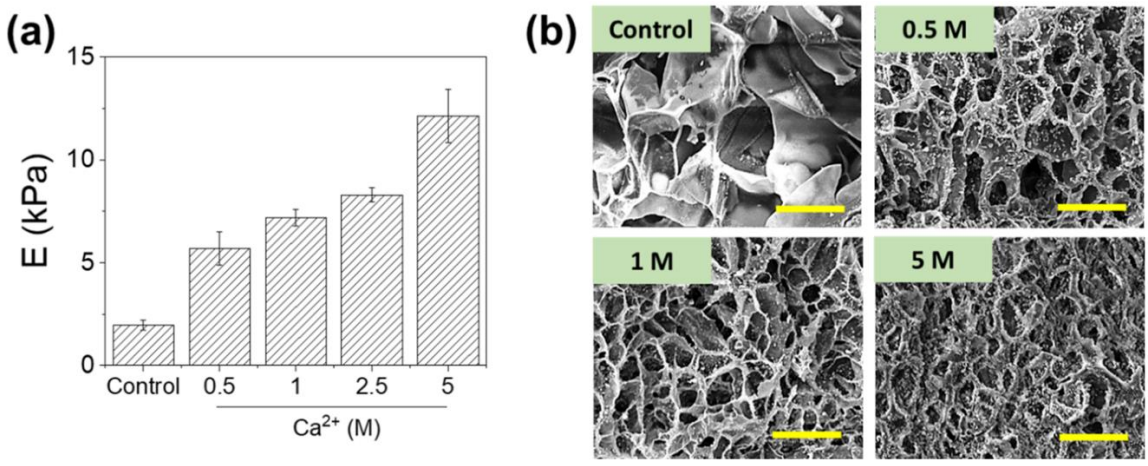

Figure 5-14. (a) Elastic moduli and (b) SEM cross-sectional images of Alg-PHEA hydrogels further cross-linked with various concentrations of Ca^{2+} up to 5 M (scale bar: 30 μm).

Ca-Alg-PHEA hydrogels were incubated in neutral buffered solution, and their degradation over time was measured to assess the effect of secondary ionic cross-linking (Figure 5-15). Alg-PHEA hydrogel

made with 15% PHEA–PEGAm600 (DS4) without Ca^{2+} cross-linking was used as the control. The control condition led to complete dissolution after 5 h. However, Ca-Alg-PHEA hydrogels showed much greater resistance to dissolution (Figure 5-15b and c). More significantly, the degradation rate and subsequent complete dissolution time were shown to effectively depend on the degree of ionic cross-linking.

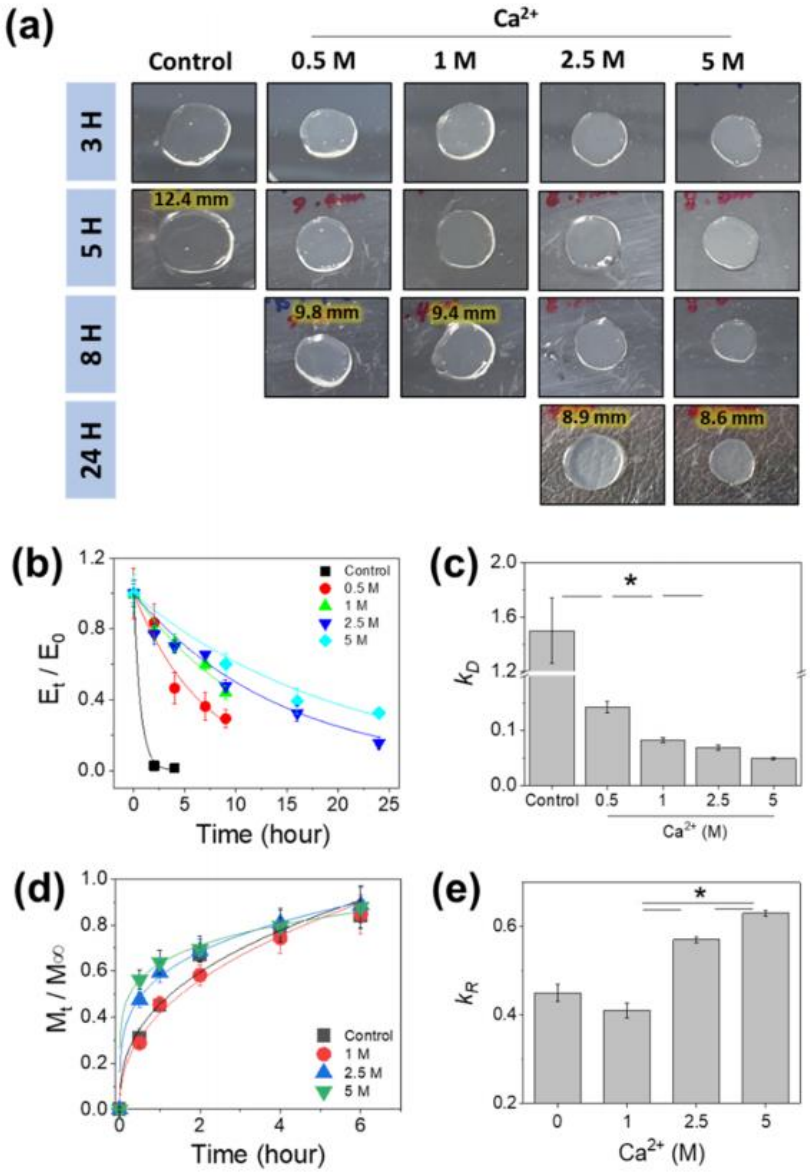

Figure 5-15. (a) Photographs of Alg-PHEA (control) and Ca-Alg-PHEA hydrogel disks, with the initial diameter of 8 mm, taken at various times during incubation in aqueous buffered solution. The concentration of Ca^{2+} cross-linker was controlled up to 5 M. The diameter before complete dissolution are noted. (b, c) Time-resolved fractional change in elastic moduli (E_t/E_0) and degradation rates (k_D), and (d, e) time-resolved fractional drug release profiles (M_t/M_∞) and release kinetics (k_R) of Alg-PHEA and Ca-Alg-PHEA hydrogels (*$p < 0.05$).

The drug release profiles using BSA as the model protein drug were also performed for the Ca-Alg-PHEA hydrogels, and the release rates (k_R) were obtained from Eq. 5-2 (Figure 5-15d and e). It is interesting to note that k_R increased with Ca^{2+} concentration, from 1 to 5 M, despite having greater mechanical properties and structural durability. It is speculated that the excess local Ca^{2+} within hydrogels at higher concentrations being released dominantly at an earlier time frame (before 2 h) likely expedited the BSA release, since BSA is negatively charged at neutral buffered conditions having an isoelectric point of 5.3 and, thus, can electrostatically interact with Ca^{2+}. [95] Taken together, in situ forming and mechanically tunable Alg-PHEA hydrogels that undergo facile dissolution could be further modulated via additional ionic cross-linking to delay and control the degradation and drug release rates.

5.4 Conclusion

In this study, an *in situ* forming and fast degrading hydrogel system was developed by inducing Schiff base formation between aldehyde-presenting alginate (Alg-ALD) and amine-presenting polyaspartamide. Since desired functional moieties can be conveniently grafted onto the polyaspartamide backbone via ring-opening addition reaction of amine-based nucleophiles with polysuccinimide, the graft architecture can be easily tuned by employing nucleophiles having linkers with varying lengths and densities. The polyaspartamide with amino poly(ethylene glycol) grafts, namely, poly(2-hydroxyethyl aspartamide)-g-amino-poly(ethylene glycol) (PHEA–PEGAm), could effectively control the mechanical properties of the resulting Alg-PHEA hydrogels in a broad range by the degree of amine substitution (DS_{Am}) and the length of PEG linker, as well as the polymer concentration. Furthermore, the polyanionic nature of PHEA–PEGAm allowed expedited dissolution of hydrogels under physiological conditions, which was also significantly influenced by the graft architecture. The potential of Alg-PHEA hydrogels as a tissue injectable delivery systems was demonstrated *ex vivo*, in which hydrogel could be stably formed within the tissue upon injection, gradually degraded over time, and eventually completely dissolved. Moreover, the degradation rate and complete dissolution could be further modulated by additional ionic cross-linking of alginate. In sum, *in situ* forming, mechanically tunable, and facile degradable polyaspartamide-linked hydrogel via graft architecture presented in this study could be a highly versatile biomaterial platform for minimally invasive implantable delivery applications.

Reprinted (adapted) with permission from (M. Kim, and C. Cha, Biomacromolecules 2020, 21(9), 3693–3703). Copyright (2020) American Chemical Society. https://doi.org/10.1021/acs.biomac.0c00806

CHAPTER 6. Summary and Future Perspective

In this study, various properties of hydrogel are controlled at various levels while maintaining their intrinsic properties to meet the specific requirements.

In chapter 2, While maintaining the intrinsic properties of PEG hydrogels, a mechanism for effectively controlling drug release kinetics was provided. By presenting pendant PEG chains with characteristic end functional groups in PEG hydrogels, their various physical properties (i.e., charge density and hydrophobicity) effectively controlled the release of proteins with different isoelectric points (pI) independent of the crosslinking density.

In chapter 3, The mechanical properties and decomposition behavior of PEGDA-PEI hydrogels prepared by *in situ* crosslinking between PEGDA and PEI via Michael addition were investigated by varying the M_W and concentration. This combination of tunable mechanical properties and degradation behavior of PEGDA-PEI hydrogels was highly effective in controlling the rate and mode of drug release by dual-mode drug release mechanisms.

In chapter 4, *in situ* formation chitosan hydrogels via Schiff base formation controlled a wide range of mechanical properties without compromising gelation kinetics. Chitosan was conjugated with PEG grafts with controlled length and density (PEG-g-Cs), allowing water solubility at physiological pH, as well as directly affecting the mechanical results of the resulting Cs-PEG hydrogel. The adhesive properties and clinical potential of Cs-hydrogels was evaluated by *ex vivo* and *in vivo* model, which showed wound closure with minimal inflammation with similar mechanical properties as commercial tissue sealants.

In chapter 5, By inducing the formation of Schiff bases between aldehyde-presented alginate (Alg-ALD) and amine-presented polyasparmide, an *in situ* formation and rapid decomposition hydrogel system was developed. The potential of Alg-PHEA hydrogels as a tissue injectable delivery system was demonstrated *ex vivo*, in which hydrogel could be stably formed within the tissue upon injection, gradually degraded over time, and eventually completely dissolved. Moreover, their degradation rate and complete dissolution could be further modulated by additional ionic cross-linking of alginate.

Through the development of *in situ* crosslinked hydrogels with controllable properties by varying the graft architecture and the modulation of the mechanical and physicochemical properties of hydrogels for refined drug release kinetics, the clinical application of hydrogels has been demonstrated in both *in vitro* and *in vivo* models. Therefore, by developing versatile hydrogels, it is expected to increase their potential use in biomedical fields.

REFERENCES

1. Mondal, S., S. Das, and A.K. Nandi, *A review on recent advances in polymer and peptide hydrogels.* Soft Matter, 2020. **16**(6): p. 1404-1454.
2. Caló, E. and V.V. Khutoryanskiy, *Biomedical applications of hydrogels: A review of patents and commercial products.* European Polymer Journal, 2015. **65**: p. 252-267.
3. Ahmed, E.M., *Hydrogel: Preparation, characterization, and applications: A review.* Journal of Advanced Research, 2015. **6**(2): p. 105-121.
4. Hu, W., et al., *Advances in crosslinking strategies of biomedical hydrogels.* Biomaterials Science, 2019. **7**(3): p. 843-855.
5. Yang, J.-A., et al., *In situ-forming injectable hydrogels for regenerative medicine.* Progress in Polymer Science, 2014. **39**(12): p. 1973-1986.
6. Choi, B., et al., *Introduction to In Situ Forming Hydrogels for Biomedical Applications*, in *In-Situ Gelling Polymers: For Biomedical Applications*, X.J. Loh, Editor. 2015, Springer Singapore: Singapore. p. 5-35.
7. Vermonden, T., R. Censi, and W.E. Hennink, *Hydrogels for Protein Delivery.* Chemical Reviews, 2012. **112**(5): p. 2853-2888.
8. Wang, C., R.R. Varshney, and D.-A. Wang, *Therapeutic cell delivery and fate control in hydrogels and hydrogel hybrids.* Advanced Drug Delivery Reviews, 2010. **62**(7): p. 699-710.
9. Drury, J.L. and D.J. Mooney, *Hydrogels for tissue engineering: scaffold design variables and applications.* Biomaterials, 2003. **24**(24): p. 4337-4351.
10. Schmidt, J.J., J. Rowley, and H.J. Kong, *Hydrogels used for cell-based drug delivery.* Journal of Biomedical Materials Research Part A, 2008. **87A**(4): p. 1113-1122.
11. Ruoslahti, E., *RGD AND OTHER RECOGNITION SEQUENCES FOR INTEGRINS.* Annual Review of Cell and Developmental Biology, 1996. **12**(1): p. 697-715.
12. Zhu, J., *Bioactive modification of poly(ethylene glycol) hydrogels for tissue engineering.* Biomaterials, 2010. **31**(17): p. 4639-4656.
13. Lin, C.-C. and K.S. Anseth, *PEG Hydrogels for the Controlled Release of Biomolecules in Regenerative Medicine.* Pharmaceutical Research, 2009. **26**(3): p. 631-643.
14. Weber, L.M., C.G. Lopez, and K.S. Anseth, *Effects of PEG hydrogel crosslinking density on protein diffusion and encapsulated islet survival and function.* Journal of Biomedical Materials Research Part A, 2009. **90A**(3): p. 720-729.
15. Hoare, T.R. and D.S. Kohane, *Hydrogels in drug delivery: Progress and challenges.* Polymer, 2008. **49**(8): p. 1993-2007.
16. Anseth, K.S., C.N. Bowman, and L. Brannon-Peppas, *Mechanical properties of hydrogels and their experimental determination.* Biomaterials, 1996. **17**(17): p. 1647-1657.

17. Cha, C., et al., *Decoupled control of stiffness and permeability with a cell-encapsulating poly(ethylene glycol) dimethacrylate hydrogel.* Biomaterials, 2010. **31**(18): p. 4864-4871.
18. Cruise, G.M., D.S. Scharp, and J.A. Hubbell, *Characterization of permeability and network structure of interfacially photopolymerized poly(ethylene glycol) diacrylate hydrogels.* Biomaterials, 1998. **19**(14): p. 1287-1294.
19. Fefelova, N.A., et al., *Mucoadhesive interactions of amphiphilic cationic copolymers based on [2-(methacryloyloxy)ethyl]trimethylammonium chloride.* International Journal of Pharmaceutics, 2007. **339**(1): p. 25-32.
20. Huynh, D.P., et al., *Controlled release of insulin from pH/temperature-sensitive injectable pentablock copolymer hydrogel.* Journal of Controlled Release, 2009. **137**(1): p. 20-24.
21. Lee, W.-F. and P.-L. Yeh, *Thermoreversible hydrogels. VIII. Effect of a zwitterionic monomer on swelling behaviors of thermosensitive hydrogels copolymerized by N-isopropylacrylamide with N,N'-dimethyl (acrylamidopropyl) ammonium propane sulfonate.* Journal of Applied Polymer Science, 1999. **74**(9): p. 2170-2180.
22. Matsusaki, M. and M. Akashi, *Novel Functional Biodegradable Polymer IV: pH-Sensitive Controlled Release of Fibroblast Growth Factor-2 from a Poly(γ-glutamic acid)-Sulfonate Matrix for Tissue Engineering.* Biomacromolecules, 2005. **6**(6): p. 3351-3356.
23. Vinogradov, S.V., T.K. Bronich, and A.V. Kabanov, *Nanosized cationic hydrogels for drug delivery: preparation, properties and interactions with cells.* Advanced Drug Delivery Reviews, 2002. **54**(1): p. 135-147.
24. Yu, L., Z. Zhang, and J. Ding, *In vitro degradation and protein release of transparent and opaque physical hydrogels of block copolymers at body temperature.* Macromolecular Research, 2012. **20**(3): p. 234-243.
25. Bae, M.S., et al., *Development of novel photopolymerizable hyaluronic acid/heparin-based hydrogel scaffolds with a controlled release of growth factors for enhanced bone regeneration.* Macromolecular Research, 2016. **24**(9): p. 829-837.
26. Kim, S., K. Lee, and C. Cha, *Refined control of thermoresponsive swelling/deswelling and drug release properties of poly(N-isopropylacrylamide) hydrogels using hydrophilic polymer crosslinkers.* Journal of Biomaterials Science, Polymer Edition, 2016. **27**(17): p. 1698-1711.
27. Akiyama, Y., Y. Nagasaki, and K. Kataoka, *Synthesis of Heterotelechelic Poly(ethylene glycol) Derivatives Having α-Benzaldehyde and ω-Pyridyl Disulfide Groups by Ring Opening Polymerization of Ethylene Oxide Using 4-(Diethoxymethyl)benzyl Alkoxide as a Novel Initiator.* Bioconjugate Chemistry, 2004. **15**(2): p. 424-427.
28. Cammas, S., Y. Nagasaki, and K. Kataoka, *Heterobifunctional Poly(ethylene oxide): Synthesis of .alpha.-Methoxy-.omega.-amino and .alpha.-Hydroxy-.omega.-amino PEOs with the Same Molecular Weights.* Bioconjugate Chemistry, 1995. **6**(2): p. 226-230.

29. Jang, J., J. Hong, and C. Cha, *Effects of precursor composition and mode of crosslinking on mechanical properties of graphene oxide reinforced composite hydrogels.* Journal of the Mechanical Behavior of Biomedical Materials, 2017. **69**: p. 282-293.

30. Cha, C., R.H. Kohman, and H. Kong, *Biodegradable Polymer Crosslinker: Independent Control of Stiffness, Toughness, and Hydrogel Degradation Rate.* Advanced Functional Materials, 2009. **19**(19): p. 3056-3062.

31. Kim, S., et al., *Comprehensive Examination of Mechanical and Diffusional Effects on Cell Behavior Using a Decoupled 3D Hydrogel System.* Macromolecular Bioscience, 2017. **17**(9): p. 1700162.

32. Cha, C., J.H. Jeong, and H. Kong, *Poly(ethylene glycol)-poly(lactic-co-glycolic acid) core–shell microspheres with enhanced controllability of drug encapsulation and release rate.* Journal of Biomaterials Science, Polymer Edition, 2015. **26**(13): p. 828-840.

33. Ferrero, C., D. Massuelle, and E. Doelker, *Towards elucidation of the drug release mechanism from compressed hydrophilic matrices made of cellulose ethers. II. Evaluation of a possible swelling-controlled drug release mechanism using dimensionless analysis.* Journal of Controlled Release, 2010. **141**(2): p. 223-233.

34. Fu, Y. and W.J. Kao, *Drug release kinetics and transport mechanisms of non-degradable and degradable polymeric delivery systems.* Expert Opinion on Drug Delivery, 2010. **7**(4): p. 429-444.

35. Siepmann, J. and N.A. Peppas, *Modeling of drug release from delivery systems based on hydroxypropyl methylcellulose (HPMC).* Advanced Drug Delivery Reviews, 2012. **64**: p. 163-174.

36. Zustiak, S.P. and J.B. Leach, *Hydrolytically Degradable Poly(Ethylene Glycol) Hydrogel Scaffolds with Tunable Degradation and Mechanical Properties.* Biomacromolecules, 2010. **11**(5): p. 1348-1357.

37. Peppas, N.A., et al., *Poly(ethylene glycol)-containing hydrogels in drug delivery.* Journal of Controlled Release, 1999. **62**(1): p. 81-87.

38. Alexander, A., et al., *Poly(ethylene glycol)–poly(lactic-co-glycolic acid) based thermosensitive injectable hydrogels for biomedical applications.* Journal of Controlled Release, 2013. **172**(3): p. 715-729.

39. Lee, W.-F. and Y.-C. Chen, *Effect of bentonite on the physical properties and drug-release behavior of poly(AA-co-PEGMEA)/bentonite nanocomposite hydrogels for mucoadhesive.* Journal of Applied Polymer Science, 2004. **91**(5): p. 2934-2941.

40. Sohn, S.S., et al., *Biomimetic and photo crosslinked hyaluronic acid/pluronic F127 hydrogels with enhanced mechanical and elastic properties to be applied in tissue engineering.* Macromolecular Research, 2016. **24**(3): p. 282-291.

41. Lai, F. and H. Li, *Modeling of effect of initial fixed charge density on smart hydrogel response to ionic strength of environmental solution.* Soft Matter, 2010. **6**(2): p. 311-320.
42. Bueno, V.B., et al., *Synthesis and swelling behavior of xanthan-based hydrogels.* Carbohydrate Polymers, 2013. **92**(2): p. 1091-1099.
43. Serra, L., J. Doménech, and N.A. Peppas, *Drug transport mechanisms and release kinetics from molecularly designed poly(acrylic acid-g-ethylene glycol) hydrogels.* Biomaterials, 2006. **27**(31): p. 5440-5451.
44. Kragh-Hansen, U., *Molecular aspects of ligand binding to serum albumin.* Pharmacol Rev, 1981. **33**(1): p. 17-53.
45. Cevik, O., D. Gidon, and S. Kizilel, *Visible-light-induced synthesis of pH-responsive composite hydrogels for controlled delivery of the anticonvulsant drug pregabalin.* Acta Biomaterialia, 2015. **11**: p. 151-161.
46. Chaturvedi, K., et al., *Polymeric hydrogels for oral insulin delivery.* Journal of Controlled Release, 2013. **165**(2): p. 129-138.
47. Holt, J.K., et al., *Fast Mass Transport Through Sub-2-Nanometer Carbon Nanotubes.* Science, 2006. **312**(5776): p. 1034-1037.
48. Thomas, J.A. and A.J.H. McGaughey, *Reassessing Fast Water Transport Through Carbon Nanotubes.* Nano Letters, 2008. **8**(9): p. 2788-2793.
49. Hoffman, A.S., *Hydrogels for biomedical applications.* Advanced Drug Delivery Reviews, 2012. **64**: p. 18-23.
50. Schexnailder, P. and G. Schmidt, *Nanocomposite polymer hydrogels.* Colloid and Polymer Science, 2009. **287**(1): p. 1-11.
51. Dragan, E.S., *Design and applications of interpenetrating polymer network hydrogels. A review.* Chemical Engineering Journal, 2014. **243**: p. 572-590.
52. Hern, D.L. and J.A. Hubbell, *Incorporation of adhesion peptides into nonadhesive hydrogels useful for tissue resurfacing.* Journal of Biomedical Materials Research, 1998. **39**(2): p. 266-276.
53. Schmedlen, R.H., K.S. Masters, and J.L. West, *Photocrosslinkable polyvinyl alcohol hydrogels that can be modified with cell adhesion peptides for use in tissue engineering.* Biomaterials, 2002. **23**(22): p. 4325-4332.
54. Nguyen, K.T. and J.L. West, *Photopolymerizable hydrogels for tissue engineering applications.* Biomaterials, 2002. **23**(22): p. 4307-4314.
55. Wenceslau, A.C., et al., *Thermo- and pH-sensitive IPN hydrogels based on PNIPAAm and PVA-Ma networks with LCST tailored close to human body temperature.* Materials Science and Engineering: C, 2012. **32**(5): p. 1259-1265.
56. Cha, C., et al., *Integrative design of a poly(ethylene glycol)-poly(propylene glycol)-alginate*

hydrogel to control three dimensional biomineralization. Biomaterials, 2011. **32**(11): p. 2695-2703.

57. Zhao, X., et al., *Photocrosslinkable Gelatin Hydrogel for Epidermal Tissue Engineering.* Advanced Healthcare Materials, 2016. **5**(1): p. 108-118.
58. Nomura, Y., et al., *Genotoxicity of dental resin polymerization initiators in vitro.* Journal of Materials Science: Materials in Medicine, 2006. **17**(1): p. 29-32.
59. Bail, R., et al., *The Effect of a Type I Photoinitiator on Cure Kinetics and Cell Toxicity in Projection-Microstereolithography.* Procedia CIRP, 2013. **5**: p. 222-225.
60. Anseth, K.S., et al., *In situ forming degradable networks and their application in tissue engineering and drug delivery.* Journal of Controlled Release, 2002. **78**(1): p. 199-209.
61. Li, Y., et al., *In situ hydrogel constructed by starch-based nanoparticles via a Schiff base reaction.* Carbohydrate Polymers, 2014. **110**: p. 87-94.
62. Darling, N.J., et al., *Controlling the kinetics of thiol-maleimide Michael-type addition gelation kinetics for the generation of homogenous poly(ethylene glycol) hydrogels.* Biomaterials, 2016. **101**: p. 199-206.
63. Zhu, H.-Z., et al., *Click synthesis of hydrogels by metal-free 1,3-dipolar cycloaddition reaction between maleimide and azide functionalized polymers.* Macromolecular Research, 2016. **24**(9): p. 793-799.
64. Choi, S.M., et al., *Synthesis and characterization of in situ gellable poly(glycerol sebacate)-co-poly(ethylene glycol) polymers.* Macromolecular Research, 2017. **25**(1): p. 85-91.
65. Wang, J., et al., *In Situ-Forming Polyamidoamine Dendrimer Hydrogels with Tunable Properties Prepared via Aza-Michael Addition Reaction.* ACS Applied Materials & Interfaces, 2017. **9**(12): p. 10494-10503.
66. Nguyen, Q.V., et al., *Injectable polymeric hydrogels for the delivery of therapeutic agents: A review.* European Polymer Journal, 2015. **72**: p. 602-619.
67. Lutolf, M.P. and J.A. Hubbell, *Synthesis and Physicochemical Characterization of End-Linked Poly(ethylene glycol)-co-peptide Hydrogels Formed by Michael-Type Addition.* Biomacromolecules, 2003. **4**(3): p. 713-722.
68. Forrest, M.L., J.T. Koerber, and D.W. Pack, *A Degradable Polyethylenimine Derivative with Low Toxicity for Highly Efficient Gene Delivery.* Bioconjugate Chemistry, 2003. **14**(5): p. 934-940.
69. Pack, D.W., et al., *Design and development of polymers for gene delivery.* Nature Reviews Drug Discovery, 2005. **4**(7): p. 581-593.
70. Hahn, M.S., J.S. Miller, and J.L. West, *Three-Dimensional Biochemical and Biomechanical Patterning of Hydrogels for Guiding Cell Behavior.* Advanced Materials, 2006. **18**(20): p. 2679-2684.

71. Liang, Y., et al., *Tuning the non-equilibrium state of a drug-encapsulated poly(ethylene glycol) hydrogel for stem and progenitor cell mobilization.* Biomaterials, 2011. **32**(7): p. 2004-2012.

72. Zuidema, J.M., et al., *A protocol for rheological characterization of hydrogels for tissue engineering strategies.* Journal of Biomedical Materials Research Part B: Applied Biomaterials, 2014. **102**(5): p. 1063-1073.

73. Weng, L., X. Chen, and W. Chen, *Rheological Characterization of in Situ Crosslinkable Hydrogels Formulated from Oxidized Dextran and N-Carboxyethyl Chitosan.* Biomacromolecules, 2007. **8**(4): p. 1109-1115.

74. Metters, A.T., C.N. Bowman, and K.S. Anseth, *A Statistical Kinetic Model for the Bulk Degradation of PLA-b-PEG-b-PLA Hydrogel Networks.* The Journal of Physical Chemistry B, 2000. **104**(30): p. 7043-7049.

75. Lee, K., et al., *Dual ionic crosslinked interpenetrating network of alginate-cellulose beads with enhanced mechanical properties for biocompatible encapsulation.* Cellulose, 2017. **24**(11): p. 4963-4979.

76. Dash, S., et al., *Kinetic modeling on drug release from controlled drug delivery systems.* Acta Pol Pharm, 2010. **67**(3): p. 217-23.

77. Ritger, P.L. and N.A. Peppas, *A simple equation for description of solute release I. Fickian and non-fickian release from non-swellable devices in the form of slabs, spheres, cylinders or discs.* Journal of Controlled Release, 1987. **5**(1): p. 23-36.

78. Piculell, L. and B. Lindman, *Association and segregation in aqueous polymer/polymer, polymer/surfactant, and surfactant/surfactant mixtures: similarities and differences.* Advances in Colloid and Interface Science, 1992. **41**: p. 149-178.

79. Anseth, K.S., C.M. Wang, and C.N. Bowman, *Reaction behaviour and kinetic constants for photopolymerizations of multi(meth)acrylate monomers.* Polymer, 1994. **35**(15): p. 3243-3250.

80. Pritchard, C.D., et al., *An injectable thiol-acrylate poly(ethylene glycol) hydrogel for sustained release of methylprednisolone sodium succinate.* Biomaterials, 2011. **32**(2): p. 587-597.

81. Saito, H., A.S. Hoffman, and H.I. Ogawa, *Delivery of Doxorubicin from Biodegradable PEG Hydrogels Having Schiff Base Linkages†.* Journal of Bioactive and Compatible Polymers, 2007. **22**(6): p. 589-601.

82. Malkoch, M., et al., *Synthesis of well-defined hydrogel networks using Click chemistry.* Chemical Communications, 2006(26): p. 2774-2776.

83. Seliktar, D., *Designing Cell-Compatible Hydrogels for Biomedical Applications.* Science, 2012. **336**(6085): p. 1124-1128.

84. Cha, C., et al., *Designing Biomaterials To Direct Stem Cell Fate.* ACS Nano, 2012. **6**(11): p. 9353-9358.

85. Loessner, D., et al., *Bioengineered 3D platform to explore cell–ECM interactions and drug*

resistance of epithelial ovarian cancer cells. Biomaterials, 2010. **31**(32): p. 8494-8506.

86. Tibbitt, M.W. and K.S. Anseth, *Hydrogels as extracellular matrix mimics for 3D cell culture.* Biotechnology and Bioengineering, 2009. **103**(4): p. 655-663.
87. Mironi-Harpaz, I., et al., *Photopolymerization of cell-encapsulating hydrogels: Crosslinking efficiency versus cytotoxicity.* Acta Biomaterialia, 2012. **8**(5): p. 1838-1848.
88. Temenoff, J.S., et al., *In Vitro Cytotoxicity of Redox Radical Initiators for Cross-Linking of Oligo(poly(ethylene glycol) fumarate) Macromers.* Biomacromolecules, 2003. **4**(6): p. 1605-1613.
89. Tromayer, M., et al., *A biocompatible diazosulfonate initiator for direct encapsulation of human stem cells via two-photon polymerization.* Polymer Chemistry, 2018. **9**(22): p. 3108-3117.
90. Van Tomme, S.R., G. Storm, and W.E. Hennink, *In situ gelling hydrogels for pharmaceutical and biomedical applications.* International Journal of Pharmaceutics, 2008. **355**(1): p. 1-18.
91. Yu, L. and J. Ding, *Injectable hydrogels as unique biomedical materials.* Chemical Society Reviews, 2008. **37**(8): p. 1473-1481.
92. Metters, A. and J. Hubbell, *Network Formation and Degradation Behavior of Hydrogels Formed by Michael-Type Addition Reactions.* Biomacromolecules, 2005. **6**(1): p. 290-301.
93. Jang, J. and C. Cha, *Multivalent Polyaspartamide Cross-Linker for Engineering Cell-Responsive Hydrogels with Degradation Behavior and Tunable Physical Properties.* Biomacromolecules, 2018. **19**(2): p. 691-700.
94. Kim, M. and C. Cha, *Integrative control of mechanical and degradation properties of in situ crosslinkable polyamine-based hydrogels for dual-mode drug release kinetics.* Polymer, 2018. **145**: p. 272-280.
95. Kim, M. and C. Cha, *Modulation of functional pendant chains within poly (ethylene glycol) hydrogels for refined control of protein release.* Scientific reports, 2018. **8**(1): p. 1-12.
96. Tan, H., et al., *Injectable in situ forming biodegradable chitosan–hyaluronic acid based hydrogels for cartilage tissue engineering.* Biomaterials, 2009. **30**(13): p. 2499-2506.
97. Liu, Y., et al., *Preparation of therapeutic-laden konjac hydrogel for tumor combination therapy.* Chemical Engineering Journal, 2019. **375**: p. 122048.
98. Wu, C., et al., *Design of injectable agar-based composite hydrogel for multi-mode tumor therapy.* Carbohydrate Polymers, 2018. **180**: p. 112-121.
99. Zheng, Y., et al., *Preparation of injectable temperature-sensitive chitosan-based hydrogel for combined hyperthermia and chemotherapy of colon cancer.* Carbohydrate Polymers, 2019. **222**: p. 115039.
100. Bonino, C.A., et al., *Real-time in siturheology of alginate hydrogel photocrosslinking.* Soft Matter, 2011. **7**(24): p. 11510-11517.
101. Berger, J., et al., *Structure and interactions in covalently and ionically crosslinked chitosan*

hydrogels for biomedical applications. European Journal of Pharmaceutics and Biopharmaceutics, 2004. **57**(1): p. 19-34.

102. Bhattarai, N., J. Gunn, and M. Zhang, *Chitosan-based hydrogels for controlled, localized drug delivery.* Advanced Drug Delivery Reviews, 2010. **62**(1): p. 83-99.
103. Chung, H. and R.H. Grubbs, *Rapidly Cross-Linkable DOPA Containing Terpolymer Adhesives and PEG-Based Cross-Linkers for Biomedical Applications.* Macromolecules, 2012. **45**(24): p. 9666-9673.
104. Qu, J., et al., *Antibacterial adhesive injectable hydrogels with rapid self-healing, extensibility and compressibility as wound dressing for joints skin wound healing.* Biomaterials, 2018. **183**: p. 185-199.
105. Alves, N.M. and J.F. Mano, *Chitosan derivatives obtained by chemical modifications for biomedical and environmental applications.* International Journal of Biological Macromolecules, 2008. **43**(5): p. 401-414.
106. Islas, L., G. Burillo, and A. Ortega, *Graft Copolymerization of 2-Hydroxyethyl Methacrylate onto Chitosan Using Radiation Technique for Release of Diclofenac.* Macromolecular Research, 2018. **26**(8): p. 690-695.
107. Bhattarai, N., et al., *PEG-grafted chitosan as an injectable thermosensitive hydrogel for sustained protein release.* Journal of Controlled Release, 2005. **103**(3): p. 609-624.
108. Harris, J.M., et al., *Synthesis and characterization of poly(ethylene glycol) derivatives.* Journal of Polymer Science: Polymer Chemistry Edition, 1984. **22**(2): p. 341-352.
109. Hong, J., et al., *Complex Tuning of Physical Properties of Hyperbranched Polyglycerol-Based Bioink for Microfabrication of Cell-Laden Hydrogels.* Advanced Functional Materials, 2019. **29**(13): p. 1808750.
110. Lih, E., et al., *Rapidly curable chitosan–PEG hydrogels as tissue adhesives for hemostasis and wound healing.* Acta Biomaterialia, 2012. **8**(9): p. 3261-3269.
111. Strehin, I., et al., *A versatile pH sensitive chondroitin sulfate–PEG tissue adhesive and hydrogel.* Biomaterials, 2010. **31**(10): p. 2788-2797.
112. Zhang, H., et al., *Mussel-inspired hyperbranched poly(amino ester) polymer as strong wet tissue adhesive.* Biomaterials, 2014. **35**(2): p. 711-719.
113. Assmann, A., et al., *A highly adhesive and naturally derived sealant.* Biomaterials, 2017. **140**: p. 115-127.
114. Vuocolo, T., et al., *A Highly Elastic and Adhesive Gelatin Tissue Sealant for Gastrointestinal Surgery and Colon Anastomosis.* Journal of Gastrointestinal Surgery, 2012. **16**(4): p. 744-752.
115. Barua, S., P. Chattopadhyay, and N. Karak, *s-Triazine-based biocompatible hyperbranched epoxy adhesive with antibacterial attributes for sutureless surgical sealing.* Journal of Materials Chemistry B, 2015. **3**(28): p. 5877-5885.

116. Askaruly, S., et al., *Quantitative Evaluation of Skin Surface Roughness Using Optical Coherence Tomography In Vivo.* IEEE Journal of Selected Topics in Quantum Electronics, 2019. **25**(1): p. 1-8.

117. Choi, G., et al., *Image-guided recording system for spatial and temporal mapping of neuronal activities in brain slice.* Journal of biophotonics, 2018. **11**(3): p. e201700243.

118. Wiegand, I., K. Hilpert, and R.E.W. Hancock, *Agar and broth dilution methods to determine the minimal inhibitory concentration (MIC) of antimicrobial substances.* Nature Protocols, 2008. **3**: p. 163.

119. Balouiri, M., M. Sadiki, and S.K. Ibnsouda, *Methods for in vitro evaluating antimicrobial activity: A review.* Journal of Pharmaceutical Analysis, 2016. **6**(2): p. 71-79.

120. Dash, M., et al., *Chitosan—A versatile semi-synthetic polymer in biomedical applications.* Progress in Polymer Science, 2011. **36**(8): p. 981-1014.

121. Jang, Y., et al., *Interfacial Compression-Dependent Merging of Two Miscible Microdroplets in an Asymmetric Cross-Junction for In Situ Microgel Formation.* Macromolecular Research, 2018. **26**(12): p. 1143-1149.

122. Qu, J., et al., *pH-responsive self-healing injectable hydrogel based on N-carboxyethyl chitosan for hepatocellular carcinoma therapy.* Acta Biomaterialia, 2017. **58**: p. 168-180.

123. Pielichowski, K. and K. Flejtuch, *Differential scanning calorimetry studies on poly(ethylene glycol) with different molecular weights for thermal energy storage materials.* Polymers for Advanced Technologies, 2002. **13**(10-12): p. 690-696.

124. Berezkin, A.V. and Y.V. Kudryavtsev, *Effect of Cross-Linking on the Structure and Growth of Polymer Films Prepared by Interfacial Polymerization.* Langmuir, 2015. **31**(44): p. 12279-12290.

125. Liu, N.C., G.P. Yao, and H. Huang, *Influences of grafting formulations and processing conditions on properties of silane grafted moisture crosslinked polypropylenes.* Polymer, 2000. **41**(12): p. 4537-4542.

126. Wang, B., et al., *Copolymerization of propylene with Si-containing α,ω-diolefins: how steric hindrance of diolefins affects long chain branch formation.* Polymer Chemistry, 2016. **7**(17): p. 2938-2946.

127. Hozumi, T., et al., *Injectable Hydrogel with Slow Degradability Composed of Gelatin and Hyaluronic Acid Cross-Linked by Schiff's Base Formation.* Biomacromolecules, 2018. **19**(2): p. 288-297.

128. Kong, H.J., et al., *Controlling Degradation of Hydrogels via the Size of Crosslinked Junctions.* Advanced Materials, 2004. **16**(21): p. 1917-1921.

129. Etemadi, H., R. Yegani, and M. Seyfollahi, *The effect of amino functionalized and polyethylene glycol grafted nanodiamond on anti-biofouling properties of cellulose acetate membrane in*

membrane bioreactor systems. Separation and Purification Technology, 2017. **177**: p. 350-362.

130. Jayakumar, R., et al., *Biomaterials based on chitin and chitosan in wound dressing applications.* Biotechnology Advances, 2011. **29**(3): p. 322-337.
131. Kroez, M., W. Lang, and G. Dickneite, *Wound healing and degradation of the fibrin sealant Beriplast® P following partial liver resection in rabbits.* Wound Repair and Regeneration, 2005. **13**(3): p. 318-323.
132. Alemdaroğlu, C., et al., *An investigation on burn wound healing in rats with chitosan gel formulation containing epidermal growth factor.* Burns, 2006. **32**(3): p. 319-327.
133. Field, C.K. and M.D. Kerstein, *Overview of wound healing in a moist environment.* The American Journal of Surgery, 1994. **167**(1, Supplement): p. S2-S6.
134. Siepmann, J. and F. Siepmann, *Modeling of diffusion controlled drug delivery.* Journal of Controlled Release, 2012. **161**(2): p. 351-362.
135. Kim, S.W., Y.H. Bae, and T. Okano, *Hydrogels: Swelling, Drug Loading, and Release.* Pharmaceutical Research, 1992. **9**(3): p. 283-290.
136. Top, A. and K.L. Kiick, *Multivalent protein polymers with controlled chemical and physical properties.* Advanced Drug Delivery Reviews, 2010. **62**(15): p. 1530-1540.
137. Hacker, M.C. and H.A. Nawaz, *Multi-Functional Macromers for Hydrogel Design in Biomedical Engineering and Regenerative Medicine.* International Journal of Molecular Sciences, 2015. **16**(11): p. 27677-27706.
138. Jalalvandi, E. and A. Shavandi, *Polysuccinimide and its derivatives: Degradable and water soluble polymers (review).* European Polymer Journal, 2018. **109**: p. 43-54.
139. Nakato, T., A. Kusuno, and T. Kakuchi, *Synthesis of poly(succinimide) by bulk polycondensation of L-aspartic acid with an acid catalyst.* Journal of Polymer Science Part A: Polymer Chemistry, 2000. **38**(1): p. 117-122.
140. Roweton, S., S.J. Huang, and G. Swift, *Poly(aspartic acid): Synthesis, biodegradation, and current applications.* Journal of environmental polymer degradation, 1997. **5**(3): p. 175-181.
141. Tomida, M., et al., *Convenient synthesis of high molecular weight poly(succinimide) by acid-catalysed polycondensation of l-aspartic acid.* Polymer, 1997. **38**(18): p. 4733-4736.
142. Pitarresi, G., et al., *Biodegradable hydrogels obtained by photocrosslinking of dextran and polyaspartamide derivatives.* Biomaterials, 2003. **24**(23): p. 4301-4313.
143. Tran, N.B., et al., *CO2-responsive swelling behavior and metal-ion adsorption properties in novel histamine-conjugated polyaspartamide hydrogel.* Journal of Applied Polymer Science, 2016. **133**(16).
144. Wang, B., et al., *Self-healable mussel-mimetic nanocomposite hydrogel based on catechol-containing polyaspartamide and graphene oxide.* Materials Science and Engineering: C, 2016. **69**: p. 160-170.

145. Cha, C., et al., *Top-down Synthesis of Versatile Polyaspartamide Linkers for Single-Step Protein Conjugation to Materials.* Bioconjugate Chemistry, 2011. **22**(12): p. 2377-2382.

146. d'Arcy, R. and N. Tirelli, *Mitsunobu Reaction: A Versatile Tool for PEG End Functionalization.* Macromolecular Rapid Communications, 2015. **36**(20): p. 1829-1835.

147. Kim, M., et al., *In situ facile-forming chitosan hydrogels with tunable physicomechanical and tissue adhesive properties by polymer graft architecture.* Carbohydrate Polymers, 2020. **229**: p. 115538.

148. Gomez, C.G., M. Rinaudo, and M.A. Villar, *Oxidation of sodium alginate and characterization of the oxidized derivatives.* Carbohydrate Polymers, 2007. **67**(3): p. 296-304.

149. Hoang Thi, T.T., et al., *Oxidized Alginate Supplemented Gelatin Hydrogels for the In Situ Formation of Wound Dressing with High Antibacterial Activity.* Macromolecular Research, 2019. **27**(8): p. 811-820.

150. Kim, S. and C. Cha, *Enhanced mechanical and electrical properties of heteroscaled hydrogels infused with aqueous-dispersible hybrid nanofibers.* Biofabrication, 2019. **12**(1): p. 015020.

151. Ritger, P.L. and N.A. Peppas, *A simple equation for description of solute release II. Fickian and anomalous release from swellable devices.* Journal of Controlled Release, 1987. **5**(1): p. 37-42.

152. Thorpe, A.A., et al., *Thermally triggered hydrogel injection into bovine intervertebral disc tissue explants induces differentiation of mesenchymal stem cells and restores mechanical function.* Acta Biomaterialia, 2017. **54**: p. 212-226.

153. D'souza, A.A. and R. Shegokar, *Polyethylene glycol (PEG): a versatile polymer for pharmaceutical applications.* Expert Opinion on Drug Delivery, 2016. **13**(9): p. 1257-1275.

154. Hou, S.-S., et al., *Self-Assembly and Hydrogelation of Coil–Sheet Poly(l-lysine)-block-poly(l-threonine) Block Copolypeptides.* Macromolecules, 2018. **51**(20): p. 8054-8063.

155. Ran, Q., et al., *Effect of the length of the side chains of comb-like copolymer dispersants on dispersion and rheological properties of concentrated cement suspensions.* Journal of Colloid and Interface Science, 2009. **336**(2): p. 624-633.

156. Lu, C., et al., *An injectable and biodegradable hydrogel based on poly(α,β-aspartic acid) derivatives for localized drug delivery.* Journal of Biomedical Materials Research Part A, 2014. **102**(3): p. 628-638.

157. Song, C.K., et al., *Dopa-Empowered Schiff Base Forming Alginate Hydrogel Glue for Rapid Hemostatic Control.* Macromolecular Research, 2019. **27**(2): p. 119-125.

158. Lu, Y., et al., *Effect of Pendant Group Structure on the Hydrolytic Stability of Polyaspartamide Polymers under Physiological Conditions.* Biomacromolecules, 2012. **13**(5): p. 1296-1306.

159. Itaka, K., et al., *Biodegradable polyamino acid-based polycations as safe and effective gene carrier minimizing cumulative toxicity.* Biomaterials, 2010. **31**(13): p. 3707-3714.

160. Augst, A.D., H.J. Kong, and D.J. Mooney, *Alginate Hydrogels as Biomaterials.*

Macromolecular Bioscience, 2006. **6**(8): p. 623-633.

161. Kuo, C.K. and P.X. Ma, *Ionically crosslinked alginate hydrogels as scaffolds for tissue engineering: Part 1. Structure, gelation rate and mechanical properties.* Biomaterials, 2001. **22**(6): p. 511-521.